EUROPEAN ORGANIZATION FOR NUCLEAR RESEARCH

CERN/EF 86-18
(CERN/EP 86-141)
26 September 1986

ON THE ENERGY RESOLUTION OF URANIUM AND OTHER HADRON CALORIMETERS

Richard Wigmans

CERN, Geneva, Switzerland
and
NIKHEF-H, Amsterdam, the Netherlands

ABSTRACT

The various components that contribute to the signal from a hadron calorimeter, and the factors that affect the energy resolution with which hadrons can be detected, are examined in detail. The role of the electromagnetic to hadronic signal ratio e/h is crucial in this respect. Its value is determined by the Z of the absorber material, the thicknesses of the passive and active layers, the signal integration time of the detector, and the properties of the readout material, in particular the free proton content and the saturation or recombination properties for few-MeV proton detection. Readout media that contain free protons offer the possiblity to tune the e/h ratio to the desired value (1.0) through the sampling fraction. Signal equalization (e/h = 1.0) does not seem to be a property unique to ^{238}U, but can also be achieved for lead and even iron calorimeters. The calculations show, on the other hand, that e/h values are larger than 1.0 for any calorimeter using liquid-argon readout. The intrinsic energy resolution for hadron detection is largely dominated by fluctuations in the binding energy losses that occur in the nuclear reactions. Efficient neutron detection can considerably reduce these effects provided that energy loss through recoil protons dominates. Calorimeters using ^{238}U, Pb or Fe absorbers, and plastic scintillator, liquid argon, silicon or TMP readout were investigated. Experimental results on e/h values and energy resolution, which are often considered confusing, are nicely reproduced and explained.

Submitted to Nuclear Instruments and Methods in Physics Research

---

EF/3213F/RW/em

1. INTRODUCTION

The use of calorimeter or total absorption techniques is rapidly gaining importance in detectors for high-energy physics experiments. Basically, a calorimeter is a block of matter in which the particle that is to be measured interacts and deposits all its energy in the form of a shower of decreasingly lower-energy particles. The block is made in such a way that a certain fraction of the initial particle energy is transformed into a measurable signal (light, electrical charge). Since this fraction is constant, the signal is proportional to the energy, at least above a certain lower energy limit. Calorimeters for electromagnetic (e.m.) shower detection have been used since a long time, either as homogeneous [e.g. NaI(Tl) or BGO] or as sampling devices. The physics on which they are based is well understood and so are the factors that limit their performance, e.g. the achievable energy resolution. This is by no means the case for hadron calorimeters.

Large hadron calorimeters will be the key instruments for particle detection in many experiments at the next generation of colliding-beam accelerators (SLC, Tevatron, HERA). Achieving the best possible energy resolution is very closely linked to the physics capabilities of these detectors [1]. Therefore, in order to be able to design them optimally it is of vital interest to understand, in as much detail as possible, the factors that limit the energy resolution.

The energy resolution of a hadron calorimeter is in general much worse than what can be achieved for e.m. shower detection. The wide variety of possible interaction processes, and the effects associated with excitation of the absorber nuclei are considered responsible for this. About ten years ago, it was realized that one dominant source of fluctuations, coming from π^o production in the shower, could be eliminated by equalizing the calorimeter response to the e.m. and purely hadronic shower components [2]. This idea, the e/h = 1 concept, appeared to work in the case of uranium/plastic scintillator calorimeters [3]. Recently, the HELIOS Collaboration at CERN measured a resolution of $0.35\ E^{-1/2}$ for 8-200 GeV pion beams with their reconstructed R807 calorimeter [4]. Various other groups [5], however, testing uranium/liquid-argon devices, found resolutions that were considerably worse and, moreover, did not scale with $E^{-1/2}$.

This indicates that the explanation of the advantageous properties of uranium absorber, given by the inventors of the idea, i.e. amplification of the hadronic signal by the nuclear fission contribution, is at best a partial one. Crucial information on hadronic shower development in uranium and lead calorimeters was recently obtained from a study of induced radioactivity [6]. These data revealed the vital role of neutrons in the formation of the hadronic calorimeter signal.

In this paper the various contributions to the energy resolution of a hadron calorimeter are investigated. Rather than going into elaborate Monte-Carlo simulations that predict a black-box result for a given design, we will discuss the various effects that play a role, and will develop simple models to estimate the consequences of each effect for the calorimeter performance. We will limit ourselves to hadrons with energies $\gtrsim$ 2 GeV. Below this value, energy loss by ionization alone will become increasingly important and the calorimeter performance may change considerably. In sect. 2, the relation between the energy resolution and the e/h value is treated. Sect. 3, examines the calorimeter response to the e.m. part of hadron showers, and sect. 4 investigates the purely hadronic part and in particular the contribution of neutrons. In sect. 5, the ultimate resolution limits of practical hadron calorimeters are discussed. Unless explicitly stated otherwise, we will consider hadron calorimeters as being of the sampling type, i.e. consisting of alternating absorber and readout planes (passive and active media).

2. THE RELATION BETWEEN e/h AND THE ENERGY RESOLUTION

In the development of a shower generated by a high-energy hadron, usually a certain number of π^o's and η's are produced. These particles decay into γ's and hence deposit their energy in the form of e.m. showers. In the purely hadronic component of the shower, some fraction of the energy will disappear without contributing to the calorimeter signal. This is, for example, the case for ν's and μ's from π and K decay which in general escape from the detector. The same is true for a certain fraction of the neutrons, which are abundantly produced in the nuclear reactions. And finally, the energy spent in breaking up the nuclei in these reactions, i.e. liberating the nucleons bound in the nucleus, is invisible as well.

This has two effects (fig. 1). First, the calorimeter response to the purely hadronic part of a hadron shower will have a much broader distribution than the response to the e.m. part, at the same energy. This is because of the large event-to-event fluctuations in the phenomena mentioned before. Secondly, the average response to the e.m. and the purely hadronic components will in general be different ($e/h^{intrinsic} \neq 1$). Since energy is lost in the case of the purely hadronic component, one expects to first order, $e/h^{intr} > 1$.

The energy sharing between the e.m. and the purely hadronic components can be very different from event to event. Much depends on the nature of the first interaction. If this interaction is of the charge exchange type, the fraction of the energy going into the e.m. component ($f_{\pi}o$) will be large; in other cases it can be very small. Fluctuations in $f_{\pi}o$ are an important ingredient for the energy resolution of a calorimeter. When the energy of the incident hadron is increased, the number of ionizations in the active layers that consitute the calorimeter signal will increase proportionally. Therefore, the width of the distributions shown in fig. 1 will decrease according to $E^{-1/2}$. However, the average position of the e.m. and the purely hadronic distributions will remain the same. If $e/h^{intr} \neq 1$, fluctuations in $f_{\pi}o$, which are of a non-Gaussian nature, will therefore cause the energy resolution <u>not</u> to scale with $E^{-1/2}$. This is a well-known experimental fact. The CDHS Collaboration [7] found that the hadronic energy resolution of their iron-scintillator calorimeter decreased much more slowly with energy than $E^{-1/2}$. Beyond 100 GeV, no further improvement was observed.

The e.m. and the purely hadronic shower components have very different characteristic dimensions, both longitudinally and laterally, especially for high-Z absorber materials where the radiation length (X_o) and nuclear interaction length (λ) are very different. If the calorimeter is sufficiently finely segmented, especially in the longitudinal direction, one may determine $f_{\pi}o$ on an event-by-event basis and hence eliminate, at least partly, the effect of the $f_{\pi}o$ fluctuations on the energy resolution.

The CDHS Collaboration developed an algorithm for this purpose; with this they were able to recuperate a purely statistical behaviour for

10-140 GeV pions. It should be noted that their detector was read out every $7X_o$ in depth. For an 8λ deep lead calorimeter this means a longitudinal subdivision in 35 independent sections. Such a requirement would cause enormous problems for the large 4π calorimeters needed in a colliding-beam environment, because of the huge number of channels involved and the difficulties in getting the signals to the outside world without creating too much dead space. The calorimeter of the Axial Field Spectrometer which operated at the CERN Intersecting Storage Rings was therefore subdivided into two longitudinal sections only [3]. Several Monte-Carlo studies, examining weighting schemes for realistic 4π calorimeters indicate that the resolution improvement that can be expected is considerably worse than in the CDHS case [8]. In the following, we will see what happens if no corrections for fluctuations in f_{π^o} can be applied on an event-by-event basis.

Obviously, the contribution of fluctuations in f_{π^o} to the energy resolution will become more important if e/h^{intr} goes further away from 1. We can write

$$\sigma(E)/E = cE^{-1/2} + X(e/h^{intr} - 1) \quad . \tag{1}$$

In order to investigate the second term, we simulated calorimeter signal distributions with a Monte-Carlo method. We made realistic assumptions concerning the various contributions to the energy resolution and varied the value of e/h^{intr}. The average value of f_{π^o} for a given hadron energy was taken as $0.12 \log(E)$. The distribution of f_{π^o} around this value was assumed to be determined by the square root of the number of π^o's produced, taken as $5 \log(E) - 4.6$ [9].

A chosen value of f_{π^o} defines the energy going into the e.m. and the purely hadronic parts of the shower, E_e and E_h. The signals from these components were assumed to be distributed around the most probable values according to a Gaussian with a sigma of $0.16/\sqrt{E_e}$ and $0.35/\sqrt{E_h}$, respectively. Adding the two signals yielded the resulting calorimeter signal. Typically 10 000 events were generated for each energy and e/h^{intr} value. The results of this exercise are given in figs 2-4.

In an experimental measurement, one never determines e/h^{intr}, but the relation between the average calorimeter signals for an electron and a

hadron of the same energy, the latter being the result of a mixture between the e.m. and the purely hadronic components. Since the average value of f_{π^o} depends on the particle energy, the experimental e/h value will depend on the energy as well, contrary to e/h^{intr} which is a constant depending on the calorimeter properties only. The experimental value of e/h as a function of energy is given in fig. 2(a), for various values of e/h^{intr}. Clearly, experimental e/h values can only be compared if they are determined at the same particle energy. One usually takes 10 GeV for this purpose.

Another consequence of the fact that $\langle f_{\pi^o} \rangle$ is energy-dependent is that the calorimeter signal for hadrons will <u>not</u> be proportional to the energy, unless $e/h^{intr} = 1$. This is shown in fig. 2(b).

Fig. 3 shows the hadron energy resolution as a function of energy. Only if $e/h^{intr} \equiv 1$ will the resolution scale with $E^{-1/2}$; in all other cases the constant c rises with energy, if the result is interpreted as $\sigma(E)/E = cE^{-1/2}$ (fig. 3(a)). In fig. 3(b) the same data are plotted using an abcissa linear in $E^{-1/2}$. This shows that the deviation from $E^{-1/2}$ scaling can be very reasonably described as a constant term, the value of which is determined by e/h (fig. 4). In order to make a comparison with experimental data more relevant, the e/h values given in figs 3 and 4 are the ones as expected to be measured at 10 GeV. The conversion to e/h^{intr}, or eventually to experimental values measured at other energies can be obtained from fig. 2(a).

These figures make it very clear that, in particular at high energies, the value of e/h^{intr} is absolutely crucial for the energy resolution that can be obtained. For the CDHS iron calorimeter (2.5 cm Fe/0.5 cm plastic scintillator) for example, where e/h has been measured to be 1.36 at 10 GeV, the resolution $\sigma(E)/E$ does not become better than ~ 7%, even at the highest energies. For calorimeters with $e/h^{intr} \equiv 1$, the energy resolution will continue to improve with increasing energy, until limitations due to instrumental effects become important. The HELIOS Collaboration, for example, measured a $\sigma(E)/E$ of 2.5% for 200 GeV pions [4], a factor of ~ 3 better than the high-energy limit for the CDHS calorimeter. Such differences are much larger than one might naïvely assume from the resolution figures that are usually quoted, which concern <u>low</u> energies (10 GeV).

Summarizing this section we conclude that a calorimeter meant to detect hadrons or hadron jets at high energies (Tevatron, HERA, SPS $\bar{p}p$ Collider, SLC, LEP) with a good energy resolution will be capable of a considerably better performance if e/h^{intr} is close to 1. In case iron or copper is used as absorber the hadronic energy resolution will be dominated and limited by the e/h^{intr} value (fig. 3). Moreover, the average response will not be proportional to the energy. This situation may be improved if the technical solutions (and the money) can be found which will permit the calorimeter to be longitudinally subdivided to such an extent that fluctuations in the fraction of energy spent on π^o production can be compensated for on an event-by-event basis. Compensating calorimeters ($e/h^{intr} \sim 1$) will ultimately be limited by instrumental effects, e.g. the uniformity of the response over the calorimeter surface. These effects, which one usally believes to be able to keep at the few percent level, determine how close e/h^{intr} should be to 1 in order not to suffer from f_{π^o} fluctuations (fig. 4).

3. THE CALORIMETER RESPONSE TO ELECTROMAGNETICALLY INTERACTING PARTICLES

In this section and the following ones we will examine in detail the calorimeter response to the various shower components. The calorimeter signal for a particular type of particle will be determined by two factors:

(i) The amount of energy that is deposited in the form of ionization in the active layers.

(ii) The ionization density of the active layers.

The latter factor is important since saturation or recombination effects are known to play a crucial role, at least in non-gaseous readout media. The amount of collected charge or scintillation light resulting from protons of a few MeV may be smaller by a large factor if compared with minimum-ionizing particles depositing the same energy in the active layers.

3.1 Muons

As a scale for the calorimeter signal, we will use the response to a minimum-ionizing particle (mip). For a given sampling calorimeter the ratio of the energy used to ionize the active and passive layers can be calculated immediately using the mean dE/dx values for mip's in the differ-

ent materials [10]. As an example, one finds that in a 3 mm uranium/2.5 mm plastic scintillator (PMMA: polymethyl methacrylate) calorimeter, 8.6% of the energy is deposited in the active layers and 91.4% in the absorber plates by a mip. It should be emphasized, however, that strictly speaking mip's are imaginary particles. The average energy deposited per unit length by real particles in realistic calorimeters will always be larger than the value calculated with the minimum in the dE/dx curves. In practice, one uses muons to set the absolute energy scale. The average energy loss by relativistic muons in matter is known to rise with energy owing to effects such as δ-ray production, bremsstrahlung, e^+e^- pair production, etc. [11]. These effects are material-dependent and hence can be quite different for the absorber and readout layers of the calorimeter. The HELIOS Collaboration found that the signal ratio e/μ of their uranium/scintillator calorimeter strongly decreased with increasing energy in the interval 8-200 GeV if the muons were assumed to be minimum-ionizing particles [4]. A careful analysis of the consequences of the various mentioned effects made it possible to extract a signal ratio e/mip from these data, which was found to be 0.67 ± 0.05, and independent of energy as it ought to be.

In order to make a comparison with other data possible, it is preferable to measure signal ratios e/μ at a well-defined energy, e.g. 10 GeV as for e/h, or to convert them to a ratio e/mip.

3.2 High-energy electron and photon showers

Although the e.m. cascade through which high-energy electrons and photons lose their energy in a block of matter is governed by one of the best established and most complete theoretical frameworks in physics (quantum electrodynamics), the signal resulting from this process when the block of matter is a sampling calorimeter has caused a lot of confusion. This signal is the result of the ionization of the active layers by all the electrons and positrons, generated in the shower development, that traverse these layers. Naïvely one might therefore expect that this signal is equivalent to the signal of muons that traverse the detector and whose combined energy deposit is equal to the initial electron or photon energy ($e/\mu = 1$). This is in practice by no means the case. Many experimental results lead to the following conclusion: in sampling calorimeters where the Z of the absorber material is larger than the (average) Z

of the active medium, the response to e.m. showers is smaller than the response to minimum-ionizing particles of equivalent energy (e/mip < 1). The larger the difference in Z, the smaller the value of e/mip becomes.

The e.m. shower code EGS4 [12], which is known to reproduce the existing experimental data in great detail, provided it is used with sufficiently low cut-off values, very clearly supports this conclusion as well. We have used the program to calculate the response to 10 GeV electrons for sampling calorimeters, using either 2.5 mm thick liquid argon or PMMA read-out layers, and Al, Fe, Sn, Pb or U absorber layers of 1 radiation length thickness. The cut-off values were 10 keV for photons and 100 keV kinetic energy for electrons and positrons. The resulting e/mip values are given in fig. 5 as a function of Z_{abs}.

Some experimental data [4,5,13] have also been included in fig. 5. Referring to what has been said in the previous subsection about the experimental determination of e/mip values, one should be careful about conclusions, but it seems beyond any doubt that the e/mip values for calorimeters with Pb or U absorbers are significantly lower than those for Fe or Cu calorimeters.

The confusion referred to at the beginning of this subsection concerns the explanation of these phenomena, which are usually called transition effects. This term was introduced by Pinkau [14], who argued that the phenomena should be attributed to effects occurring at the boundary between layers of materials with different Z. His argument is based on the difference in critical energy which will lead to a somewhat different shower development in the energy region 5-50 MeV for both materials. The critical energy is defined as the energy below which the electrons and positrons lose more energy by ionization than by bremsstrahlung, and corresponds approximately to the energy below which the cross section for Compton effect by photons becomes larger than the one for e^+e^- pair production. The shower tree will have more branches in a high-Z (low critical energy) material. Hence, the total energy will be deposited in a smaller number of radiation lengths, and the density of charged particles at a given depth will be larger than in a low-Z material.

Qualitatively, this is correct. Quantitatively, however, this effect will play a very minor role in realistic calorimeters. Any significant change in the shower composition will only appear after a significant fraction of a radiation length. When a shower crosses the boundary between two layers with different Z, it will only adapt adiabatically to the new situation. Realistic calorimeters consist of absorber layers that are typically $0.5\text{-}2X_o$ thick, whilst the readout layers are only $\sim 0.01X_o$ thick. Therefore, the shower development in the calorimeter will be completely governed by the properties of the absorber material, and the change in charged-particle density induced by the active layers is, at maximum, something of the order of a few percent.

Recently, Flauger [15] studied the transition effects in some detail, using the EGS shower simulation program. He subdivided the active and passive layers of a fine-sampling calorimeter into sublayers, and found that the energy deposit in the different sublayers of one layer was virtually the same. From this, the author concluded that transition effects occur very rapidly. In this data we find support for our conclusion that transition effects, as discussed here, play no significant role at all.

The main contribution to the e/mip < 1 effect is, in fact, a very simple one, and has to do with the way in which low-energy ($\lesssim$ 1 MeV) γ's lose their energy in matter. Fig. 6(a) shows the mass attenuation coefficients for γ's in different materials, as a function of energy [16]. Roughly speaking, for any element the Compton cross section is the largest component in the energy region 1–5 MeV. This cross section is proportional to Z, and it decreases slowly as the energy increases. At high energies the pair production cross section dominates, it is proportional to Z^2 and increases slowly with energy. The mass absorption coefficients asymptotically approach the value $1/X_o$. Consequently, the total absorption cross section has a minimum at some intermediate energy. At low energies, the photoelectric effect may become important. However, since the cross section is proportional to Z^5, the contribution of this effect will be extremely material-dependent. That is why the mass attenuation coefficients for Pb and U increase more steeply below 1 MeV than do those for the other elements given (logarithmic scale!).

The consequences of this behaviour for the e/mip value of a sampling calorimeter are decisive. A large fraction of the initial electron energy is going into low-energy photon production during the shower development; hence the way in which these photons deposit their energy is absolutely crucial. Analysis of the EGS4 data shows that for a 10 GeV electron shower in a uranium calorimeter, only 12% of the initial energy is deposited through ionization by electrons and positrons faster than 20 MeV (fig. 6(b)). Below this energy the photon mass attenuation coefficients for uranium and low-Z readout materials strongly deviate from proportionality; hence considerable effects on the e/mip value may be expected. More than 60% of the energy is deposited by particles that are softer than 4 MeV, where the electron range is only $0.5X_o$. For these particles the calorimeter signal will be determined by the photon cross sections, since the sampling of electrons in becoming very incomplete. And ~ 40% of the energy is deposited by particles that are softer than 1 MeV, where the contribution of photoelectric effect to the photon interaction cross sections makes a big difference between high-Z and low-Z materials. The EGS4 results on the energy sharing as a function of the Z of the absorber material are summarized in fig. 6(b).

Let us consider, as an example, what happens to a 511 keV γ in the uranium/PMMA calorimeter discussed in the previous subsection. The EGS calculations showed that in the shower development of a 1 GeV electron, on an average 65 positrons are created, which means that already ~ 7% of the total initial energy is carried by these 511 keV positron annihilation γ's. The data from fig. 6(a) tell us that ~ 70% of such γ's will interact in a 3 mm uranium plate that they meet on their way, whilst only 2% will interact in a 2.5 mm PMMA plate. The 511 keV will be partly (Compton effect) or totally (photoelectric effect) transferred to an electron, whose range is in any case so short compared with the plate thickness that the process, to a good approximation, may be considered as a local energy deposition at the point of the interaction. So the fraction of the energy deposited in the active layers by these γ's is to a first approximation 2/70 = 2.9%, which is only one third of the fraction deposited by minimum-ionizing particles (subsect. 3.1).

In a more sophisticated treatment, the γ's are isotropically emitted from a source which is homogeneously distributed in depth over one uranium

plate, and the energy deposition is followed over $20X_o$ in all directions using EGS4 with cut-off values of 10 keV and 100 keV for photons and electrons, respectively. This treatment showed that the fraction of the energy deposited in the active layers by these γ's is 6-7 times smaller than for a minimum-ionizing particle.

These calculations show that the calorimeter response to low-energy photons, which are abundantly produced in the e.m. shower development, is considerably suppressed compared to mip's, and this will lead to e/mip values which are different from 1 to an extent which is determined by the Z-values of the passive and active layers. It is also clear that in order to make reliable predictions, the EGS program has to be used with cut-off values that are low enough to correctly treat the energy deposit by 0.1-1 MeV photons and electrons.

The EGS4 results mentioned earlier clearly show that the e/mip ratio decreases with the increasing depth or age of the shower. This is illustrated in fig. 7(a). This plot was obtained by comparing the energy deposited in each individual active layer with the average energy in the two passive layers sandwiching it. The ratio of these two numbers is plotted on a scale normalized to the dE/dx ratio for minimum-ionizing particles. Results are given for 1 GeV electrons in calorimeters with $1X_o$ thick Pb, Fe or Al absorber plates and 2.5 mm liquid argon or PMMA readout.

In order to be able to correct for systematic effects due to the shower profile we also computed Ar/Ar. The curves in fig. 7(a) are corrected for these effects. If the depth is increased a larger fraction of the shower consists of low-energy photons, and hence the e/mip value decreases with increasing depth. In the case of Al/LAr, where the Z of the absorber is lower than the Z of the readout medium, e/mip increases with depth. The integrated e/mip value is also > 1 in this case (fig. 5).

We also investigated the effect of the thickness of the absorber plates. The results are given in fig. 7(b). Low energy γ's from the e.m. shower development may convert by Compton or photoelectric effect into an electron sufficiently close to the surface of an absorber plate for the electron to escape and contribute to the measured signal. The calorimeter signal can be expected to increase if the absorber plates are

being made thinner, since the fraction of such processes will increase. Fig. 7(b) indeed shows this effect, but for plates thicker than ~ 3 mm it plays appparently no role anymore, since the e/mip value stays constant.

Summarizing, we conclude that the calorimeter response to high-energy electron and photon showers sensitively depends on the Z-values of the active and passive layers. This is due to the way in which low-energy γ's from these showers interact with matter. In particular, for high-Z absorbers the response is considerably reduced (to ~ 60%) with respect to the equivalent mip response. This is of course an important ingredient for equalizing the calorimeter response to the e.m. and purely hadronic parts of a hadron shower (sect. 4).

3.3 Gammas from nuclear processes

In the shower development of a hadron a large number of γ's will be produced in the processes that occur at the nuclear level. In the spallation reactions caused by the fast hadrons from the shower the final state nucleus will be produced in an excited state, from which it decays to the ground state predominantly by γ-emission.

Neutrons that scatter inelastically will also excite the nuclei and hence convert their kinetic energy loss into photons (n,n'γ reactions). And in uranium fission γ's from nuclear processes, i.c. the deexcitation of the nuclei of the fission products, will be produced as well. The vast majority of all these γ's is prompt since the typical lifetime of an excited nuclear state is orders of magnitude smaller than the signal integration time of a calorimeter. Their energy spectra depend on the characteristic nuclear level structure of the nuclides involved, but in general it is true that > 90% of these γ's have an energy below 2 MeV.

In the previous subsection we saw that the calorimeter response to such γ's is very material and energy-dependent. The participation of such γ's in the shower development of high-energy electrons is largely responsible for the e/mip ratio being different from 1. We investigated with EGS4 the response to such γ's for various calorimeters as a function of energy, in the same way as described for the e^+ annihilation γ in the previous subsection. The results are given in fig. 8, where the

signal is given as a fraction of the equivalent mip response. The calorimeters appear to be very inefficient for nuclear γ-rays, particularly at low energies (fig. 8(a)) and for high-Z absorbers (fig. 8(b)). Since the results are very much energy-dependent we also investigated the response to a typical spectrum of γ's from ^{238}U fission taken from ref. [17]. It turns out that the signal is only 40% of the equivalent mip signal (fig. 8(b)). The γ/mip ratio turned out to vary in the same way with the thickness of the absorber plates as the e/mip ratio (fig. 7(b)). These data are essential for estimating the amplification of the purely hadronic signal due to nuclear γ-detection.

4. THE PURELY HADRONIC PART OF THE SHOWER

We now turn to the calorimeter signal for the purely hadronic part of the shower, or to be more precise the signal resulting from the energy deposited in another form than e.m. showers generated at the particle level, e.g. π^o and η decay (E_h).

In the previous section we saw that understanding of the calorimeter response to e.m. showers requires insight in the processes occurring in the last stages of the shower development. The same is true for hadronic showers. However, because of the wide variety of processes that may occur at all stages of the shower development, the description of these showers, and the calculation of the resulting calorimeter response are considerably more complex.

4.1 Spallation

If an incoming high-energy hadron strikes an atomic nucleus the most likely process to occur is spallation. In this process two stages have to be distinguished: a fast intranuclear cascade followed by a slower evaporation step, which also may involve nuclear fission for heavy elements. The incoming particle makes quasifree collisions with nucleons within the nucleus. The nucleons struck in this way obtain enough energy themselves to travel through the nucleus and to hit other nucleons. In this way a cascade of fast nucleons develops. In this stage, also pions and other hadrons may be created if the energy transferred is sufficiently high.

Some of the particles taking part in this cascade reach the nuclear boundary and escape. Others get caught and distribute their kinetic energy among the remaining nucleons in the nucleus.

The second step of the spallation reaction consists of a deexcitation of the resulting intermediate nucleus. This is achieved by evaporating a certain number of particles, mainly free nucleons, until the excitation energy is less than the binding energy of one nucleon. The remaining energy, typically a few MeV, is emitted in the form of γ-rays. For heavy elements, the excited intermediate nucleus can also fission (subsect. 4.2).

A lot of experimental information on spallation reactions has been accumulated during the last decades. Rudstam [18] has given an empirical formula, valid within broad limits either of energies (> 50 MeV) or of mass numbers (A > 20), which gives a satisfactory description of spallation cross sections. When a particle of energy E hits a target with mass number A_T the relative cross sections σ for producing spallation products (Z_f, A_f) are given by the relation

$$\sigma(Z_f,A_f) \sim \exp\,[-P(A_T-A_f)] \times \exp\,[-R|Z_f-SA_f + TA_f^2|^{3/2}]\ , \qquad (2)$$

where $P = 20E^{-0.77}$ for E (in MeV) $\leq$ 2100 MeV,

$P = 0.056$ for E > 2100 MeV,

$R = 11.8A_f^{-0.45}$,

$S = 0.486$,

$T = 0.00038$.

Fig. 9 shows the cross sections for nuclides that can be produced from ^{238}U spallation induced by a 2 GeV hadron, computed with this formula. Hundreds of different reactions occur with comparable probabilities. The largest cross section for an exclusive reaction amounts only to ~ 2% of the total spallation cross section, and there are ~ 300 different reactions that contribute > 0.1% to the total spallation cross section. We wrote a Monte-Carlo program, that first computes all the relevant spallation cross sections for the energy of the incoming particle considered, and then generates events with a probability distribution obeying these cross sections. The binding energies for all known nuclides from the periodic table, taken from ref. [19], were put into a data base for this

program. Figs 10 and 11 show some results of this exercise, which are relevant for our study. In fig. 10(a), the distribution of the binding energy loss, per interaction of a 1 GeV hadron, is given. On an average, 90 MeV is lost, but the fluctuations about this number are huge. The $\sigma_{r.m.s.}$ of the distribution is ~ 70% of the mean value. This last feature is almost energy-independent. Fig. 10(b) shows the distribution of the number of neutrons emitted in the spallation reactions induced by 1 GeV hadrons. On an average, 12 neutrons are released, and the fluctuations about this number are similar to the ones seen in the binding energy loss. Fig. 11 shows the energy dependence. In fig. 11(a), the average fraction of the incoming energy spent on binding energy losses is given, together with the $\pm$ 1 $\sigma_{r.m.s.}$ boundaries of the distributions. Fig. 11(b) shows the average numbers of protons and neutrons released, as a function of the energy of the incoming particle. It turns out that, below 200 MeV, the probability of at least one proton being emitted drops below 50%. On an average, still ~ 6 neutrons come off at this energy. This indicates that the protons that are produced in spallation processes in very heavy nuclei are almost exclusively produced in the fast cascade step. This is not amazing, since the Coulomb barrier for protons in uranium is ~ 14 MeV; therefore, in the evaporation stage where fragments are released with a kinetic energy of typically a few MeV (some fraction of the binding energy per nucleon), one does not expect to find many charged particles coming out. The Coulomb barrier for α-particles or heavier nucleon aggregates is a multiple of the 14 MeV mentioned for protons. Although production of such light nuclei from the cascade step will play a role at some level in the first generations of collisions in a high-energy hadron shower, it is probably limited for the shower as a whole, where most of the spallation reactions are caused by particles below ~ 100 MeV. In the calculations mentioned here the production of nucleon aggregates is neglected and therefore the curves from figs 10 and 11 are, strictly speaking, upper limits for the number of particles produced and lower limits for the binding energy lost.

In the fast cascade step, protons and neutrons will be emitted in a ratio that, on an average, corresponds to the one for the presence of these nucleons in the target nucleus. The same is true for the energy carried away by protons and neutrons. This means that, on an average, for high-energy hadron-induced spallation reactions, neglecting the energy

carried away by evaporation neutrons, protons take 92/146 = 63% of the energy carried by neutrons in reactions on uranium, 65% for lead and 87% for iron.

These considerations also allow to split the total neutron production in spallation reactions into a cascade fraction and an evaporation fraction (fig. 11(b)).

The evaporation neutrons will be isotropically emitted, the escaping cascade particles will have a dominating momentum component along the direction of the incoming particle. Therefore, the residual target nucleus will undergo a net recoil; the energy taken by the nucleus depends on the nucleon multiplicity, and may therefore rise up to ~ 5%, on an average at ~ 2 GeV (fig. 11(a)). Beyond that energy, pion production becomes important and because of the small pion mass the fraction of the energy spent on target recoil, will diminish. The fluctuations about the average value are in this case even larger than for binding energy losses, since the angular distribution of the emitted particles will also play a role. Target recoil will, in general, not contribute to the measurable calorimeter signal at any significant level and therefore, has to be considered as lost energy.

The calorimeter signal for a hadron shower is primarily the result of the ionization by protons and pions produced in this process. As will be shown later, in particular non-relativistic protons give a dominating contribution. Fig. 12 gives the average amount of energy released by ionization before a proton interacts, as a function of the proton energy. The fraction of the initial energy that goes into ionization is given too. These curves were computed using the dE/dx tables from ref. [10], by numerically integrating the product of the interaction probability and the remaining proton energy, in steps of 10^{-3} nuclear interaction lengths, up to the point where the remaining kinetic energy is 0, the proton range. Fig. 12 shows that minimum-ionizing hadrons lose, on an average, 220 MeV before interacting and that below 150 MeV, more than 90% of the protons lose their energy by ionization alone; they reach the range without causing any nuclear interaction. The calorimeter signal for such low-energy hadrons will be similar to the one for muons of the same kinetic

energy. Since no losses occur, the signal per unit of energy is considerably larger than for high-energy hadrons. From fig. 12 one may get an impression concerning the energy at which this alinearity in the response to hadrons will start to occur. If $e/\mu = 0.6$ and $e/h = 1.0$ (uranium), the deviation from linearity will be ~ 5% at 2 GeV, ~ 15% at 1 GeV and ~ 35% at 0.5 GeV, which is approximately in agreement with experimental observations [13].

The curves from figs 11 and 12 make it possible to get a feeling as to how an "average" purely hadronic shower could develop. Let us consider as an example a 5 GeV proton that enters a uranium calorimeter. Let us assume that in the first collision a π^+ and a π^- with an energy of 1.2 GeV each are created. According to the averages from figs 11 and 12 the shower develops as shown in table 1.

Before interacting, the proton loses 240 MeV by ionization. After subtracting the 2.4 GeV going into pions, 2360 MeV remains for the nuclear part of the interaction, to be shared amongst cascade nucleons, evaporation neutrons, γ's, binding energy and target recoil. Fig. 11 tells us that, on an average, 8 evaporation neutrons and 10 cascade nucleons will be produced. Binding energy and target recoil take away 120 and 150 MeV, respectively, the evaporation neutrons and γ's will consume ~ 30 MeV. The remaining 2060 MeV is to be shared amongst the 10 cascade nucleons. A fraction 92/238 = 38.7% of this goes into protons, yielding 4 protons with a total kinetic energy of 790 MeV. Six neutrons will take care of the remaining 1270 MeV, for example in the way proposed in the table.

In the following lines of the table the spallation caused by some of the particles (the underlined ones) produced in the first interaction is analyzed in a similar way, taking energy fractions and particle multiplicities from figs 11 and 12. The same is done for some particles created in the second generation of interactions. We have only written down the spallation reactions for those particles which are relevant for the production of ionizing particles and, therefore, will contribute to the calorimeter signal. What is left after these reactions have taken place, are protons which are so soft that they will lose practically all their energy by ionization, and neutrons which will not produce any more new protons at a level that is significant for the calorimeter signal. They will continue

to produce reactions, yielding new, softer neutrons and increased binding energy losses. The fraction of the initial energy spent on ionization in this example can, therefore, be found by summing up all the italic numbers. The result is 44%. About 80% of the signal is due to protons, and only 20% to pions. One also can make a sort of shower profile for the event in this example, since the ionization by the incoming particle is likely to be produced between 0 and 1 nuclear interaction lengths (λ), the pions will ionize the medium between 1λ and 2λ, etc. The maximum of the energy deposit occurs somewhere between 1λ and 2λ.

Although the event in this example is only one amongst an infinite number of possibilites, it makes some interesting conclusions possible:

(a) Protons from spallation reactions are more important for the hadronic calorimeter signal than charged pions. This is a consequence of the multiplicities involved. The two pions assumed for the 5 GeV interaction in our example will, as an average, not be far away from reality. The conclusion also holds for much higher energies. Let us consider as an extreme case a 50 GeV hadron that produces in its first interaction ten charged pions of 5 GeV each, and transfers no energy to the target nucleus. These pions will all together lose $10 \times 0.24 = 2.4$ GeV before interacting and their interactions will, on an average, be reasonably described by the example given earlier. The 2.4 GeV lost by the pions represents less than 5% of the initial particle energy and hence does not modify our conclusion. As in the case of the e.m. showers, the hadronic calorimeter signal is predominantly determined by processes that occur in the late stages of the shower development, where pion production plays a very modest role indeed.

(b) The fraction of the initial particle energy that goes into ionization by protons, and hence the hadronic calorimeter signal, depends on the Z and A-values of the absorber medium. First, the cascade protons take a fraction Z/A of the available energy transferred to the nucleus. The value of Z/A in iron is, for example, 20% larger than in uranium. These 20% will apply to each next generation of interactions caused by the cascade nucleons and therefore, will have a cumulative effect on the calorimeter signal that is even larger.

Secondly, the Coulomb barrier for escaping charged particles is determined by $ZA^{-1/3}$. In iron, where the Coulomb barrier for protons is only 5 MeV, proton emission in the evaporation stage is likely to play a non-negligible role. The consequence of both phenomena is that in high-Z materials a smaller fraction of the hadronic energy is spent on ionization and a larger fraction is going into neutron production than in low-Z absorber materials.

Since protons from spallation reactions are apparently a very important component for the hadronic calorimeter signal, the calorimeter response to those predominantly non-relativistic particles deserves a separate study. The signal ratio spallation proton/mip (p/mip) may deviate from 1 because of the following effects:

(i) The range of low-energy protons in calorimeter absorber materials is limited. The frequently used 3 mm thick uranium plates are sufficient to stop perpendicularly entering 40 MeV protons. Therefore, at the low-energy side of the proton spectrum sampling inefficiencies that will tend to reduce the p/mip value will play a role.

(ii) The ratio $(dE/dx)_{readout}/(dE/dx)_{absorber}$, a measure for the calorimeter signal, can be very different from the mip value for non-relativistic particles. The magnitude of this effect depends on the material combination and may be quite substantial. This is shown in fig. 13(a), where this ratio is given as a function of the proton energy for various calorimeters. Especially for U and Pb calorimeters the p/mip ratio may considerably increase due to this effect.

(iii) Saturation or recombination effects in the readout material may occur for densily ionizing low-energy spallation protons. This effect will decrease the p/mip signal ratio, and depends sensitively on the properties of the readout material. It is practically absent in case of silicon readout, but may be quite important for plastic scintillator and liquid argon.

(iv) Multiple scattering of very soft protons will decrease the p/mip ratio, for calorimeters with high-Z absorber material.

The combined effect of all these phenomena was investigated with a Monte-Carlo technique. Spallation protons were generated at a random depth inside an absorber plate of a given calorimeter and transported through the structure, with a step length chosen such that ~ 0.1 MeV is lost.

For the dE/dx and multiple scattering data the tables of ref. [10] were used. Birk's law was used to treat saturation or recombination effects (see subsect. 4.3 for details about this point). Results are given in fig. 13. Fig. 13(b) shows the p/mip ratio as a function of the energy of the spallation protons for 3 mm U/2.5 mm PMMA calorimeters. The upper curve shows the energy deposit in the active layers. The effect of proton absorption inside the layer where it is produced, clearly appears below 50 MeV. The lower curve shows the actual signal, obtained by including the saturation effects in the light production by the stopping protons, relative to minimum-ionizing particles. As expected, the p/mip signal ratio is strongly energy-dependent. In fig. 13(c), this ratio is given for protons distributed according to an exponentially decreasing energy spectrum. The abcissa gives the average energy of the protons, which is directly related to the average number of spallation protons produced per unit energy. Due to the saturation and absorption effects the p/mip ratio decreases if the proton spectrum gets softer. In practice, the average number of protons per GeV will be 3-4 (fig. 11(b) and table 1), which leads to a final p/mip ratio of ~ 0.94 for this type of calorimeter.

Fig. 13(d) shows the influence of the plate thicknesses on the results (note the blown-up vertical scale). The p/mip signal ratio does not change very much if the thickness of the absorber plates is varied within practical limits, but the thickness of the plastic plates clearly plays an important role. The p/mip ratio decreases considerably with increasing scintillator plate thickness, presumably since an increasing fraction of the protons will stop inside the active layers and hence produce relatively little light compared to the amount of energy deposited.

All these results concern U/PMMA calorimeters. Similar calculations were performed for many other devices. The resulting p/mip signal ratios are summarized in table 2. We assumed that four protons were produced per GeV hadronic energy. Apart from silicon, whose response is not saturating for the low-energy protons considered here, the net result of all the

mentioned effects is that the calorimeter signal for spallation protons is reduced compared to minimum-ionizing particles. This reduction is larger if the kB value of the medium (a measure for the saturation properties) is increased. A thin readout and a large Z-value of the absorber medium increase the relative calorimeter response.

The fact that the silicon response does not saturate for low-energy protons may be quite interesting for hadron calorimetry. Table 2 shows that due to this effect, the hadronic signal may be up to ~ 20% larger, and hence the e/h ratio correspondingly smaller compared to other (saturating) readout materials.

We now return to our 5 GeV event example (table 1). As we have seen, 44% of the energy goes into ionization by charged particles, 4% into target recoil and a few percent into γ's. The remaining 50% is shared between kinetic neutron energy and binding energy losses. The cascade neutrons that are not further followed in the example will undergo reactions of the type (n,xn) until their energy is too low for these processes, each time liberating a certain amount of binding energy and creating some evaporation neutrons. The sharing of the 50% amongst kinetic neutron energy and nuclear binding energy is, therefore, governed by the ratio of the typical kinetic energy of an evaporation neutron and the average binding energy of the last say 20-30 nucleons in the absorber nucleus. The evaporation neutrons are usually assumed to have a thermal or Maxwellian energy spectrum,

$$N(E) \sim \sqrt{E} \exp(-E/T),$$

with a temperature T ~ 2 MeV, yielding an average kinetic energy of ~ 3 MeV per neutron. The average binding energy of the last nucleons amounts to ~ 6.4 MeV in uranium, 7.6 MeV in lead and 10.5 MeV in iron. Therefore, of the total available amount for binding energy + kinetic neutron energy ~ 32%, 28% and 22% will go into the latter component for uranium, lead and iron, respectively. So in our 5 GeV event example ~ 16% of the total energy will be spent on kinetic energy for neutrons, and 35% will get lost to liberate binding energy.

The purpose of the described example is to show where the energy in a hadronic shower is going, which processes are important for the formation

of the calorimeter signal, and how the choice of materials influences the energy sharing and, in particular, the energy components that will determine the calorimeter signal. It will be clear that a precise quantitative evaluation requires a very sophisticated Monte-Carlo program, that takes into account all the details that were outlined above. Gabriel [20] has done this with his HETC code. He has simulated 5 GeV proton showers in uranium, lead and iron calorimeters. The results on the mean energy sharing amongst the various components of the purely hadronic part of the showers are given in table 3.

These numbers nicely confirm the tendencies described above. The fraction of the energy deposited by ionization decreases with increasing Z (or rather decreasing Z/A), and the ratio kinetic energy neutrons/binding energy loss increases with Z. Moreover, the absolute numbers are in good agreement with the ones derived from our "average event" example. His calculations also confirm our conclusion that a dominating part of the energy deposited in the form of ionization comes from spallation protons (70-75%).

In the following calculations on signal equalization and energy resolution, we will use the numbers from table 3 as a starting point. Before going into these calculations, however, we will first discuss one other point, the role of nuclear fission in ^{238}U.

4.2 Nuclear fission

If we want to investigate the role of nuclear fission, we have to distinguish between two stages in the shower development:

(a) Fission as part of the spallation reactions, induced by fast particles (protons, neutrons, pions).

(b) Fission as part of the energy loss mechanism of the abundantly produced slow (few MeV) neutrons.

In the previous section we already mentioned that for spallation reactions on the heaviest known elements, the intermediate nucleus that remains after the fast cascade nucleons have escaped, might fission rather than decay through neutron evaporation and γ-emission. Also a combination

of both processes, i.e. emission of some evaporation neutrons followed by fission is possible. The fission probability is very sensitively dependent on the Z^2/A value of the intermediate nucleus [21] and, therefore, on the number and type of nucleons that escaped in the fast cascade step. On an average, more nucleons will escape if the energy increases, and the ratio of the numbers of escaping protons and neutrons will be the same as in the struck nucleus. Therefore, the Z^2/A value of the resulting intermediate nucleus will, on an average, decrease with increasing energy, and so will the fission probability. We recently measured the fission probability in 591 MeV p-^{238}U collisions to be 48 ± 6% [6]. In particular, spallation reactions of the type (p,xn) will contribute to this. Each emitted proton in reactions of the type (p,xpyn) requires at least four accompanying neutrons to keep the Z^2/A value the same as for ^{238}U. For high-energy showers in uranium, (n,xn) reactions that are the main processes occurring at $E_n \lesssim 200$ MeV (fig. 11(b)) will be frequently accompanied by nuclear fission.

In a ^{238}U fission a lot of energy is liberated, ~ 200 MeV. However, ~ 90% of this energy is going into recoil of the fission fragments and will, because of the extremely small range of these fragments (typically 10 mg/cm^2), virtually not contribute to the measured signal in practical calorimeters. The remaining energy is used to produce evaporation neutrons and γ's that deexcite the states in which the fission fragments are produced.

Fission processes at this stage of the shower development compete with the normal deexcitation mechanism of the intermediate nucleus to the ground state of a spallation reaction product. The only difference is that there are two (or exceptionally three) final state nuclei in the case of fission. The particles that eventually might contribute to the measurable calorimeter signal are of the same nature in both cases: soft evaporation neutrons and γ's.

The fact that there are two nuclei to be deexcited if fission takes place, does not at all mean that the average evaporation neutron multiplicity and the amount of energy carried by these particles doubles with respect to single intermediate spallation nucleus decay. First, the average binding energy of the evaporating nucleons is, on an average, smaller for

intermediate spallation nuclei which are candidate for fission (mainly U, Pa or Th isotopes) than for fission products. This means that if both types of nuclei were to be excited to the same energy, say 30 MeV, the number of evaporation neutrons would be smaller for fission products. On the other hand, the average energy going into γ's (the last step of the deexcitation) is larger. Secondly, the excitation energy of the nuclear fission fragments is in general considerably smaller than for the intermediate spallation nucleus, which will also lead to a smaller evaporation neutron multiplicity.

This can be concluded from the fact that the Maxwell temperature T of the fission neutrons is lower than for evaporation neutrons from spallation reactions. Typical values for ^{238}U are 1.3-1.5 MeV for fission neutrons and ~ 2 MeV for spallation neutrons [17,21]. Therefore, not only the average multiplicity of neutrons emitted by a fission fragment will be lower than for an intermediate spallation nucleus, but also the average kinetic energy per nucleon ($\bar{E} = 3/2\ T_{Maxwell}$).

Experimental data on ^{238}U fission show that the average number of neutrons produced by both fragments together is small, typically $\lesssim 4$ [17]. Fig. 11(b) shows that by evaporation of the intermediate spallation nucleus, 2-8 neutrons will be produced, depending on the energy transferred to the uranium nucleus.

All these considerations lead to the conclusion that the effects of nuclear fission in the spallation stage of the hadronic shower development are probably rather limited. The total energy carried by slow neutrons will increase somewhat, and their spectrum will be a bit softer, but it is unlikely that these effects exceed ~ 20%. The energy carried by soft γ's might double with respect to the situation in which nuclear fission would be switched off, but compared to the total kinetic energy of the neutrons this is a small effect too.

The numbers given by Gabriel (table 3) support this conclusion. Nuclear fission by fast particles was included in his calculations. The fraction of the total energy carried by slow neutrons is only slightly larger in ^{238}U than in lead (15% versus 12%). Fission γ's produced in this stage make up for ~ 3% of the initial particle energy, according to him.

Nuclear fission disturbs the energy balance, the total amount of energy deposited in one form or another being larger than the energy carried by the incoming particle. Therefore, the fraction used for binding energy losses in uranium (table 3) is given in brackets: it is 100% minus the rest, and therefore does not take into account the enormous amount of binding energy liberated in nuclear fission.

The main problem of treating the role of fission in spallation reactions in a more quantitative manner is the absence of experimental data. This is totally different as soon as the neutron energy drops below ~ 20 MeV. The cross sections for the various reactions that may occur are there very precisely known (fig. 14(a)). Therefore, one can easily find out how neutrons of a given energy will lose their energy in a series of interactions before they finally get absorbed. One sees that beyond 6.2 MeV, the binding energy of the last neutron, nuclear reactions of the type (n,xn) still occur, eventually accompanied by fission of the uranium nucleus. Below this energy, where the majority of the evaporation neutrons will be produced, the number of processes becomes very limited. The neutrons can be scattered either elastically or inelastically or get absorbed either by being captured (only important below ~ 0.1 MeV) or by fissioning a uranium nucleus. In the latter case, the relative gains are very important. A 2 MeV neutron that induces ^{238}U fission creates, on an average, 2.5 new neutrons of about the same energy, plus 7.4 MeV in the form of prompt γ-rays. These new fission neutrons might themselves induce nuclear fission as well, so that potentially, an important amplification of the amount of energy deposited in the form of kinetic neutron energy and soft γ's may occur. The extent of this will sensitively depend on the competition offered by other mechanisms through which the slow neutrons may lose energy. Once the neutron energy drops below ~ 1.2 MeV, nuclear fission ceases to play a role (fig. 14(a)). In uranium calorimeters this competition does not only come from elastic and inelastic neutron scattering off uranium nuclei, but also from processes in the readout material. In particular, the presence of free protons in this material is of crucial importance. We have shown experimentally that the number of fissions per unit energy drops considerably if plastic scintillator plates are inserted in between the uranium plates, and that the neutrons are thermalized much faster in this case [6]. Such effects were not observed if iron plates (simulating liquid argon readout) were used instead of

plastic. Fig. 14(b) shows the cross section for elastic neutron scattering by free protons. The neutrons lose half of their energy in this process, against only half of a percent for elastic scattering off uranium nuclei. Below ~ 3 MeV the cross section for n-p scattering also becomes larger than the one for inelastic scattering by uranium. Therefore, the presence of a significant fraction of free protons in the uranium calorimeter stack will crucially influence the way neutrons lose their energy and the role played by nuclear fission in this process.

4.3 The calorimeter response to neutrons

We would now like to answer the following question. Consider a purely hadronic shower, i.e. a shower in which no π^o's are produced. How large is the signal of a given calorimeter in which the shower is fully contained relative to an equivalent minimum-ionizing particle, and hence what is the signal ratio e/h?

In the previous sections we saw that there are three components in such a shower that may contribute to the measurable calorimeter signal:

(a) Ionizing particles. We saw that a fraction f_{ion} of the energy is deposited in the form of ionization, which varies from 38% for uranium to 57% for iron (table 3). The effects of the dominating spallation proton component on the calorimeter signal were discussed in subsect. 4.1.

(b) Gamma rays, a fraction f_γ of the energy of the incoming particle.

(c) Soft neutrons, at a fraction f_n.

Relating all calorimeter responses to minimum-ionizing particles one can write:

$$e/h = \frac{e/mip}{f_{ion} \cdot ion/mip + f_n \cdot n/mip + f_\gamma \cdot \gamma/mip} \quad . \tag{3}$$

Curves for e/mip were given in fig. 5. The ion/mip values can be found from tables 2 and 3. About 70-75% of the ionization is due to spallation protons (table 3), for which the calorimeter response relative to mip's is given in table 2; the rest comes from pions which we assume to be minimum-ionizing particles. If the efficiency for detecting nuclear

γ-rays and soft neutrons were to be zero, e/h values between 1.3 (U-Si) and 1.8 (Fe-plastic) would be found for the configurations from table 2.

In subsect. 3.3 we showed that in particular calorimeters with high-Z absorbers are very inefficient in detecting nuclear γ's, i.e. the signal ratio γ/mip is considerably less than 1 (fig. 8(b)). Therefore, it would need huge values of f_γ to bring e/h close to 1. In this section we concentrate on the signal ratio n/mip.

We first investigated in detail in which form the neutrons deposit their kinetic energy before they are finally captured, for calorimeters of a given composition, and for neutrons from 0-20 MeV. We used the cross sections from ref. [22] for this purpose. Examples of these cross sections are given in fig. 14, for ^{238}U and hydrogen. Other elements that we used were carbon and oxygen (components of plastic scintillator), silicon, argon, iron and lead. For a neutron at a given energy an interaction was selected according to a probability distribution defined by the product of cross section and nuclear abundance. The neutron loses a certain fraction of its energy in some form, both dependent on the selected process. The procedure was repeated for the lower-energy neutron until the selected process turned out to be neutron capture.

If the selected process was fission, the neutron was given a weight equal to the multiplicity of fission neutrons (ranging from 2.5-5.2) for the incoming energy E_n, and its new energy was selected according to a distribution $\sqrt{E}\ \exp(-E/T)$, with $T = 1.3 + 0.012 \times E_n$ [17]. Energy deposit in the subsequent processes was multiplied by the weight factor.

If the selected process was elastic scattering, a fraction $1/(A+1)$ of the neutron energy was transferred into target recoil, A being the mass number of the hit nucleus.

In inelastic scattering the neutron brings the nucleus into an excited state from which it decays by γ-emission. The neutron loses some fraction f of its energy in this event. The question is what value of f to use. In principle, the neutron may bring the nucleus into any of the possible excited states that requires less than the neutron's kinetic energy. The probability distribution depends strongly on nuclear physics

details. On the one hand, one may say that since the level density increases strongly with the excitation energy, the neutron is likely to lose a large fraction of its energy. On the other hand, if the nuclear excitation energy increases the configuration of the nucleons will, in general, be more and more different from the one in the nuclear ground state, and hence the transition will be less likely. We estimated the average f value as follows (fig. 14(a)). If the energy transfer is larger than the binding energy of the last neutron (6.2 MeV), this neutron will be released: we have a (n,2n) reaction. One sees that at ~ 9.0 MeV the probability that this neutron is released equals the probability that it is not released and hence the average value of f is 6.2/9.0 ~ 0.7. We used this value and found that our results are only marginally dependent on this choice.

If (n,2n) or (n,3n) reactions were selected binding energy gets lost. Moreover, γ-rays were assumed to be produced according to our f value. The remaining energy was divided by 2 (3) and the new neutron was given a weight factor 2 (3) that was applied to the energy deposited in all subsequent processes.

Fig. 15(a) shows some results of these calculations, for a 3 mm ^{238}U - 3 mm plastic scintillator (PMMA, chemical composition $C_5H_8O_2$) calorimeter. The figure shows in which form the energy is deposited, as a function of the energy of the starting neutron. We distinguish binding energy, γ's from inelastic scattering, fission γ's, target recoil (U,C,O) and recoil protons. The curves are given as a fraction of the energy of the starting neutron and because of fission contributions they do not add up to 100%.

Particularly interesting are the recoil protons. They are produced inside the scintillator plates. Their energy spectrum is soft, since it is especially at low neutron energies that the probability of n-p scattering becomes the dominating process (fig. 14). The energy deposited through this process is not sampled by the calorimeter. As the thickness of one scintillator plate corresponds to the range of a 17 MeV proton one may say that practically all the energy carried by the recoil protons directly contributes to the measurable calorimeter signal. Fig. 15(a) shows that a 3 MeV neutron deposits 50% of its kinetic energy in this way in this

calorimeter. For a minimum-ionizing particle this is, for this calorimeter configuration, only ~ 10%. From this one may, however, not conclude that the calorimeter <u>signal</u> is enhanced by a factor of 5 with respect to mip's. Saturation effects will, at these low energies, be extremely important. One usually uses Birks' law to describe these effects

$$\frac{dL}{dx} = \frac{dE/dx}{1 + kB \cdot dE/dx} \quad \text{or} \quad L/E = \left[\int_0^{x_{range}} (1 + kB \cdot \frac{dE}{dx})\, dx\right]^{-1} , \qquad (4)$$

where L is the amount of light produced by a particle of energy E, normalized in such a way that L/E = 1 for a mip.

The factor kB was measured to be 0.00978 ± 0.00009 g/MeV • cm^2 for this type of scintillator [23]. Fig. 15(b) shows the value of L/E as a function of the proton energy, calculated with the dE/dx values from ref. [10]. The L/E value was computed for each recoil proton produced in the previously described Monte-Carlo program for slow neutron transport. This made it possible to obtain the contribution of recoil protons to the calorimeter signal, relative to mip's of the same neutron energy. The result is given in fig. 15(c). The vertical scale is given in the same units as for fig. 15(a). One sees that the signal, on an average, is reduced by a factor of 5 due to saturation effects, and therefore is not too far away from the mip value. This is purely by accident. Had the saturation effects be very different, the result would have been very different as well. Another effect of saturation is that the signal distribution as a function of neutron energy (fig. 15(c)) is somewhat flatter than the distribution of the fractional energy deposit in the form of recoil protons (fig. 15(a)). This is due to the contribution of the > 2 MeV protons, for which saturation is less important, to the signal of the higher energy neutrons. This is a nice thing, since it means that the signal gets less dependent on the neutron energy distribution, due to saturation.

The energy deposited in the form of recoil protons is <u>not</u> sampled by the calorimeter. This means that the calorimeter response to neutrons is <u>not</u> proportional to the sampling fraction of the calorimeter, that is the ratio ΔE (readout)/[ΔE (absorber) + ΔE (readout)], where ΔE denotes the mean energy loss by a mip in one readout or absorber layer. This can be demonstrated with a simple example (fig. 15(a)). At 1 MeV, 70% of the neutron energy goes into recoil protons. If we now double the thickness

of the scintillator plates the sampling fraction, and hence the mip signal, will almost double as well. However, the neutron signal cannot double. Instead of 70% now 80% of the neutron energy goes into recoil protons. This leads immediately to one of our most important conclusions:

The neutron/mip ratio of calorimeters containing free protons in the readout medium depends on the sampling fraction.

For calorimeters with a large sampling fraction (i.e. relatively thick scintillator) the contribution of neutrons to the hadron signal will be smaller than for calorimeters with a small sampling fraction (i.e. relatively thick absorber plates). And therefore, the e/h value of the calorimeter will decrease with the sampling fraction (eq. (3)).

It is also clear that the precise magnitude of these effects sensitively depends on two factors:

(i) The fraction of free protons in the readout medium. A larger value means a larger reducing effect on e/h.

(ii) Saturation of the readout medium. Less saturation means a larger reducing effect on e/h.

The conclusions formulated above are supported by experimental data. In fig. 16 the results on e/h and energy resolution obtained from four different measurements with uranium-plastic scintillator calorimeters [3,4,24,25] are plotted as a function of the sampling fraction. The e/h value shows the expected behaviour, a decrease with decreasing sampling fraction. For the energy resolution we took the non-sampling component, i.e. the part that remains after quadratically subtracting the contribution of sampling fluctuations [13] from the total measured energy resolution. This energy resolution reaches a minimum value for e/h ~ 1.0.

Other experimental evidence comes from tests of uranium calorimeters using proportional wire chamber readout [26]. These tests revealed that the hadron signal sensitively depends on the fraction of free protons in the chamber gas. More protons means a larger hadron signal and hence a lower e/h signal ratio. The authors found that the e/h value varied from

0.6-1.4, depending on the gas mixture. A small sampling fraction and the absence of saturation effects make that the hadron signal is largely dominated by recoil protons from neutron scattering in this case.

4.4 The e/h signal ratio

The only remaining ingredient that is needed before we can proceed to e/h calculations is the energy spectrum of the neutrons below 20 MeV. This spectrum contains two components. Firstly, there is the soft component consisting of evaporation and (in the case of uranium) fission neutrons. Secondly, there are the low-energy (< 20 MeV) cascade neutrons. We used Maxwell distributions to describe the energy spectra of both components: $N(E) \sim \sqrt{E}\ \exp(-E/T) = F_M(E,T)$. The Maxwell temperatures were chosen 1.5 and 6 MeV, for the first and second component, respectively. So the input spectrum for our soft neutron transport Monte-Carlo was as follows: $N(E) \sim F_M(E,1.5) + xF_M(E,6)$, where x was taken 0.1 for uranium and 0.3 for non-fissioning materials. This in order to account for the fact that the first term is relatively more important for uranium because of the contribution of fission neutrons created in spallation reactions. The average neutron energy amounted to 4.3 MeV for uranium and 5.6 MeV for non-fissioning materials. It turned out that the results on the neutron signal are only very weakly dependent on the parameter choice, as long as the parameters stay within reasonable limits. For example, the n/mip ratio changes by less than 3% if the neutron spectrum of lead is used for uranium. We found a nice way to check the validity of our assumptions, since the proposed neutron spectra, together with the total kinetic energy carried by these neutrons (table 3) make it possible to calculate the number of fissions per GeV and the number of neutron captures per GeV, and to compare these to experimental results [6]. This comparison is shown in table 4. It turns out that the experimental data are remarkably well described. The difference in neutron multiplicity between uranium and lead, the effect of the scintillator on the number of fissions, the fraction of neutrons inducing fission in uranium and lead/uranium calorimeters are all nicely reproduced. Moreover, the experimentally observed differences in the spatial distribution of captured neutrons [6] are qualitatively explained, since a neutron has to undergo 2-3 times as many interaction processes before being captured if no free protons are present in the readout medium.

These results are rather sensitive to the choice of the neutron spectrum. We think that the agreement with the experimental data can still be further improved, especially if also fissions caused by neutrons beyond 20 MeV are taken into account. But since the effect of this fine-tuning on the neutron signal is anyway marginal, and because of the computer time involved, we considered this result sufficiently satisfactory.

In the previous section we showed that the signal from recoil protons sensitively depends on the sampling fraction of the calorimeter. A more practical variable for calorimeters, however, is the ratio of the thicknesses of absorber and readout material, R_d, which is to first order inversely proportional to the sampling fraction. A large value of R_d means a small sampling fraction and hence a relatively large contribution of recoil protons to the calorimeter signal. We will present our results on n/mip signal ratios and e/h values as a function of R_d. Apart from the factors mentioned in the previous section, i.e. the fraction of free protons and saturation effects, also the density ratio of the absorber and readout materials will therefore affect the results. Materials with the same fraction of free protons and the same kB value, but with different densities, will yield different results for a given value of R_d.

Fig. 17(a) shows the signal ratio neutron/mip split up in its various contributions, as a function of R_d, for uranium/PMMA calorimeters. We distinguish between recoil protons, excitation and fission γ's and γ's released in thermal neutron capture. The recoil proton component rises sharply with increasing R_d for reasons that were discussed in the previous section. The contribution of excitation and fission γ's also increases, but only to the extent that a larger fraction of the neutron energy is deposited in the form of excitation γ's and more fissions occur if R_d increases. A signal ratio γ/mip of 0.37 (fig. (8b)) was assumed for the detection of these γ's.

An interesting contribution comes from the capture γ's. When the neutrons have lost practically all of their kinetic energy, they are captured by ^{238}U nuclei, transforming those into ^{239}U. In this process 4.8 MeV, being the difference in binding energy between ^{239}U and ^{238}U is released in the form of γ-rays. Especially in uranium, there is a large

amount of energy involved in this process, since the number of neutrons is very large, ~ 40-50 times 4.8 MeV, i.e. ~ 200-250 MeV/GeV. The curve for capture γ's in fig. 17(a) assumes that all this energy is released in the detector, with a γ/mip ratio of 0.37, as for the other γ's. However, neutron capture is a relatively slow process. The neutrons travel a long distance, mostly at keV energies before finally being captured (table 4). According to Brückmann [27] it takes ~ 1 μs before they are all captured. In 100 ns, which is a typical signal integration time for calorimeters employing scintillator readout, only ~ 25% of the neutrons would be captured, according to his calculations. Moreover, some fraction of the neutrons will always escape from the front face of the detector. This fraction can be estimated to be 10-20% [6] and, therefore, is it rather likely that only ~ 20% of the γ's from neutron capture contribute to the calorimeter signal of scintillator calorimeters.

Fig. 17(b) shows the total hadronic signal, as a function of R_d, for U/PMMA calorimeters. Due to the increased contribution of neutron detection, this signal rises with R_d. Beyond $R_d = 3$, neutrons even form the largest contribution to the hadron signal. It turns out that detection of all the capture γ's makes up for 10-15% of the hadronic signal. This in is agreement with experimental findings. Brückmann and Kowalski [28] measured the electron and pion response of a uranium/scintillator calorimeter as a function of the gate width, ranging from 50-600 nsec. The e/h ratio decreased by ~ 7% over this range, due to this effect.

So finally, we have all the ingredients to compute e/h ratios. According to formula (3) seven numbers are needed:

(a) e/mip — The value depends on the Z of the absorber and (to a less extent for the cases considered here) on the readout (fig. 5). The value is constant, except for thin absorber plates (fig. 7(b)).

(b) f_{ion} — A constant determined by the Z of the absorber (table 3).

(c) ion/mip — The value does practically not change with the thickness of the absorber plates, but decreases with the thickness of the active layers (fig. 13(d)). The values of table 2 were used for the calculations.

(d) f_n A constant determined by the Z of the absorber (table 3).

(e) n/mip Strongly dependent on the properties of the readout medium and varying with the ratio of the thicknesses of passive and active layers, in case the latter contain free protons (fig. 17(a)). For the fraction of the kinetic neutron energy released in the form of γ's the γ/mip signal ratio applies. The value also depends on the gate width of the detector.

(f) f_γ A constant determined by the Z of the absorber (table 3). In case of uranium, 3% has to be added to account for fission γ's produced by particles faster than 20 MeV (subsect. 4.2).

(g) γ/mip The value depends on the Z of the absorber and readout media (fig. 8(b)), and is taken constant except for very thin absorber plates (fig. 7(b)).

The results for a particular combination of materials will, therefore, depend on the thickness of the passive layers (e/mip,γ/mip), on the thickness of the active layers (ion/mip), and on the ratio of both thicknesses R_d (n/mip). The results on the e/h ratios will be shown as a function of R_d fixing the thickness of the active layers to a practical value. The variations of e/mip and γ/mip with the thickness of the absorber plates are in this way automatically accounted for. The effect of a change in the thickness of the active layers will be shown separately.

4.4.1 Uranium

Fig. 17(c) shows the results on the e/h ratio for uranium calorimeters, with 2.5 mm PMMA readout. Three curves are given, for 0%, 20% and 100% contribution of the γ-rays from neutron capture. This is to illustrate to which extent the e/h value of a given calorimeter might eventually be influenced by changing the gate width. The e/h value turns out to be sensitively dependent on the sampling fraction, or R_d. Taking the middle curve as the most likely one of these three, one may expect the

best results on the calorimeter performance (e/h = 1) for R_d values close to 1. Detectors with a larger R_d (a smaller sampling fraction) will overcompensate, i.e. e/h < 1, a smaller R_d value will lead to undercompensation.

We investigated how sensitive the results are with respect to the various assumptions that went into the calculations. Fig. 17(c) is in fact an example of this. Other uncertainties concern the outcome of the HETC hadron shower simulations (table 3), and in particular the values for the fraction of the hadron energy spent on ionization (f_{ion}) and neutron production (f_n). Fig. 17(d) shows how the e/h results are affected by a 10% change in the adopted numbers. The effect of a 10% change in the number of spallation protons per unit energy is also shown in this figure. And finally, the effect of doubling the thickness of the readout layers is shown. It turns out that the R_d value where e/h equals 1, is rather sensitive to such changes. Differences of ~ 25% are observed between the various curves in fig. 17(d). On the other hand, the variation of e/h as a function of R_d looks very similar in all cases. Doubling the absorber thickness with respect to the optimal value leads to an e/h of 0.88 ± 0.01, tripling to 0.82 ± 0.01, etc. As a consequence, the predictions of the changes in e/h with the sampling fraction should be considered much more reliable than the absolute e/h values. One reliable experimental point will allow to accurately predict the optimal geometry.

Fig. 18 shows the e/h curves for uranium calorimeters employing different readout materials, namely two different types of plastic scintillator (PMMA and SCSN-38, a polystyrene-based material), silicon, liquid argon (LAr) and tetramethylpenthane (TMP). The scintillator curves are based on 20% capture γ detection (0.1 μs gate), for Si and liquid argon the effect of a change in gate width is illustrated by giving the results for short (20% capture γ detection) and long (80%) gates.

Experimental results are included in this graph. So far, only results obtained with plastic scintillator or liquid argon readout are known. Most authors do not give experimental error bars. We believe that those should be at least 5%. Fig. 17(b) shows how important efficient neutron detection is for the hadronic signal. Experimentally, we have shown that these neutrons can travel long distances, especially also in the lateral

directions [6]. Since most of the experimental results were obtained with test calorimeters of rather limited size, neutron leakage might play a non-negligible role leading to a systematic overestimation of the experimental e/h value.

The curves for the two types of scintillator are slightly different, because of differences in the chemical composition (fraction of free protons), the material density and the saturation effects. Although the experimental values are slightly larger than the predicted ones (which might be an experimental problem as indicated before), the agreement may be considered remarkable. In particular, the predicted trend of a decreasing e/h value with increasing R_d seems to be very well confirmed experimentally. Moreover, one might see an indication that confirms the predicted difference between PMMA and SCSN-38.

It should be stressed once more, that the uncertainties in these calculations concern details on the shower development which affect the absolute value of the vertical scale, but not the variation of e/h with R_d, nor the differences between the various readout materials.

The curves for liquid argon are practically flat for $R_d > 2$. Since, in this case, no recoil protons are contributing only the small changes in the number of fissions due to interactions in argon affect the result. Below $R_d \sim 2$ the e/h values rises due to the increasing e/mip value. The e/h value is significantly larger than 1 in all cases, which seems to be confirmed by experimental data. The difference between the e/h values for long and short gates amounts to about 15%.

The curves for silicon show the same characteristics as for liquid argon, be it that the flat plateau starts slightly beyond the right side boundary of the figure. This is because 0.4 mm silicon plates were assumed, instead of 2.5 mm for the other materials. The plateau values for e/h are 1.09 and 0.97 for a 100 ns and 1 µs gate, respectively. Thanks to the absence of saturation effects in the detection of spallation protons, signal equalization seems to be possible with silicon readout, using the gate width for fine-tuning.

A very interesting material is TMP. No experimental data exists so far. The very large fraction of free protons (chemical composition C_9H_{20}) and the low density (0.72 g/cm^3) give a large weight to the contribution of recoil protons to the calorimeter signal in this case, much larger than for the plastic scintillators discussed. Absolutely crucial for the predictions are, therefore, the saturation or rather recombination properties of this liquid. As far as we know, no measurements on the suppression of the signal from soft protons have been performed up to now. Results have been reported for α-particle detection showing that the recombination effects are dependent on the applied electric field strength. This might be interesting since the calorimeter performance could be tuned with the high voltage. Two curves are given, one assuming that the recombination effects are the same as for liquid argon (Birk's law with kB = 0.0045 g/MeV $\cdot$ cm^2), and the other one assuming that the kB value for PMMA (0.00978) has to be applied. One sees that in any case the optimal point (e/h = 1) requires a very large sampling fraction, and that for practical calorimeters overcompensation is predicted.

4.4.2 Lead

Fig. 19 shows the n/mip and e/h curves for calorimeters using lead as absorber, for the same readout materials. Fig. 19(a) shows the n/mip values as a function of R_d, for devices with a hydrogen containing readout. The contribution of recoil protons shows the same tendency as for ^{238}U; it rises with increasing R_d, be it that the absolute values are lower because of the absence of the fission neutron multiplication effect. The capture γ's deserve special interest in this case. The cross section for thermal neutron capture by lead is extremely small, 0.17 b compared to 2.7 b for ^{238}U. This means that the mean free path of a neutron, even if it is thermalized, amounts to ~ 180 cm in lead, against 8 cm in ^{238}U. Neutron capture will, therefore, play a very minor role in calorimeters with Pb absorber, unless one adds some other material with a sufficiently large cross section. Table 5 gives a list of materials that are well suited for this purpose. In particular, cadmium looks interesting, not only because one needs very little material to capture the thermalized neutrons efficiently, but also because a large amount of energy is released (9 MeV) per captured neutron. Iron is a reasonable alternative. The effect is that a larger signal is obtained from neutrons and, therefore, the e/h value gets smaller for a given R_d value.

Fig. 19(a) also shows the contribution of capture γ's to the n/mip signal ratio in case the neutrons are captured in iron or cadmium. Fig 19(b) shows the results for e/h, as a function of R_d. The thickness of the readout layers is 2.5 mm, except for Si (0.4 mm), where the horizontal scale is shifted by one decade to include practical devices. The same tendencies are observed as for uranium, be it that all curves are shifted towards larger R_d values. For both scintillator types two curves are given; one for plain lead (assuming no contribution of capture γ's), and the other one in case 20% of the neutrons are captured in cadmium, the 20% being taken for the same reason as in the ^{238}U calorimeters. A recent experimental result from a Pb-SCSN calorimeter prototype without any additives to convert thermal neutrons [29] is also included in this figure. One sees that also for Pb-scintillator calorimeters signal equalization can be achieved. The calculations predict e/h to become 1 at R_d values that are four to five times the optimal values for uranium/scintillator devices. Adding a tiny little bit of cadmium reduces these numbers by 20%.

For liquid argon and silicon three curves are given in each case. One for plain lead, the upper one, where no contribution of capture γ's is assumed; the other two curves are for lead containing a little bit of cadmium, for long (80% of the thermal neutrons convert in Cd) and short (20%) gates. Particularly for these readouts, the e/h value can be considerably improved by adding a thermal neutron converting impurity. In practical liquid argon calorimeters one will anyway have to use some other metal because of the mechanical instability of the lead plates, so one might as well use something that converts the thermal neutrons efficiently. The results for iron-coated lead are only marginally different from the cadmium-doped ones. The experimental e/h value obtained with an iron-coated Pb/LAr prototype for the SLD Experiment is nicely reproduced by these calcultions. The e/h values for Si readout are systematically ~ 8% lower than the equivalent LAr values, because of the absence of saturation in the response to spallation protons (subsect. 4.1). Values close to 1.1 seem to be achievable.

As in the case of uranium, the calculations for TMP readout were done with two different kB values. It looks as if lead is an ideal absorber for TMP. If the kB value is somewhere in between the two chosen values, the R_d for a calorimeter with e/h = 1 is in the practical range.

4.4.3 Iron

Fig. 20 shows the results for calorimeters with iron absorber, and the same readouts as before. Conversion of thermal neutrons is here no problem. The n/mip values as a function of R_d were computed as usual with the slow neutron transport Monte-Carlo. The results are given in fig. 20(a) for the hydrogen containing readout media. As in the case of lead and uranium, the contribution of recoil protons increases with R_d. Compared to lead (fig. 19(a)), the recoil proton/mip ratios are smaller. This is because the number of nuclei/cm^3 in iron is considerably larger than in lead (in fact lead is anomalously light), so that the neutrons lose a smaller fraction of their energy in collisions with protons and a larger fraction in scattering off iron nuclei. Moreover, in lead, the cross section for inelastic neutron scattering (the main competing process at low neutron energies) is considerably suppressed with respect to iron, ^{208}Pb being a very stable "double magic" nucleus. This also leads to a relative increase of the contribution of γ's to the neutron signal in iron, which effect is enhanced by the increased γ/mip signal ratio.

Fig. 20(b) shows the resulting e/h curves, as a function of R_d. The previously mentioned effect plus the relatively small fraction of energy carried by neutrons in this case make it hard to compensate for the difference between the response to the e.m. and the ionizing hadronic part, except maybe for TMP at very small sampling fractions (large R_d). Fig. 20(b) also contains some experimental points taken from ref. [2] for liquid argon and from refs [7,30,31] for iron-plastic scintillator calorimeters. The experimental scintillator points clearly show a decreasing e/h value with increasing R_d. The slope of a line drawn through the three experimental points is, however, considerably steeper than the one for our predicted curves. It suggests an intercept with the e/h = 1 line at $R_d \sim 15$. The points at R_d = 5 and 8.3 were measured by the same group (the CDHS Collaboration), so that it is not very likely that the observed phenomena are due to a completely different interpretation of the various sets of data.

This observation made us reconsider the calculations. The variation of the e/mip value as a function of the thickness of the absorber plates is given in fig. 7(b). We concluded that for plates thicker than 3 mm the e/mip value is constant, an assumption that went into all the calculations.

No calculations were done for plates thicker than 20 mm. It will, however, be clear that at some point, the e/mip value will further drop, and eventually reach zero, since the e.m. shower will be completely absorbed by the first plate, while mip's still go through. In practice, the relevant processes for the e/h ratio are the π^o showers, that start somewhere inside a plate. We ran EGS4 for high-energy e.m. showers starting at a random point inside a very thick absorber plate. It was found at the expense of very much computer time, that in this case even for very thick absorber plates the e/mip ratio did not change significantly from the values found for ~ 5 mm thick plates, provided that the starting point of the shower was homogeneously distributed inside the absorber plates. The explanation for this is that there is always an appropriate fraction of showers that start sufficiently close to the boundary to contribute to the measured signal. However, if we are talking about very thick plates, the starting point of the shower will <u>not</u> be homogeneously distributed, but decay like $\exp(-z/\lambda)$, z being the depth in the calorimeter and λ the nuclear interaction length. For π^o's created in the later generations of the shower development this will not be exactly true, but in general most of the energy going into π^o production will be spent in the first interaction for hadrons $\lesssim$ 100 GeV.

We investigated with EGS4 simulations how the calorimeter response varies for e.m. showers generated in very thick iron plates with a starting point distributed as $\exp(-z/\lambda)$. The result is given in fig. 21(a). The e/mip value clearly decreases with increasing plate thickness, with some indication that the effect gets stronger for lower energy showers. For 10 cm thick plates a 10% effect on the e/mip ratio is observed which directly translates into a 10% effect on the e/h ratio. The relevant quantity for this effect is λ, so that a similar effect may be expected for 6 cm uranium plates, whilst the thickest absorber plates which were experimentally used are only 1.5 cm thick. It is therefore fair to say that this effect does not at all modify our conclusions for uranium and lead calorimeters. For iron, however, measurements with absorber thicknesses up to 15 cm (0.9 λ) have been reported [7]. Fig. 21(b) shows how the model calculations are modified due to this effect for very thick absorber plates. Since the effect depends on the plate thickness rather than on R_d, the results are given as a function of this thickness, and e/h is predicted to become 1 for plates of ~ 11 cm.

Of course, no one would ever conceive an iron/scintillator calorimeter with 11 cm thick absorber plates with the aim to optimize the energy resolution and, therefore, this might just seem an academic exercise, since no one has ever measured the e/h ratio for such a device neither. This is, however, not true. The CDHS Collaboration have measured, five years ago, the hadronic energy resolution as a function of the energy for iron/scintillator calorimeters with 2.5, 5, 10 and 15 cm thick absorbers [7]. The results are plotted in fig. 22(a)(*). In sect. 2 it was shown that $e/h \neq 1$ causes the energy resolution not to scale as $cE^{-1/2}$, the deviation being larger if $|e/h - 1|$ is increased (fig. 3). This scaling deviation is clearly observed in fig. 22(a). The c-value for 140 GeV is 38% larger than at 50 GeV, for 2.5 cm absorbers. For 10 cm absorber plates, this difference is only 7%. The experimental points clearly cluster in this case. An additional, unpublished point at 75 GeV, was found at exactly the same c-value as for 140 GeV. For 15 cm absorber plates the points are drawn apart again.

This indicates that the e/h value is very close to 1 for the 10 cm absorber plates and that the 15 cm device, as a consequence, operated in an overcompensated mode. Additional evidence for this conclusion can be found from fig. 22(b). In this figure the energy resolution obtained after the weighting procedure which is the subject of ref. [7] is plotted as a function of the absorber thickness Δx, on a scale linear in $\sqrt{\Delta x}$. The dashed line gives the contribution of sampling fluctuations, computed with the formula given by Fabjan [13], to this resolution. The quadratic difference between the experimental values and the dashed line, which is a measure for the intrinsic energy resolution, clearly reaches a minimum near the 10 cm plates, indicating that e/h is close to 1 (cf. also fig. 16).

This excercise yields additional support for the framework on which the calculations are based, and for the conclusion that signal equalization is not a unique property of uranium. Moreover, it illustrates the statement made in sect. 2 that $e/h = 1$ is particularly important for the very high-energy showers, since the energy resolution will scale with $E^{-1/2}$

(*) I would like to thank J. Wotschack for providing me with the detailed numbers that made it possible to draw this figure.

down to the few percent level. The authors of ref. [7] measured with their 10 cm Fe/0.6 cm scintillator detector an energy resolution of 10% at 140 GeV, and in principle there is no reason why they should not have been able to measure 1% at 14 TeV with this instrument, without the need of a weighting procedure and the necessary fine-grained longitudinal readout.

Summarizing this section we conclude that the calorimeter response to the purely hadronic part of hadron showers can be tuned and be made equal to the signal of an e.m. shower by making an appropriate use of the neutrons that are abundantly produced in high-Z absorber materials. Essential for this is the presence of free protons in the readout medium. Elastic neutron scattering off such protons becomes, in that case, a dominant mechanism and since the energy deposited in this way is not sampled like for minimum-ionizing particles the contribution of this process to the calorimeter signal sensitively depends on the sampling fraction. Details of the calorimeter response to neutrons depend on the chemical composition of both absorber and readout materials, on saturation effects and on the material densities. The e/h value can be tuned using the sampling fraction and, to a less extent the signal integration time, as parameters. Signal equalization, or compensation does not seem to be property unique to ^{238}U; lead and of course other materials in the same Z-range that unfortunately are less available (Au, Pt, W) offer possibilities as well. There are experimental indications that even iron calorimeters can be made (over) compensating.

5. THE ENERGY RESOLUTION OF HADRON CALORIMETERS

After having discussed in detail the e/h signal ratio and the factors that determine its value we now return to the aim of this paper, i.e. trying to understand the energy resolution of hadron calorimeters, and the factors that limit their performance in this respect. The energy resolution of a hadron calorimeter is determined by four factors:

(a) Sampling fluctuations, for devices that consist of separate absorber and readout layers.

(b) Deviations from e/h = 1, which lead to an energy-dependent contribution.

(c) Detector imperfections.

(d) The intrinsic energy resolution.

Sampling fluctuations are due to the fact that only a small fraction of the hadron energy is deposited in the active medium. They are determined by the energy deposited in one sampling layer ΔE. We will not discuss these any further and use the expression derived by Fabjan [13]

$$\sigma_{SAMP}/E = 0.09\ [\Delta E\ (MeV)/E\ (GeV)]^{1/2} .$$

The energy-dependent term that results from $e/h \neq 1$ was discussed in sect. 2. By detector imperfections are meant all the instrumental effects that increase the fluctuations when transforming the light or electrical charge produced in the shower development into a detector signal, and the effects of incomplete shower containment. Since the contribution of such effects does not scale as $E^{-1/2}$, they limit the high-energy performance. It is believed that for well-designed calorimeters their contribution can be limited to $\sigma/E \sim 1\%$. The fact that total energy resolutions for pions of better than 3% (at 200 GeV) have been measured [4] supports this belief.

In this section we will concentrate on the intrinsic energy resolution. It should be emphasized that here we use a definition that is slightly different from the one used by other authors, since we want to distinguish between the effect of $e/h \neq 1$ on the energy resolution, and other physics limitations. As was shown in subsect. 4.1, a considerable fraction of the hadronic energy is spent on binding energy losses that occur in nuclear spallation reactions, on an average ~ 40% in high-Z materials. It was also shown that the fluctuations about this average are huge (figs 10 and 11). The distribution of the binding energy loss per interaction is very asymmetric (fig. 10(a)). Fluctuations in the combined binding energy loss on an event-by-event basis intrinsically limit the achievable energy resolution. By convoluting many distributions of the type shown in fig. 10(a) for realistic events we estimated that the fluctuations in the total combined binding energy loss may be as large as 30-35% at 1 GeV hadronic energy.

What does this mean for the calorimeter signal? Since the average binding energy loss is about equal to the energy released in the form of ionizing hadrons from the shower development in high-Z materials, one may conclude that if the effects of neutron and γ-detection are neglected,

fluctuations in binding energy losses give rise to an intrinsic energy resolution of 30-35%/√E. For iron, where the binding energy loss is about a factor two lower than the energy going into ionizing shower particles, the contribution of this effect to the intrinsic energy resolution would be half this value.

However, the effects of neutron and γ-detection can not be neglected, since they form as we saw in the previous section a crucial component of the hadronic signal. This leads to a very interesting phenomenon. The amount of energy going into neutrons is evidently correlated to the binding energy loss. A relatively large binding energy loss, therefore, means that a relatively large fraction of the hadron energy is spent on kinetic neutron energy as well, which corrects at least partially for the relatively small signal from ionizing particles for the event concerned, and vice versa. If the neutrons were to be detected with a good energy resolution themselves, the intrinsic energy resolution due to the large fluctuations in binding energy losses would be substantially reduced because of this effect. The energy resolution of neutron detection is, therefore, crucial to the intrinsic energy resolution.

The energy resolution of neutron detection is, just as the e/h value, closely linked to the way the neutrons lose their energy, i.e. dependent on the presence of free protons in the readout medium. The reason for this is twofold:

(i) The average calorimeter response (signal per unit of energy) is much less energy-dependent for low-energy recoil protons than for low-energy γ's (the alternative for recoil protons). This can be concluded from a comparison of figs 15(c) and 8(a).

(ii) The fluctuations about the mean value are huge for low-energy γ's, since the calorimeter signal originates from very soft electrons with a range that is a small fraction of the thickness of an absorber plate, escaping from the absorber plates into the active medium (subsect. 3.3). For neutrons that convert their kinetic energy into recoil protons which are part of the active medium, fluctuations of this type are absent.

The effects of this were investigated quantitatively with a Monte-Carlo simulation based on the one used for the calculation of the e/h values. We evaluated the combined signal resulting from all the recoil protons produced by slow neutron elastic scattering, making up for a total kinetic neutron energy of 1 GeV. The neutrons were selected according to the energy spectrum discussed in subsect. 4.4 and were followed through all the successive steps by which they lose (or gain, in the case of some fissions) energy until they were finally captured. This procedure was repeated until the total kinetic energy of the neutrons reached 1 GeV, yielding the total signal from recoil protons, including the saturation effects, per GeV. By generating many events in this way the signal distribution for recoil protons from elastic neutron scattering was obtained. In fig. 23 the width of this distribution is given for uranium calorimeters with 2.5 mm PMMA readout, as a function of the thickness of the uranium plates. The same figure shows the results for the γ-detection, obtained with a similar procedure, using EGS4 to generate γ's according to some fixed energy spectrum (the one observed for prompt ^{238}U fission γ's) up to 1 GeV total energy. The latter resolution rises as expected linearly with the square root of the absorber plate thickness, while the resolution for neutron detection through recoil protons only rises very slowly with the plate thickness. For practical calorimeters where the plate thickness of the absorbers is at least 2 mm, the resolution for neutron detection through recoil protons is considerably better than through γ's (from inelastic scattering, fission, or capture). Therefore, the total energy resolution of neutron detection, i.e. the combined effect of γ's and recoil protons improves considerably if the latter dominate the neutron signal, and hence will be worse for liquid argon calorimeters than for detectors with plastic scintillator or TMP readout.

The curves shown in fig. 23 and the equivalent ones for other calorimeters, were used to compute the total contribution of fluctuations in the binding energy loss to the intrinsic energy resolution. It was assumed that the total amount of kinetic neutron energy is proportional to the binding energy loss on an event-by-event basis. The calculation went as follows for a given calorimeter design. For each event, first the binding energy loss was chosen, acccording to a Gaussian distribution with the fraction given in table 3 as an average value, and a $\sigma_{r.m.s.}$ of $0.35\ E^{-1/2}$. This defines then also the fraction of the energy carried by neutrons and

excitation γ's, because of the proportionality assumption. The remaining energy was deposited in the form of ionization by the charged shower particles, the signal of which was found by multiplying with the appropriate ion/mip value (table 2). The total signal was obtained by adding to this the signals from proton recoil and γ-detection. The γ-signal was chosen from a Gaussian distribution with a mean value given by the product of the total γ-energy and the appropriate γ/mip value (fig. 8(b)) and a width defined by fig. 23, or the equivalent curve for other absorber/ readout combinations. The signal from neutron detection through proton recoil was also chosen from a Gaussian distribution, around a mean value defined by the product of the kinetic neutron energy and the appropriate n/mip value, which depends on the choice of the absorber/ readout combination and the sampling fraction (figs 17(a), 19(a) and 20(a)). The width of the distribution was taken from the previously described calculation (fig. 23). This procedure was repeated for a large number (typically 10 000) of events and yielded the total purely hadronic signal distribution, the width of which gives the overall contribution of binding energy losses to the intrinsic energy resolution. Some results are given in fig. 24, for various types of uranium calorimeters, as a function of R_d. Curves showing similar features were also obtained for lead and iron devices. From fig. 24, one clearly sees the improvement in the intrinsic energy resolution caused by neutron detection through recoil protons. The smallest values are in principle reached near the point where the mip-equivalent energy carried by neutrons and γ's equals the mean binding energy loss, and are largely determined by the energy resolution for neutron detection for the absorber plate thickness concerned. That is why the minimum in the curves for TMP is lower than for scintillator and lower for thin than for thick readout layers. The requirement for getting a minimum intrinsic energy resolution is different from the one for $e/h = 1$, and therefore leads to a different R_d value. Fig. 25 suggests that both requirements might lead to approximately the same R_d values for optimal performance both in terms of energy resolution and energy dependence of the resolution for absorbers with $Z \sim 50$-70.

The curves for the intrinsic energy resolution in liquid argon or any other readout material without free protons do not show such a minimum (fig. 24), because the contribution of γ-detection (proton recoil is obviously not occurring here) to the hadronic signal is to first order a

constant fraction. As was discussed before, this fraction depends on the contribution of slow neutron capture (gate width). Fig. 24 shows that the intrinsic energy resolution is in most of the practical cases considerably better if the calorimeter readout material does contain free protons. The same conclusion can be drawn for calorimeters using absorbers other than uranium.

It should be emphasized that this computation of the contribution of fluctuations in the binding energy losses to the intrinsic energy resolution yields a lower limit. This is in particular true if

(a) the particle energy is so low that pion production plays only a modest role in the shower development, i.e. $\lesssim$ 10 GeV, or

(b) the Z of the absorber material is low.

The reason for this is the following. A relatively small loss in nuclear binding energy means that a relatively large fraction of the initial particle energy is spent on the production of ionizing particles. The nuclear binding energy loss tells us how many nucleons have been released in the various nuclear reactions that took place in the shower development and is, therefore, also correlated with the number of (spallation) protons produced. In low-Z materials, like iron, where the Coulomb barrier is relatively low, and therefore many protons can be produced at the evaporation stage of the nuclear reactions, this correlation will be much stronger than for materials like lead and uranium where the number of protons produced in the shower is, on an average, up to a factor of ten lower than the number of neutrons. If this correlation is strong (low Z) or if the signal from ionizing particles is almost completely determined by spallation protons (low energy, c.f. tables 1 and 3), a small binding energy loss yielding a large signal from ionizing particles necessarily means that the energy distribution of the spallation protons, and hence the ion/mip value (fig. 13) have to be quite different from the ones for an average event. Such effects were not taken into account in the calculations. The results as shown in fig. 24 will, therefore, only yield a reasonable impression of the intrinsic energy resolution if there is no strong correlation between the binding energy loss and the energy spectrum of the spallation protons contributing to the signal. This is the case as soon as charged pions can account for variations of the order of $0.3\ E^{-1/2}$ in the hadronic signal of calorimeters with high-Z absorber material.

Keeping this restriction in mind, we can now proceed to the calculation of the total hadronic energy resolution which is of more practical use than the rather academic interest of the intrinsic limits. For this purpose, one also has to include the contributions of sampling fluctuations and of the fluctuations in the fraction of the energy spent on π^o production. The latter were derived from fig. 4. This means that the longitudinal detector segmentation was assumed to be insufficient to determine f_{π^o} event-by-event. Fig. 26 shows the contribution of sampling fluctuations as a function of the thickness of the absorber layers. As in all following figures, the abcissa is plotted linear in the square root of this thickness, which yields a straight line for this contribution. All resolutions are expressed in terms of $\sqrt{E} \times \sigma/E$, with the hadron energy E in GeV. The total resolution was obtained as follows. First the contributions of the sampling fluctuations and the fluctuations in the binding energy losses were quadratically added. Then the energy-dependent $e/h \neq 1$ term was linearly added to this result (sect. 2).

In the following figures, the total energy resolution is given for two energies, 10 and 100 GeV. As was discussed before, the calculation for lower energies will lead to an underestimation of the resolution for those geometries where the intrinsic component contributes considerably. In the figures, both the total energy resolution and the various contributions to it are given. When available (a representative choice of) experimental results obtained for energies $\geq$ 10 GeV are included as well.

Figs 27 to 30 show the results for calorimeters with uranium absorbers and various readout media, i.e. scintillator (fig. 27), liquid argon (fig. 28), silicon (fig. 29) and TMP (fig. 30). In fig. 27 the energy resolutions are given for uranium calorimeters with 2.5 and 5 mm PMMA (the differences with SCSN-38 are marginal) readout. The curves show the following features. The total energy resolution reaches a minimum for an absorber thickness which is close to the one for which $e/h = 1$ (fig. 18). This is certainly true at very high energies. At lower energies effects of sampling fluctuations and intrinsic contributions may slightly shift the optimal uranium plate thickness. One sees that for the PMMA thicknesses considered (2.5 and 5 mm) fluctuations in binding energy loss and sampling fluctuations contribute roughly equally to the total energy resolution at the minimum of the curves, where energy-dependent ($e/h \neq 1$)

terms are absent. The best values are 0.32/√E and 0.37/√E for 2.5 and 5 mm PMMA, respectively, in good agreement with the experimental values reported [3, 4, 25]. This figure clearly illustrates an effect that was already mentioned several times: only if e/h = 1 the energy resolution scales with $E^{-1/2}$. The only common point for the 10 and 100 GeV curves is found for configurations that fulfil this requirement. The experimental results obtained by the WA78 Experiment [24] nicely confirm the predicted scaling violation for non-optimal configurations (fig. 27(b)).

In fig. 28 the results for U/liquid argon detectors are presented. As for the e/h value, two cases were considered, differing in the contribution of captured thermalized neutrons to the hadronic signal. The results appear to be rather sensitive to this contribution. Not only do the achievable energy resolutions improve considerably if the fraction of contributing captured neutrons is increased, but the results also become less energy-dependent. Perfect scaling with $E^{-1/2}$ is, however, not reached since $e/h \neq 1$ for all configurations. Getting 80% of the neutrons to contribute to the hadronic signal through their capture in uranium is, however, far from trivial. It requires not only a sufficiently long gate width (~ 1 μs [27,28]), but also a calorimeter that is sufficiently large, in particular also in the lateral directions [6]. Experimental tests done so far with prototype modules did probably not fulfil the latter condition. Representative results from several tests are included both in figs 28(a) and 28(b). In particular, the results obtained by the DØ Collaboration [5] who did measurements over a wide range of energies (10-150 GeV) indicate that the energy resolution does not scale with $E^{-1/2}$. Fabjan et al. [2] measured an extremely good energy resolution at 10 GeV, for a fine-sampling U/LAr calorimeter. The difference between this result and the ones obtained with SLD and DØ prototypes at the same energy are larger than predicted by our calculations. Rehak, one of the authors of ref. [2], has argued [32] that their results were obtained with a biased selection of events. An unbiased reanalysis of the data increased the resolution from 30 to 46%/√E, according to him. This result is also included in the plots and leads to a much more consistent picture. It seems, therefore, that the contribution of γ's from neutron capture to the hadronic signal of the various mentioned devices was rather limited and that a significant improvement may be expected for full scale detectors.

The curves for uranium/silicon devices (fig. 29) show similar features as the ones for liquid argon. Because of the absence of saturation effects in the detection of the spallation proton component, the e/h value is closer to 1 (fig. 18) and, therefore, the ideal situation of resolution scaling with $E^{-1/2}$ is already reasonably approximated for a relatively modest contribution of γ's from neutron capture to the hadronic signal. If this contribution becomes large (large detectors, 1 μs gate), very good energy resolutions may be expected. No experimental results have been reported up to now.

The recombination properties of TMP are very crucial to the achievable energy resolution, in particular in combination with uranium absorber. Fig. 30 shows the predictions (no experimental results were reported so far) for the two different assumptions with respect to the kB value of the medium that were mentioned before. The calculations show that extremely good energy resolutions (25-30%/$\sqrt{E}$) for all energies can be obtained, provided that uranium plates of ~ 1 mm are used. For 3 mm plates, the resolution at 100 GeV may be anything between 65 and 100%/$\sqrt{E}$, depending on the kB value, because of the overcompensation.

The properties of TMP, in particular the low density combined with the relatively large free proton content, are such that optimal performance in terms of energy resolution probably requires an unpractically large sampling fraction. Amongst other things, this has the disadvantage that the <u>average interaction length</u> is considerably larger for such a calorimeter than for one employing another readout method (table 6). This quantity amounts to 26-35 cm in U/TMP, depending on the recombination properties, against ~ 20 cm for scintillator devices, down to ~ 12 cm for silicon readout. For detectors operating in a colliding-beam environment, the volume for a detector corresponding to a certain number of nuclear interaction lengths is determined by the third power of this quantity, which illustrates its importance.

More practical calorimeters using TMP readout might be constructed with lead absorber. Fig. 31 shows the predictions for the energy resolution of Pb/TMP devices, always with the same assumptions concerning the kB value. If 2.5 mm TMP gaps are used in combination with 2-4 mm lead plates the energy resolution might be as good as 0.3 $E^{-1/2}$, for all

energies. A disadvantage of compensating Pb/TMP calorimeters is the large average nuclear interaction length (table 6), although the value is not worse than for optimal U/TMP devices.

The results for the other type of lead calorimeter with which signal equalization can be obtained, i.e. using scintillator readout, are shown in fig. 32. Fig. 32(a) shows the energy resolution curves for Pb calorimeters with 2.5 mm PMMA readout. Scaling with $E^{-1/2}$ is predicted for ~ 10 mm Pb plates and the resolution would be ~ 42%/√E at all energies. The contribution of sampling fluctuations to this value is larger than for optimal U/PMMA devices, so that a somewhat better performance for low-energy (10 GeV) hadrons may be expected for thinner lead plates, at the expense of e/h not being equal to 1.

Fig. 32(b) shows the effect of adding a little cadmium on the energy resolution. Because of the contribution of neutron capture to the hadronic signal the e/h = 1 condition is now fulfilled for ~ 8 mm lead plates, and the resolution at this point may be as good as 38%/√E. Doubling the scintillator thickness shifts the optimal point to ~ 20 mm Pb plates, where an energy resolution of 52%/√E is predicted (fig. 32(c)). The only test of Pb/scintillator calorimeters that we know of was done with scintillator plates of this thickness, and 4/5 mm lead plates, and was limited to low-energy pions [29].

Thanks to the relatively thick lead plates needed for optimal performance, the average nuclear interaction length for a compensating lead/scintillator calorimeter is almost equal to the one for an optimal uranium/scintillator (table 6), in spite of the large difference in density between uranium and lead.

Fig. 33 shows the predictions for lead calorimeters with liquid argon (fig. 33(a)) and silicon (fig. 33(b)) readout, for which e/h = 1 can not be achieved. This figure shows that the high-energy performance can be considerably improved if the thermal neutrons can be made to contribute efficiently to the hadronic signal, e.g. by capture in cadmium. At 100 GeV, the best possible energy resolution is ~ 7 % (LAr) and ~ 5 % (Si), respectively, the difference being due to the non-saturation of silicon for densily ionizing spallation protons. Just as in the case of uranium

absorbers, where 1 m of detector may contain ~ 8 nuclear interaction lengths, silicon offers also in combination with lead the advantageous possibility to construct very compact devices (table 6).

Finally, we consider iron calorimeters, repeating the statement that the intrinsic energy resolution is probably severely underestimated in this case. Therefore, in those cases where the intrinsic resolution contributes considerably to the final result, the latter should not be taken too seriously (thin plates). In spite of this one may conclude from fig. 34 that in any case liquid argon or silicon readout will lead to large deviations from $E^{-1/2}$ scaling. At 100 GeV, the resolution can not be expected to be better than 7-9% for liquid argon, and 5.5-7.5% for silicon readout, depending on the fraction of neutrons that are captured while the signal gate is open.

Fig. 35 shows the results for the only type of detector with iron absorber for which signal equalization and a reasonable energy resolution in the range of 10^{10}-10^{12} eV might be realized, Fe/TMP. As before, the performance will crucially depend on the recombination properties. For 2.5 mm TMP layers, signal equalization may be obtained for 15-20 mm iron plates if the recombination properties are similar to liquid argon. The energy resolution would then be 45%/$\sqrt{E}$.

The last configuration studied is iron/5 mm scintillator (fig. 36). In this case we calculated the energy resolution curves for 15, 50, 100 and 140 GeV hadrons since systematic experimental measurements were reported at these energies [7]. The experimentally observed deviation of $E^{-1/2}$ scaling is reasonably reproduced, just as the clustering of experimental results at ~ 120%/$\sqrt{E}$ for ~ 10 cm plates (e/h = 1!).

Table 6 shows that in spite of the fact that the density of iron is 2.4 times smaller than the density of uranium, compensating iron calorimeters are more compact than compensating uranium calorimeters, a surprising result of which one may take advantage when designing calorimeters that will operate in multi-TeV environments. There, 10 cm Fe/5 mm scintillator detectors with a resolution of 120%/$\sqrt{E}$ <u>at all energies</u>, and 5-6 nuclear interaction lengths per meter detector might be very competitive instruments.

The agreement between the experimental points and the predicted curves in fig. 36 is certainly not perfect. Several factors are likely to be responsible for this. The underestimation of the contribution of fluctuations in the binding energy loss in case of iron absorber was already mentioned. The fact that the experimental e/h values are systematically larger than the predicted ones (fig. 20(b)) leads to an underestimation of the energy-dependent $e/h \neq 1$ term, which causes the predicted differences between the energy resolutions at low and high energy to be too small. Moreover, several experimental points were obtained with 6 mm rather than 5 mm thick scintillator plates, while the curves concern 5 mm.

In subsect. 4.4 it was shown that uncertainties in the assumptions that went into the calculations can easily shift the optimal thickness ratio (where $e/h = 1$) by ~ 25%. Such uncertainties will of course also affect the results discussed in this subsection, since the curves representing the energy-dependent $e/h \neq 1$ term might have to be moved a little bit to the left or to the right in figs 27-36. The aim of these calculations was, however, not primarily to reproduce as many sets of experimental data in as much detail as possible, but rather to try to understand which factors affect the energy resolution and to what extent. Therefore, all the assumptions that went into the calculations were based on first principles, on known physics. Not a single parameter was fitted such as to reproduce experimental energy resolution or e/h data.

Keeping that in mind, the picture that emerges from a comparison of all these predictions with the existing experimental data, which have often been found confusing, can be considered amazingly consistent and in many ways instructive.

6. SUMMARY AND CONCLUSIONS

We investigated in detail the various components that contribute to the signal of hadron calorimeters and the factors that affect the energy resolution with which hadrons are detected. The e.m. to hadronic signal ratio, e/h plays a central role in this matter. Unless a very fine longitudinal segmentation is applied, any deviation from $e/h = 1$ will cause the energy resolution not to scale with $E^{-1/2}$ and the signal not to be proportional to the particle energy, because of the non-Gaussian fluctuations

in the fraction of the hadron energy that is spent on π^0 production. The effects of this are particularly important at ultrahigh energies. Our analysis shows, for example, that if one wants to detect jets in the TeV energy range, a calorimeter using 10 cm iron as an absorber and 5 mm scintillator readout will yield a better energy resolution than 2 cm uranium absorber plates and the same readout. The e/h value is determined by the Z-value of the absorber material, by the thicknesses of both the absorber and the readout material, by the properties of the readout medium (density, saturation effects), by the signal integration time of the detector, and finally by the sampling fraction.

The Z-values of the absorber and readout materials determine to what extent the signal from the e.m. part is reduced with respect to minimum-ionizing particles. This reduction is found to be due to phenomena that occur in the last stages of the shower development, especially photo-electric and Compton effect. In these processes, low-energy photons transfer their energy to an electron, almost exclusively in the absorber layers in case high-Z material is used. The range of these electrons is such that only a very small fraction of them will escape from the layer in which they are produced and hence contribute to the measurable signal.

The calorimeter signal from low-energy γ's is, therefore small compared to an equivalent mip as well, and has huge fluctuations. The Z-value of the absorber determines, moreover, what fraction of the energy is going into low-energy neutron production. The detection of few-MeV neutrons is the other crucial ingredient to the e/h value. It turns out that if the readout medium contains free protons, an important fraction of the kinetic neutron energy is transferred by elastic scattering into recoil energy of these protons. This component of the energy deposit is not sampled and, therefore, contributes in a totally different way to the calorimeter signal than minimum-ionizing particles do. It was found that the neutron/mip signal ratio, and hence the e/h value can be tuned using the sampling fraction as a variable. The smaller the sampling fraction, the larger the relative contribution of neutrons to the calorimeter signal. The numerical details depend on the fraction of free protons in the readout medium, on the density of the readout material and on the saturation or recombination properties for few MeV proton detection.

The fission occurring in ^{238}U certainly increases the fraction of the energy carried by slow neutrons and, therefore, allows one to tune the e/h value over a rather broad range. However, signal equalization (e/h = 1) does not seem to be a property unique to uranium calorimeters. Lead/scintillator and probably lead/TMP calorimeters with e/h = 1 seem to be feasible as well, particularly if precautions are taken to profit from thermal neutron capture. Analysis of experimental data indicated that already more than five years ago compensating iron/scintillator calorimeters were operating.

The e/h value of calorimeters employing liquid argon readout can not be tuned to the value 1 through the sampling fraction. The kinetic energy of the neutrons is mainly transferred into low-energy γ's, for which the detector is very inefficient. The calculations show that in all cases e/h stays significantly above 1.

Calorimeters with Si readout do also not profit from efficient neutron detection, but because of the absence of saturation effects for the detection of spallation protons, that were found to dominate the direct ionization component, e/h = 1 seems to be achievable in the case of U/Si.

The intrinsic energy resolution of hadron calorimeters is largely influenced by fluctuations in the binding energy loss that occurs in the nuclear reactions. We found contributions of 0.2-0.4 $E^{-1/2}$ from this source. Efficient detection of slow neutrons may considerably reduce these effects because of the correlation between the total kinetic neutron energy and the binding energy loss. The energy resolution of neutron detection through recoil protons is much better than for neutrons that convert their kinetic energy into nuclear excitation γ's. The intrinsic energy resolution is, therefore, dependent on the extent to which both processes contribute. As a consequence, the $E^{-1/2}$ scaling term in the resolution is smaller for calorimeters using scintillator readout than for liquid argon, if the contributions of e/h and sampling fluctuations are the same. For practical calorimeters, an energy resolution of 0.2 $E^{-1/2}$ seems to be the ultimate limit. The possibilities of TMP look also potentially very interesting in this respect, particularly in combination with non-U absorber material. Absolutely crucial for the performance of such

calorimeters are the (so far unknown) recombination properties that determine the response to low-energy protons.

Many interesting topics were not discussed in this paper. Gaseous readouts were almost completely ignored. Because of the virtual absence of recombination effects e/h values can be tuned over a very broad range without completely rebuilding the calorimeter, a fact which was experimentally observed and supports the framework of our calculations. The gas composition and/or its presssure can be used as the tuning variables. The achievable energy resolution is, however, worse than with other techniques because specific effects like Landau and path length fluctuations and escape of recoil protons, will contribute considerably.

Other ideas that deserve serious attention are the use of hydrogen containing admixtures, like methane, to liquid argon, or the use of absorber material mixtures to correct for overcompensation (TMP?), or to limit the effects of radiation damage by uranium while maintaining the advantages of uranium for calibration purposes (scintillator).

Hadron calorimeters are used in high-energy physics experiments. The users of these instruments tend to describe their properties in terms of units typical to high-energy physics, e.g. radiation length, critical energy, nuclear interaction length. This study has shown that in order to fully understand the signal from these devices one needs to descend to an energy level where these units are meaningless, to the nuclear and atomic processes, because that is where finallly the bulk of the initial particle energy is dissipated.

Acknowledgements

I am indebted to Yves Sirois who helped me with the EGS simulations. The work described in this paper has benefited considerably from many discussions with Chris Fabjan, Hans Specht and Bill Willis. They also carefully read the manuscript and gave valuable suggestions for improvement.

REFERENCES

[1] ZEUS Collaboration, ZEUS, a detector for HERA, Letter of Intent.

[2] C.W. Fabjan and W.J. Willis, in Proc. Calorimeter Workshop, Batathrough Ill. (1975), M. Atac, ed., p. 1;

C.W. Fabjan et al., Nucl. Instrum. Methods 141 (1977) 61.

[3] T. Akesson et al., Nucl. Instrum. Methods A241 (1985) 17.

[4] F. Corriveau et al., CERN HELIOS, Int. Note 145 (1986), unpublished.

[5] B. Cox, Uranium-liquid argon calorimetry; preliminary results from the DØ tests, presented at the DPF Meeting of the American Physical Society, University of Oregon, Eugene, Oreg., 1985, FERMILAB - Conference 86/14-E;

D. Hitlin, SLD liquid argon prototype tests, in Proc. Workshop on Compensated Calorimetry, Pasadena, 1985, CALT-68-1305.

[6] C. Leroy, Y. Sirois and R. Wigmans, An experimental study of the contribution of nuclear fission to the signal of uranium hadron calorimeters, CERN-EP/86-66 (1986).

[7] H. Abramowicz et al., Nucl. Instrum. Methods 180 (1981) 429.

[8] A. Rothenberg, Weighting schemes for the UA2 calorimeter, in Proc. Workshop on Compensated Calorimetry, Pasadena, 1985, CALT-68-1305;

M. Shaevitz, Weighting schemes for Fe Calorimeters, idem;

C. Milstene, Compensation by longitudinal segmentation, idem.

[9] U. Amaldi, Phys. Scripta 23 (1981) 409.

[10] J.F. Janni, Atomic Data and Nuclear Data Tables 27 (1982) 147-529.

[11] W. Lohmann, R. Kopp and R. Voss, Energy loss of muons in the energy range 1-10 000 GeV, Yellow Report CERN 85-03 (1985).

[12] W.R. Nelson, H. Hirayama and D.W.O Royers, The EGS4 Code System, SLAC-Report-165 (1985).

[13] C.W. Fabjan, Calorimetry in high-energy physics, CERN-EP/85-54 (1985).

[14] K. Pinkau, Phys. Rev. B139 (1965) 1548.

[15] W. Flauger, Nucl. Instrum. Methods A241 (1985) 72.

REFERENCES (Cont'd)

[16] Photon cross sections, attenuation coefficients and energy absorption coefficients from 10 keV to 100 GeV, NSRDS-NBS 29 (1969).

[17] V.M. Gorbachev, Y.S. Zamyathin and A.A. Lbov, Nuclear reactions in heavy elements, a data handbook (Pergamon Press, London, 1980) and references therein.

[18] G. Rudstam, Zeitschr. für Naturforsch. 21a (1966) 7.

[19] K. Bos and A.H. Wapstra, Atomic Data and Nuclear Data Tables 19 (1977) 177.

[20] T.A. Gabriel, Nucl. Instrum. Methods 150 (1978) 145;

T.A. Gabriel, The physics of HETC, in Proc. Workshop on Compensated Calorimetry, Pasadena, 1985, CALT-68-1305.

[21] M. Barbier, Induced radioactivity, North Holland, Amsterdam (1969).

[22] R.J. Howerton, Semi-empirical neutron cross sections, Univ. of California, Livermore, 1958, UCRL-5351.

[23] ZEUS Collaboration, Technical proposal for the ZEUS Detector, DESY Hamburg (1986) 5-45.

[24] M. de Vincenzi et al., Nucl. Instrum. Methods A243 (1986) 348.

[25] J. Engelen and H. Tiecke, Energy and position resolution of a uranium test calorimeter for ZEUS, private communication.

[26] Y. Galaktionov et al., The performance of a uranium gas-sampling calorimeter, CERN-EP/86-46 (1986).

[27] H. Brückmann, Hadron calorimetry - a puzzle of physics, in Proc. Workshop on Compensated Calorimetry, Pasadena, 1985, CALT-68-1305

[28] H. Brückmann and H. Kowalski, The dependence of calorimeter responses on the gate width, DESY, Hamburg, ZEUS - Int. Note 86/026 (1986).

[29] C. Daum et al., Description and first results of a hadron test calorimeter for ZEUS, DESY, Hamburg, ZEUS Int. Note 86/13 (1986).

[30] M. Holder et al., Nucl. Instrum. Methods 151 (1978) 69.

[31] V. Böhmer et al., Nucl. Instrum. Methods 122 (1974) 313.

[32] P. Rehak, Uranium/liquid argon calorimeter studies, in Proc. Workshop on Compensated Calorimetry, Pasadena, 1985, CALT-68-1305.

TABLE CAPTIONS

TABLE 1 Example of a 5 GeV proton shower in uranium (the numbers are energies in MeV).

TABLE 2 The spallation proton/mip signal ratio.

TABLE 3 Energy deposition in 5 GeV proton showers neglecting the π^{o} component.

TABLE 4 Comparison of soft neutron transport Monte-Carlo results with experimental data [6].

TABLE 5 Properties of metals that convert thermal neutrons into γ's.

TABLE 6 Average nuclear interaction length for (almost$^{(*)}$) compensating calorimeters (cm).

TABLE 1

Incoming particle	Ionization	Binding energy	Evaporation neutrons	γ's	Cascade particles p	n	π^+	π^-	Target recoil
5000 (p)	*240*(a)	120	8 * 3	4	500	600	1200	1200	150
					200	300			
					50(b)	150			
					40(b)	100			
						80			
						40			
1200 (π^+)	*230*(b)	90	7 * 3	4	170	250			30
					100(c)	140			
					45(c)	70			
						50			
1200 (π^-)	*230*(b)	90	7 * 3	4	170	250			30
					100(c)	140			
					45(c)	70			
						50			
600 (n)		70	7 * 3	4	*130*(c)	170			5
					60(c)	90			
						50			
300 (n)		50	6 * 3	4	*65*(c)	100			
					20(c)	45			
250 (n)		45	6 * 3	4		185			
250 (n)		50	6 * 3	4	*70*(d)	110			
500 (p)	*250*(b)	50	6 * 3	4	*50*(c)	130			
200 (p)	*170*(b)	20	3 * 3						
170 (p)	*150*(c)	15	2 * 3						
170 (p)	*150*(c)	15	2 * 3						

(a) First generation ionizing particles.
(b) Second generation ionizing particles.
(c) Third generation ionizing particles.
(d) Fourth generation ionizing particles.

TABLE 2

Readout	kB value $g/cm^2.MeV$	Absorber	p/mip	Absorber	p/mip	Absorber	p/mip
2.5 mm PMMA	0.00978	3 mm U	0.937	6 mm Pb	0.917	6 mm Fe	0.831
5.0 mm PMMA			0.896		0.883		0.812
2.5 mm SCSN	0.00835	3 mm U	0.961	6 mm Pb	0.942	6 mm Fe	0.855
5.0 mm SCSN			0.920		0.909		0.833
2.5 mm LAr	0.0045	3 mm U	0.994	6 mm Pb	0.973	6 mm Fe	0.884
5.0 mm LAr			0.960		0.944		0.862
0.4 mm Si	0	3 mm U	1.148	6 mm Pb	1.131	6 mm Fe	1.014
0.4 mm Si			1.132		1.112		0.995

TABLE 3

Absorber	U	Pb	Fe
Ionization (fraction due to spallation protons)	38% (0.70)	43% (0.72)	57% (0.74)
Excitation γ's	2%	3%	3%
Neutrons < 20 MeV	15%	12%	8%
Invisible energy (binding energy + target recoil)	(45%)	42%	32%

TABLE 4

	M.C.	Exp.
# neutrons per GeV		
^{238}U	59	43 ± 7(*)
Pb	21	14 ± 3(*)
$Pb/^{238}U$	0.36	0.32 ± 0.05
# n-induced fissions per GeV		
^{238}U	10.5	8.7 ± 1.3
3 mm U - 2.5 mm PMMA	7.1	6.9 ± 1.1
9 mm U - 2.5 mm PMMA	9.1	7.8 ± 1.2
3 mm U - 2.5 mm LAr	10.4	8.8 ± 1.4
Pb(**)	6.2	4.6 ± 0.8
$Pb/^{238}U$(**)	0.59	0.53 ± 0.05
# n-induced fissions / # neutrons captured		
^{238}U	0.18	0.20 ± 0.01
3 mm U - 2.5 mm PMMA	0.12	0.14 ± 0.01
9 mm U - 2.5 mm PMMA	0.15	0.15 ± 0.01
3 mm U - 2.5 mm LAr	0.18	0.21 ± 0.01
Pb(**)	0.30	0.33 ± 0.03
# interactions before capture		
^{238}U	53	
3 mm U - 2.5 mm PMMA	20	
9 mm U - 2.5 mm PMMA	29	
3 mm U - 2.5 mm LAr	49	

(*) The experimental results should be a bit lower than the Monte-Carlo prediction, since backward escaping neutrons were not taken into account in the published results.

(**) Here we do not mean fission in lead, but fission observed in thin uranium plates inserted in a massive lead block (see ref. [6] for details).

TABLE 5

Element	Z	$\sigma(n, \gamma)$ (b)	Mean free path (cm)	ΣE_γ (MeV)
Fe	26	2.55	4.6	7.7
Co	27	37	0.30	7.5
Ag	47	64	0.27	7.0
Cd	48	2450	0.01	9.0
Ta	73	21	0.86	6.1
W	74	18.5	0.86	5.7
Ir	77	426	0.03	6.1
Au	79	99	0.17	6.5

TABLE 6

Readout	Absorber		
	U	Pb	Fe
PMMA	19.5	20.2	17.5
SCSN-38	21.5	21.7	17.8
LAr	16-19	-	-
Si	12-15	17.5-18.2	-
TMP	26-35	25-32	18-19

(*) For LAr and Si readout e/h < 1.1 is taken.

FIGURE CAPTIONS

Fig. 1 Schematic view of the response of a hadron calorimeter to the e.m. and purely hadronic components of a hadron shower.

Fig. 2 (a) The relation between the e.m. to purely hadronic signal ratio, e/h^{intr}, and the measured e/h value as a function of energy.

(b) The calorimeter signal per GeV for hadrons, normalized to the signal for a 10 GeV hadron, as a function of energy, for various values of e/h^{intr}.

Fig. 3 (a) Monte-Carlo results on the hadronic energy resolution as a function of energy, for various values of e/h (10 GeV). See text for details.

(b) The same results plotted on a scale linear in $E^{-1/2}$.

Fig. 4 The constant term in the energy resolution, as a function of e/h (10 GeV). See text for details.

Fig. 5 The e/mip signal ratio for sampling calorimeters as a function of the Z-value of the absorber, for 2.5 mm liquid argon and plastic scintillator readout. The absorber layers are $1X_o$ thick. Results from EGS4 Monte-Carlo simulations.

Fig. 6 (a) The mass attenuation coefficients for γ's in different materials, as a function of energy.

(b) The fraction of the energy of a 10 GeV electron shower, that is deposited through ionization by electrons and positrons slower than 1 or 4 MeV or faster than 20 MeV as a function of the Z of the calorimeter absorber.

Fig. 7 (a) The e/mip signal ratio as a function of shower depth, or age, for various calorimeter configurations. Results from EGS4 Monte Carlo simulations.

(b) The e/mip signal ratio as a function of the thickness of the passive layers for U/LAr and U/PMMA calorimeters. Results from EGS4 Monte-Carlo simulations.

FIGURE CAPTIONS (Cont'd)

Fig. 8 (a) The γ/mip signal ratio as a function of the γ-ray energy for a 3 mm U/2.5 mm PMMA calorimeter. Results from EGS4 Monte-Carlo simulations.

(b) The γ/mip signal ratio as a function of the Z of the absorber material, for $1X_o$ thick absorber layers, and 2.5 mm liquid argon or PMMA readout. The γ-ray spectrum is the spectrum of prompt γ's emitted in ^{238}U fission. Results of EGS4 Monte-Carlo simulations.

Fig. 9 Cross sections for nuclides that are produced by spallation of ^{238}U induced by a 2 GeV hadron. The nuclide is defined by the number of protons (ΔZ) and neutrons (ΔN) that escaped from the ^{238}U nucleus.

Fig. 10 (a) The binding energy lost in spallation reactions induced by 1 GeV hadrons on ^{238}U nuclei.

(b) The number of neutrons produced in such reactions.

Fig. 11 (a) The average fraction of the hadron energy spent on binding energy losses and target recoil in the primary spallation reactions on uranium, as a function of the hadron energy. The dashed lines give the $\pm 1\ \sigma_{r.m.s.}$ boundaries of the distributions.

(b) The average numbers of protons and neutrons produced in the primary spallation reactions on uranium, as a function of the energy of the incoming hadron. The neutrons are split up in an evaporation and a cascade component (see text).

Fig. 12 The average amount of energy released by protons before they interact in uranium, as a function of the proton energy. Results are given in MeV (dashed curve), and as a fraction of the proton energy (full curve).

FIGURE CAPTIONS (Cont'd)

Fig. 13 The calorimeter response to spallation protons:

(a) The ratio of the energy deposition by ionization dE/dx, in the active and passive layers of various calorimeters, relative to minimum-ionizing particles as a function of the proton energy.

(b) The energy deposit (upper curve) and the calorimeter signal (lower) for stopping protons, relative to mip's, as a function of the proton energy, for 3 mm U/2.5 mm PMMA calorimeters.

(c) The p/mip signal ratio for protons distributed according to an exponentially decreasing energy spectrum, as a function of the average number of spallation protons produced per GeV hadronic energy (lower scale), or the average proton energy (upper scale), for 3 mm U/2.5 mm PMMA calorimeters.

(d) The effect of the thickness of the active and passive layers on the p/mip signal ratio, for U/PMMA calorimeters

Fig. 14 The cross sections for neutron-induced reactions on ^{238}U nuclei (a) and protons (b).

Fig. 15 The response of a 3 mm U/3 mm PMMA calorimeter to low-energy neutrons:

(a) The various forms in which the kinetic neutron energy is deposited. Because of the contribution of fission the total can be larger than 100%. The curves are drawn to guide the eye.

(b) The fraction of the recoil proton energy that is converted into light, normalized to a mip, as a function of the proton energy (saturation effects).

(c) The calorimeter signal resulting from the recoil protons, relative to the signal for minimum-ionizing particles of equivalent energy, as a function of the neutron energy.

FIGURE CAPTIONS (Cont'd)

Fig. 16 Experimental results on the non-sampling part of the energy resolution and the e/h value, measured with uranium-plastic scintillator calorimeters as a function of the sampling fraction. The curves are drawn to guide the eye.

Fig. 17 (a) The signal ratio neutron/mip split up in its various contributions, for U/PMMA calorimeters, as a function of the ratio of the thicknesses of absorber and readout layers.

(b) The hadronic signal of U/PMMA calorimeters, split up in its various components, as a function of the ratio of the thicknesses of the absorber and readout layers.

(c) The signal ratio e/h for U/2.5 mm PMMA calorimeters as a function of the ratio of the thicknesses of the passive and active layers, assuming that 0,20 or 100% of the γ's released in thermal neutron capture contribute to the hadronic signal.

(d) The effects of changes in the parameters used to calculate the e/h signal ratio for U/PMMA calorimeters. See text for details.

Fig. 18 The signal ratios e/h for uranium calorimeters employing different readout materials as a function of the ratio of the thicknesses of absorber and readout layers. Results of experimental measurements are included. See text for details.

Fig. 19 (a) The signal ratio neutron/mip for lead calorimeters using various readout media, as a function of the ratio of the thicknesses of the absorber and readout layers. The full lines give the contribution of recoil protons. The other lines give the contribution of excitation and capture γ's for SCSN readout, assuming that capture takes place in iron or cadmium (see text).

FIGURE CAPTIONS (Cont'd)

Fig. 19 (b) The signal ratio e/h for lead calorimeters employing different readout materials, as a function of the ratio of the thicknesses of the absorber and readout layers. For Si readout the horizontal scale should be read multiplied by ten. See text for details.

Fig. 20 (a) The signal ratio neutron/mip for iron calorimeters using various readout media, as a function of the ratio of the thicknesses of the absorber and readout layers. The full lines give the contribution of recoil protons. The other lines give the contribution of excitation and capture γ's for SCSN readout. See text for details.

(b) The signal ratio e/h for iron calorimeters using different readout media, as a function of the ratio of the thicknesses of the absorber and readout layers. For Si readout the horizontal scale should be read multiplied by ten. See text for details.

Fig. 21 (a) The e/mip ratio for iron/scintillator calorimeters, as a function of the (very large) thickness of the iron absorber plates, for various energies. Results of EGS4 Monte-Carlo simulations.

(b) The consequence of the effect observed in fig. 21(a) for the e/h signal ratio. The full line gives the uncorrected result, the dashed line the corrected one.

Fig. 22 (a) The energy resolution for iron-scintillator calorimeters, as reported by the CDHS Collaboration [7].

(b) The energy resolution for the same calorimeters obtained after a weighting procedure, as a function of the thickness of the iron plates, plotted on a scale linear in the square root of this variable.

FIGURE CAPTIONS (Cont'd)

Fig. 23 The energy resolution for detecting neutrons and γ's in the MeV energy range, in U/PMMA calorimeters, as a function of the thickness of the uranium plates.

Fig. 24 The contribution of the fluctuations in the binding energy loss to the intrinsic resolution of various types of uranium calorimeters, as a function of the ratio of the thicknesses of the passive and active layers.

Fig. 25 The e/h value at which the intrinsic energy resolution reaches a minimum value, for various kinds of hydrogen containing readout materials, as a function of the Z of the absorber.

Fig. 26 The contribution of fluctuations in the fraction of the energy that is sampled by the readout layers to the total energy resolution.

Fig. 27 The total energy resolution and the various factors contributing to it, for detection of 10 and 100 GeV hadrons in U/PMMA calorimeters, as a function of the uranium plate thickness. The thickness of the scintillator plates amounts to 2.5 mm (a) or 5.0 mm (b). The numbers in brackets denote other energies at which experimental results were reported.

Fig. 28 The total energy resolution and the various factors contributing to it, for detection of 10 and 100 GeV hadrons in U/liquid argon calorimeters, as a function of the uranium plate thickness. The liquid argon gap is 2.5 mm wide. The calculations assume that 20% (a) or 80% (b) of the thermalized neutrons are captured in the detector and contribute to the hadron signal.

FIGURE CAPTIONS (Cont'd)

Fig. 29 The total energy resolution and the various factors contributing to it, for detection of 10 and 100 GeV hadrons in U/silicon calorimeters, as a function of the uranium plate thickness. The silicon wafers are 0.4 mm thick. The calculations assume that 20% (a) or 80% (b) of the thermalized neutrons are captured in the detector and contribute to the hadron signal.

Fig. 30 The total energy resolution and the various factors contributing to it, for detection of 10 and 100 GeV hadrons in U/TMP calorimeters as a function of the uranium plate thickness. Two different assumptions on the recombination properties of TMP were used: kB = 0.00978 (a) or 0.0045 g/MeV • cm^2 (b). The TMP gap is 2.5 mm wide.

Fig. 31 The total energy resolution and the various factors contributing to it, for detection of 10 and 100 GeV hadrons in lead/TMP calorimeters as a function of the thickness of the lead plates. The TMP gap is 2.5 mm wide. Two different assumptions concerning the recombination properties of TMP were used: kB = 0.00978 (a) or 0.0045 g/MeV • cm^2 (b).

Fig. 32 The total energy resolution and the various factors contributing to it, for detection of 10 and 100 GeV hadrons in lead/PMMA calorimeters as a function of the thickness of the lead plates. Three cases were considered:

(a) Plain lead in combination with 2.5 mm PMMA.
(b) Lead + 1% Cd, in combination with 2.5 mm PMMA.
(c) Plain lead in combination with 5.0 mm PMMA.

Fig. 33 The total energy resolution and some of the factors contributing to it, for detection of 10 and 100 GeV hadrons in lead/2.5 mm liquid argon (a) and lead/0.4 mm silicon (b) calorimeters, as a function of the thickness of the lead plates. In each case, three situations are considered as far as the contribution of γ's from thermal neutron capture to the hadron signal is concerned: 0% (plain lead), 20% and 80% in cadmium added to the lead.

FIGURE CAPTIONS (Cont'd)

Fig. 34 The total energy resolution and some of the factors contributing to it, for detection of 10 and 100 GeV hadrons in iron/2.5 mm liquid argon (a) and iron/0.4 mm silicon (b) calorimeters, as a function of the thickness of the iron plates. The calculations assume that 20 or 80% of the thermalized neutrons are captured in the detector and that the γ's from this process contribute to the hadron signal.

Fig. 35 The total energy resolution and the various factors contributing to it, for detection of 10 and 100 GeV hadrons in iron/TMP calorimeters, as a function of the thickness of the iron plates. The TMP gap is 2.5 mm wide. Two different assumptions concerning the recombination properties of TMP were used: kB = 0.00978 (a) or 0.0045 g/MeV $\cdot$ cm^2 (b).

Fig. 36 The total energy resolution and the various factors contributing to it, for detection of 15, 50, 100 and 140 GeV hadrons in iron/PMMA calorimeters, as a function of the thickness of the iron plates. The scintillator plates are 5 mm thick. Experimental results for pions at the four different energies are included.

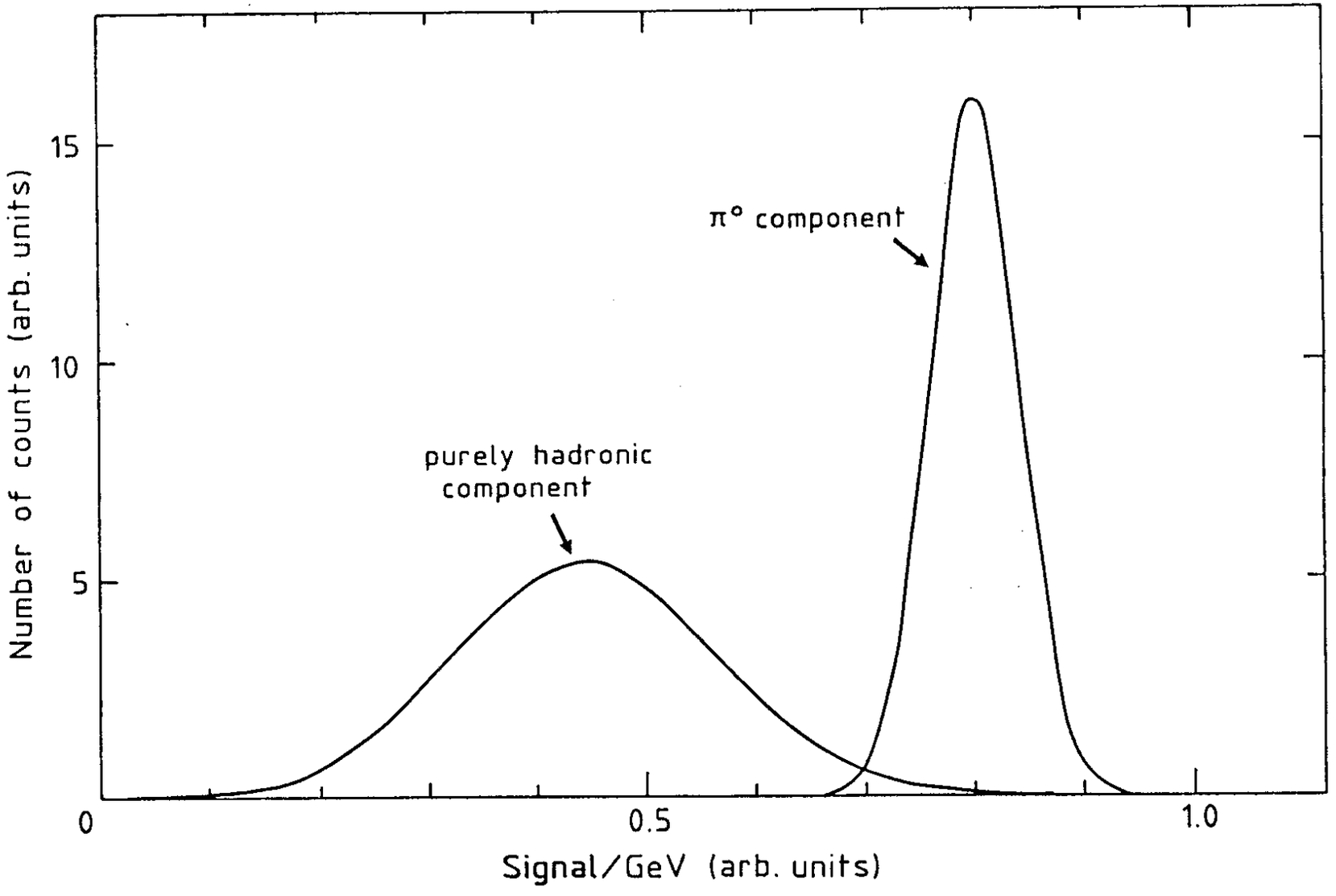
Number of counts (arb. units)
15
10
5
0
0.5
1.0
Signal/GeV (arb. units)
π° component
purely hadronic component

FIGURE 1

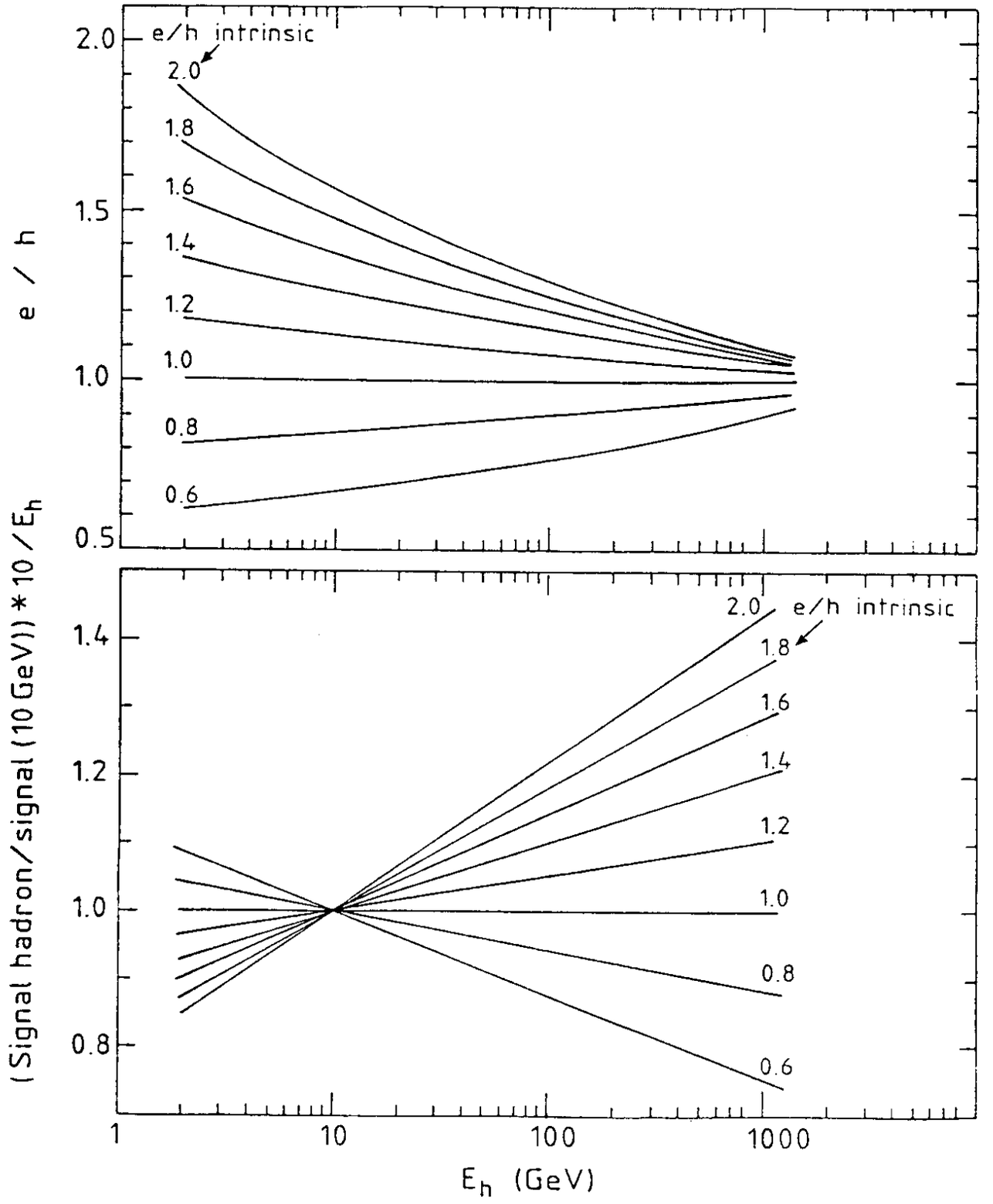
e/h intrinsic
2.0
1.8
1.6
1.4
1.2
1.0
0.8
0.6
e / h
2.0
1.5
1.0
0.5
(Signal hadron/signal (10 GeV)) * 10 / E_h
1.4
1.2
1.0
0.8
1
10
100
1000
E_h (GeV)

FIGURE 2

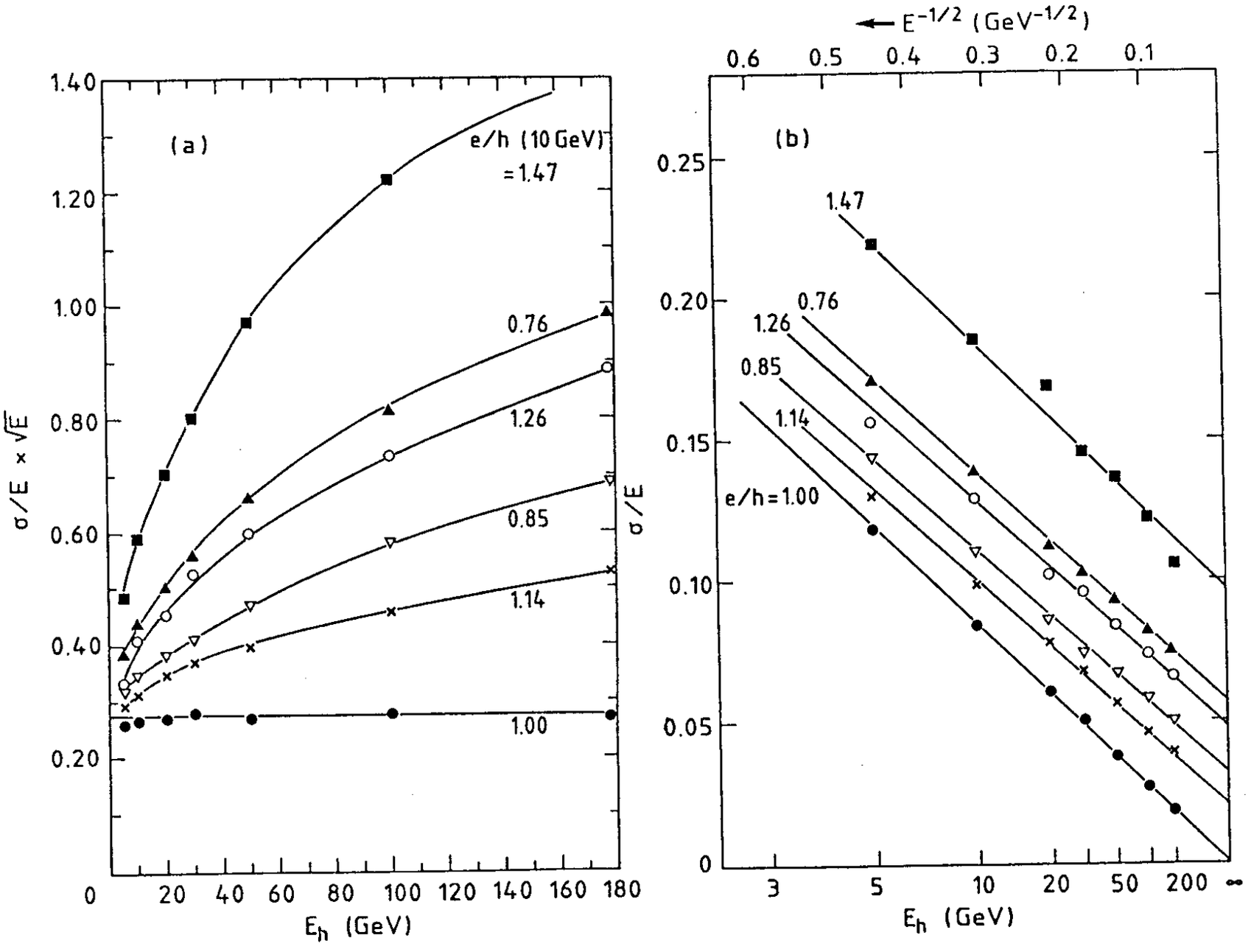
(a)
e/h (10 GeV) = 1.47
0.76
1.26
0.85
1.14
1.00
σ/E × √E
E_h (GeV)
(b)
E^-1/2 (GeV^-1/2)
1.47
0.76
1.26
0.85
1.14
e/h = 1.00
σ/E
E_h (GeV)

FIGURE 3

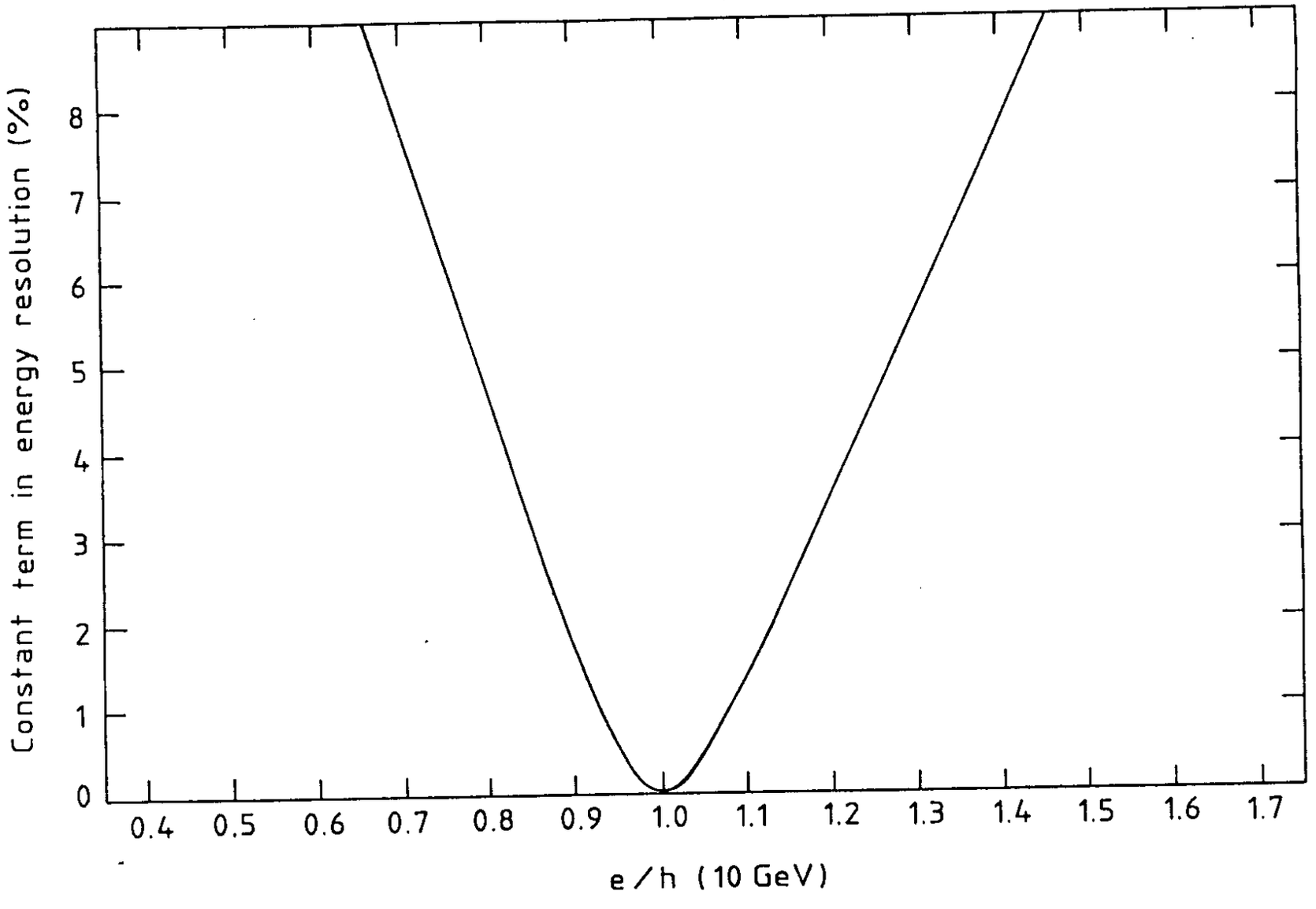
Constant term in energy resolution (%)
0
1
2
3
4
5
6
7
8
0.4
0.5
0.6
0.7
0.8
0.9
1.0
1.1
1.2
1.3
1.4
1.5
1.6
1.7
e / h (10 GeV)

FIGURE 4

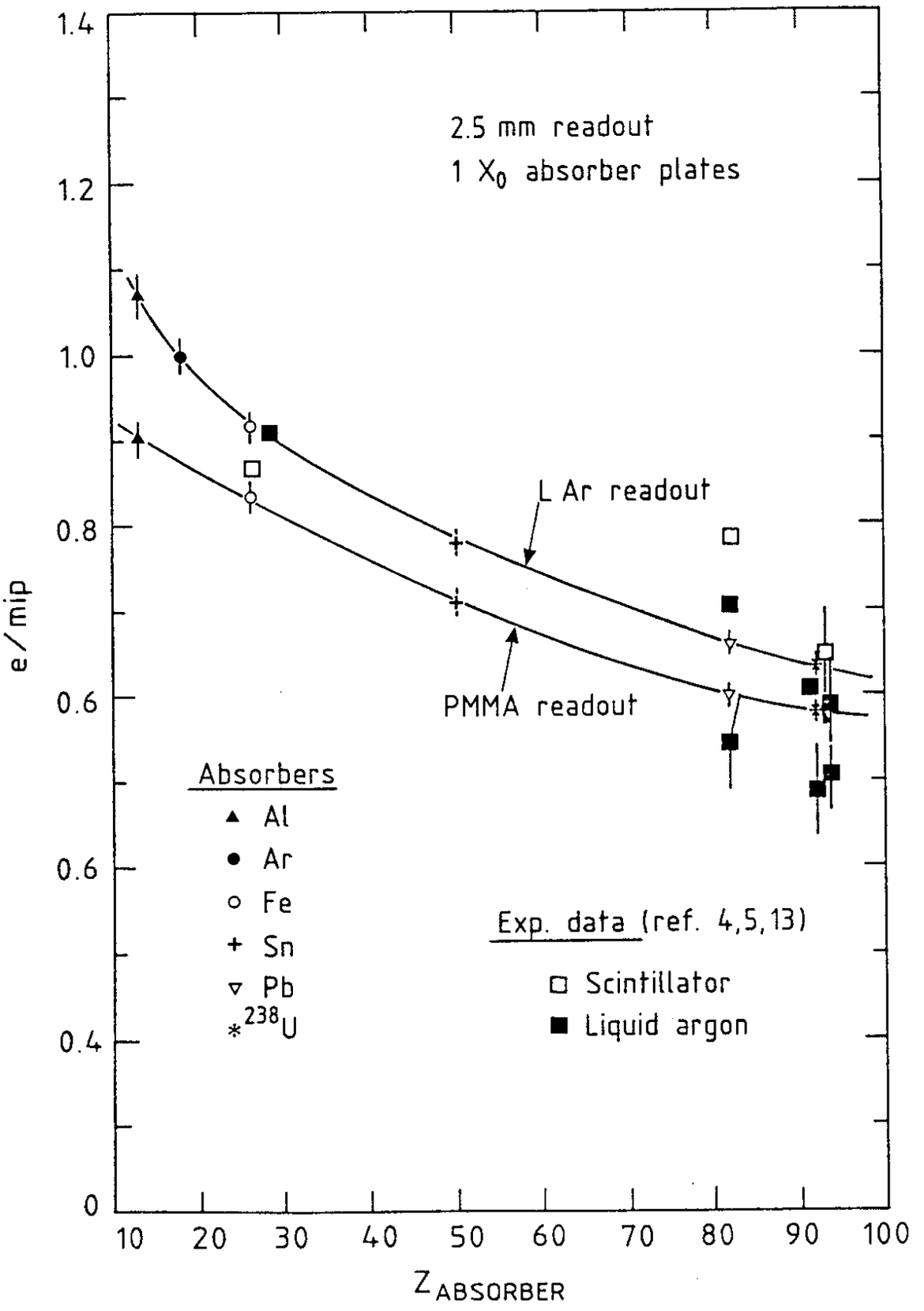
2.5 mm readout
1 X_0 absorber plates
L Ar readout
PMMA readout
Absorbers
Al
Ar
Fe
Sn
Pb
*^{238}U
Exp. data (ref. 4,5,13)
Scintillator
Liquid argon
e/mip
$Z_{ABSORBER}$
1.4
1.2
1.0
0.8
0.6
0.6
0.4
0
10
20
30
40
50
60
70
80
90
100

FIGURE 5

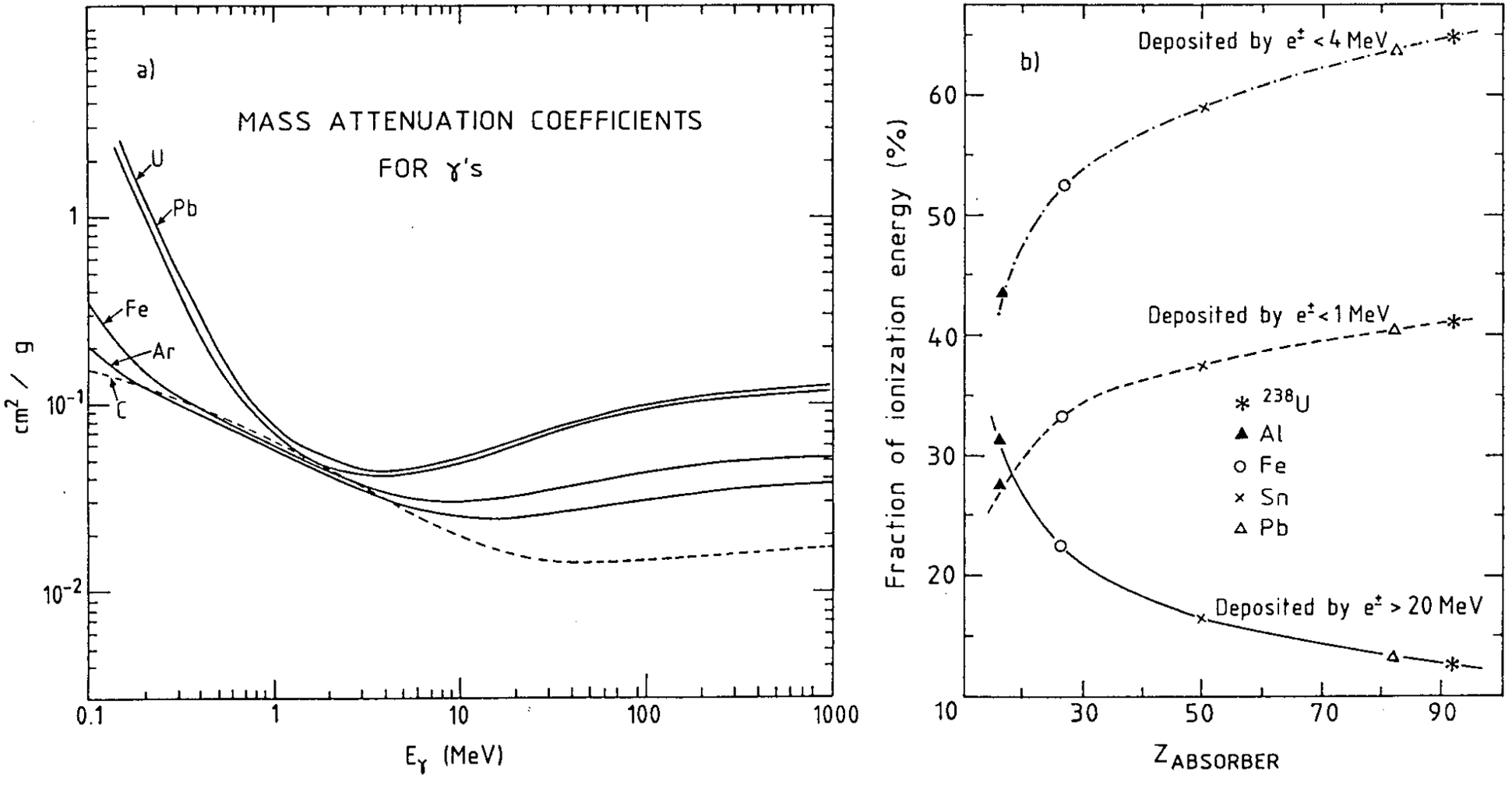
a)
MASS ATTENUATION COEFFICIENTS
FOR γ's
U
Pb
Fe
Ar
C
cm² / g
1
10⁻¹
10⁻²
0.1
1
10
100
1000
Eγ (MeV)
b)
Deposited by e± < 4 MeV
Deposited by e± < 1 MeV
Deposited by e± > 20 MeV
* 238U
▲ Al
o Fe
× Sn
△ Pb
Fraction of ionization energy (%)
60
50
40
30
20
10
30
50
70
90
ZABSORBER

FIGURE 6

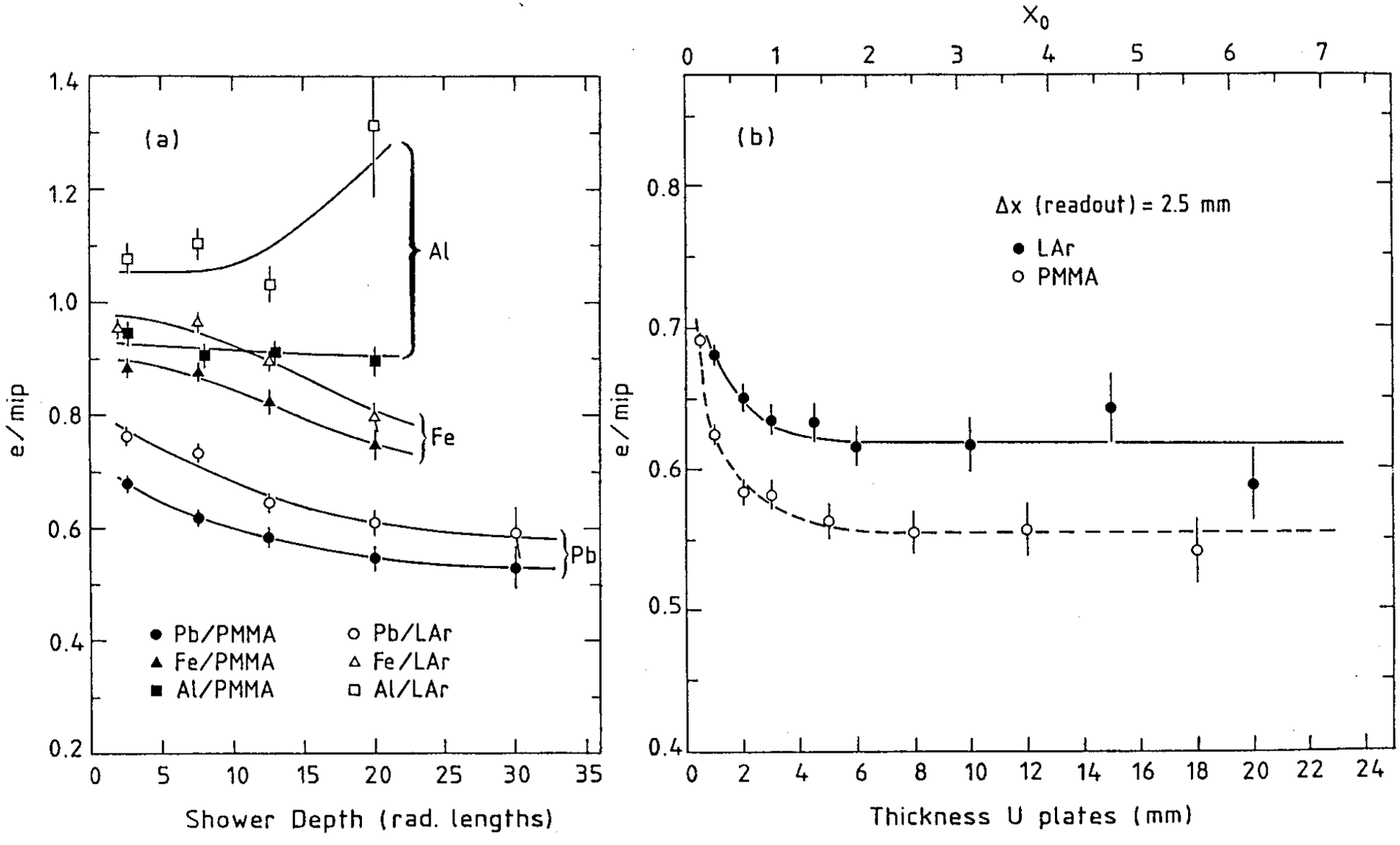
(a)
e / mip
Shower Depth (rad. lengths)
Al
Fe
Pb
Pb/PMMA
Fe/PMMA
Al/PMMA
Pb/LAr
Fe/LAr
Al/LAr
(b)
X_0
Δx (readout) = 2.5 mm
LAr
PMMA
e / mip
Thickness U plates (mm)

FIGURE 7

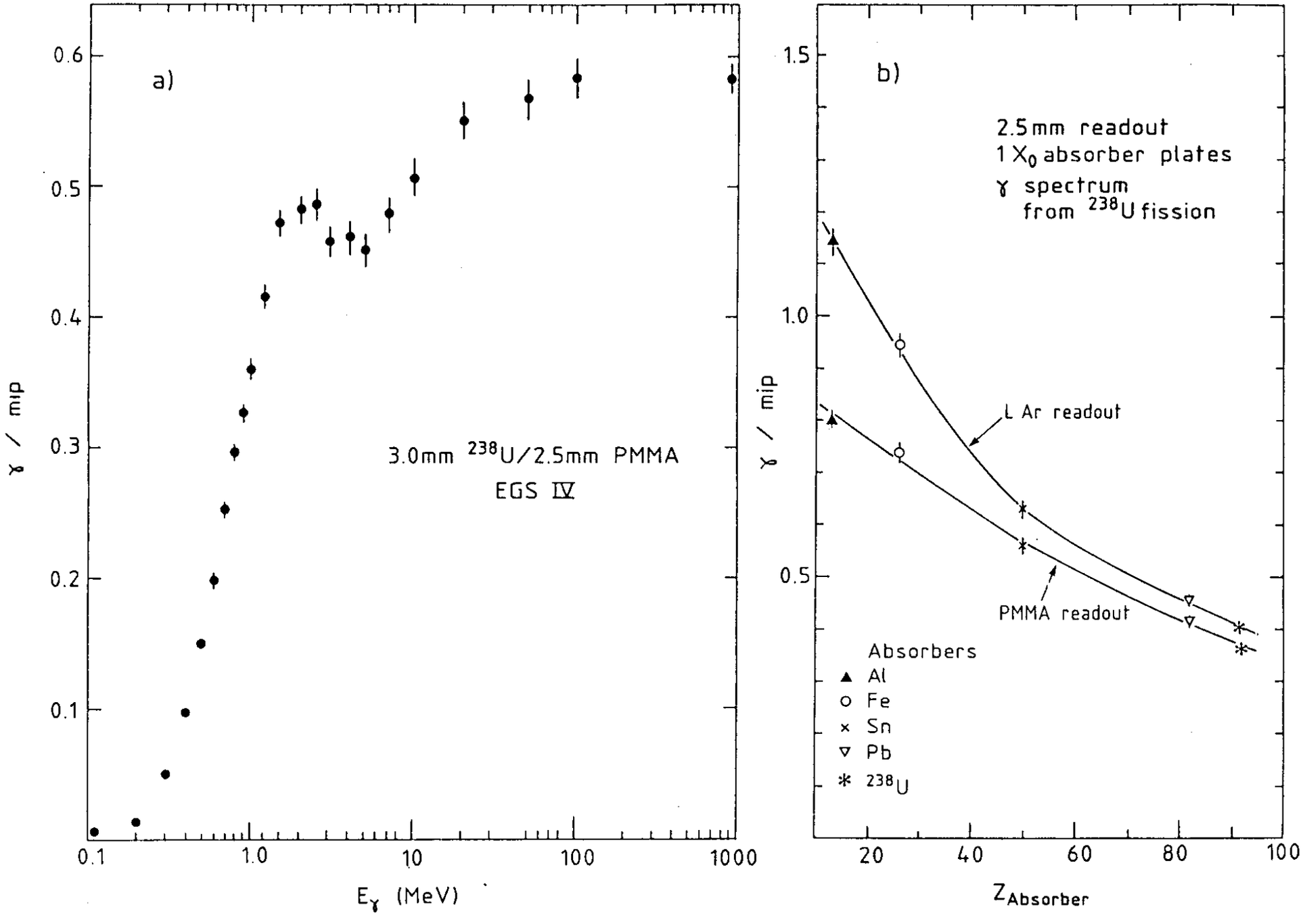
a)
3.0mm ^{238}U/2.5mm PMMA
EGS IV
γ / mip
E_γ (MeV)
0.1
1.0
10
100
1000
0.6
0.5
0.4
0.3
0.2
0.1
b)
2.5mm readout
1 X_0 absorber plates
γ spectrum
from ^{238}U fission
L Ar readout
PMMA readout
Absorbers
Al
Fe
Sn
Pb
^{238}U
γ / mip
$Z_{Absorber}$
1.5
1.0
0.5
20
40
60
80
100

FIGURE 8

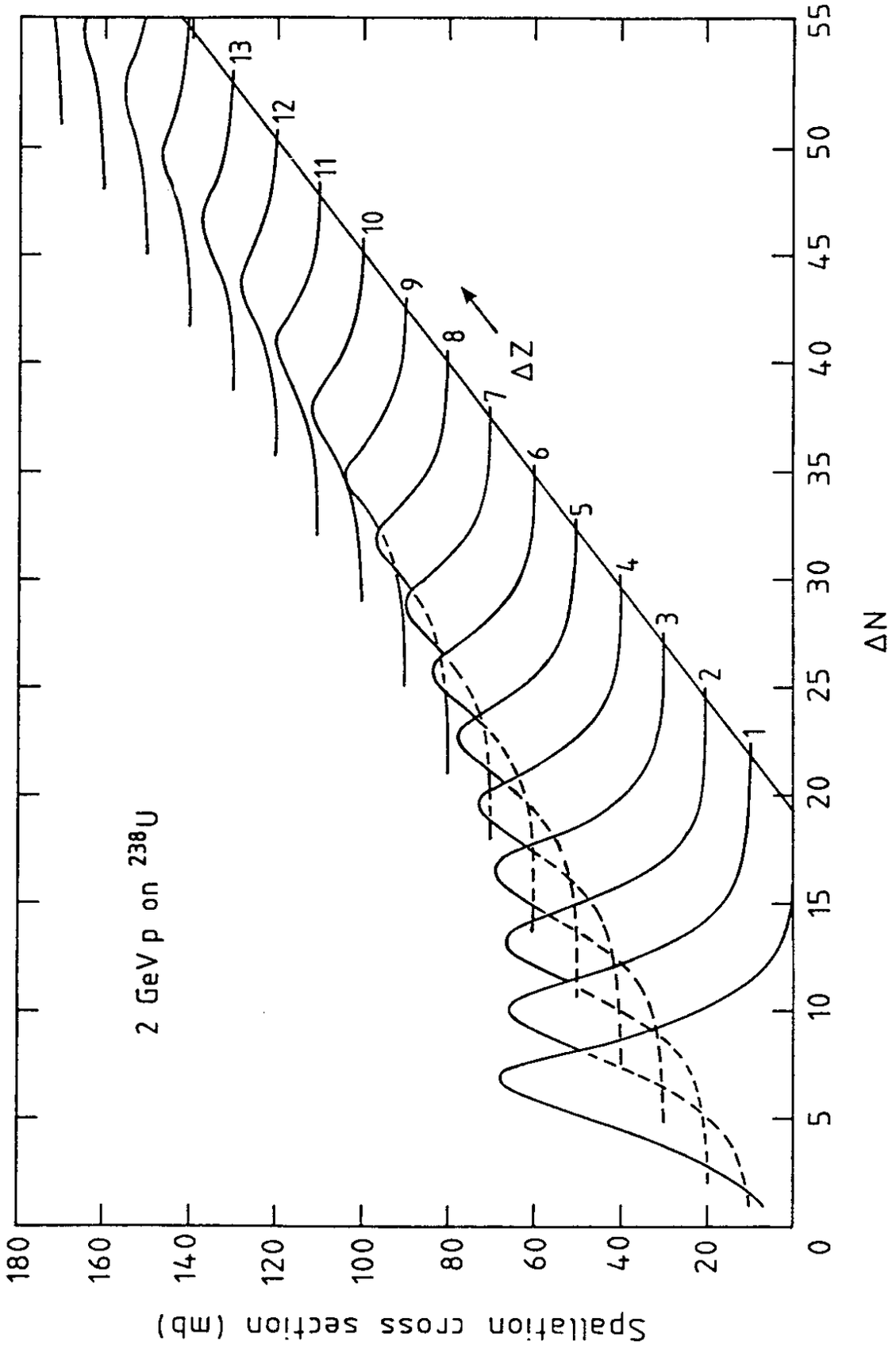
Spallation cross section (mb)
ΔN
2 GeV p on ^{238}U
ΔZ
1
2
3
4
5
6
7
8
9
10
11
12
13

FIGURE 9

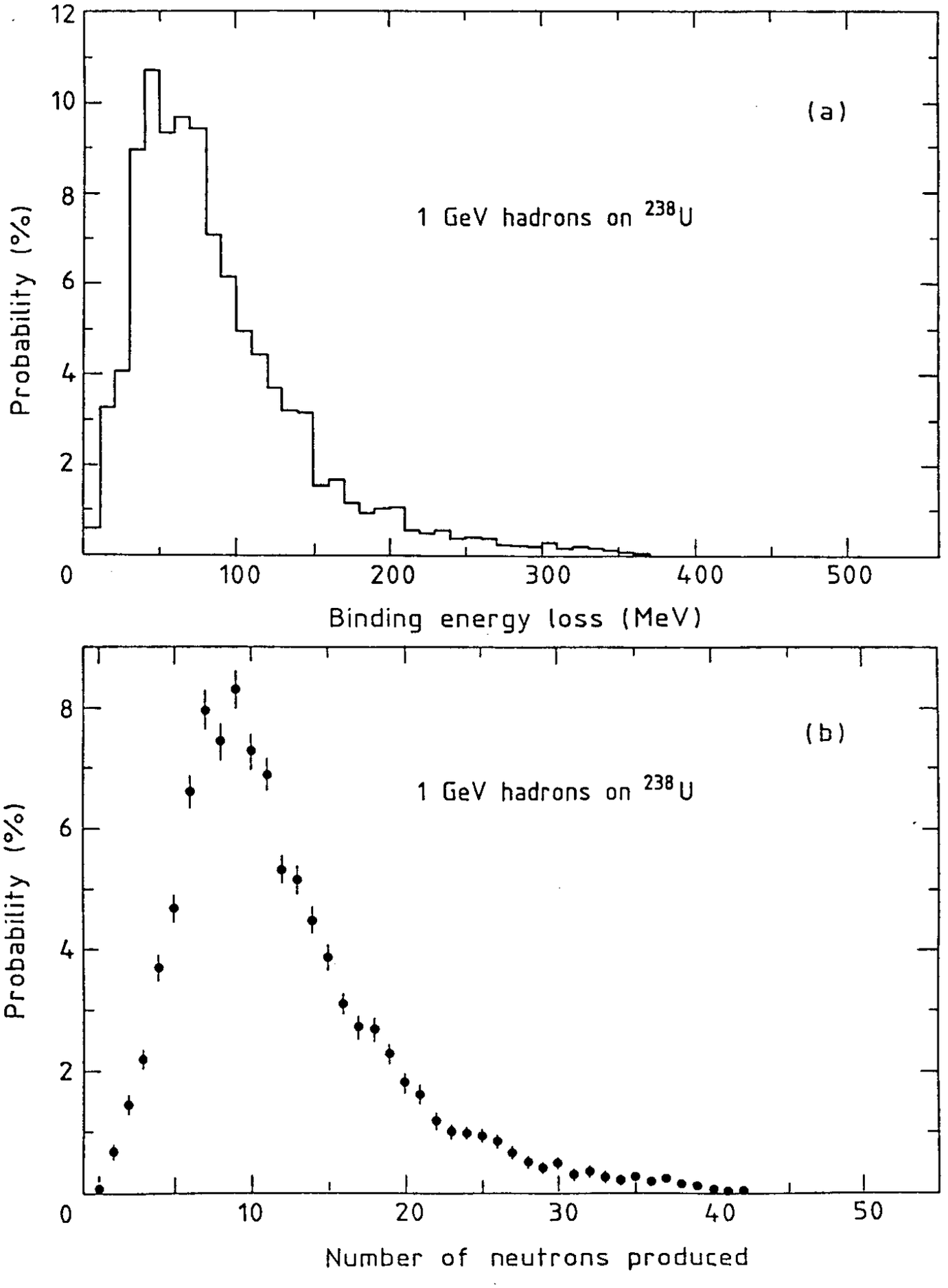
(a)
1 GeV hadrons on ^{238}U
Probability (%)
Binding energy loss (MeV)
0
2
4
6
8
10
12
100
200
300
400
500
(b)
1 GeV hadrons on ^{238}U
Probability (%)
Number of neutrons produced
0
2
4
6
8
10
20
30
40
50

FIGURE 10

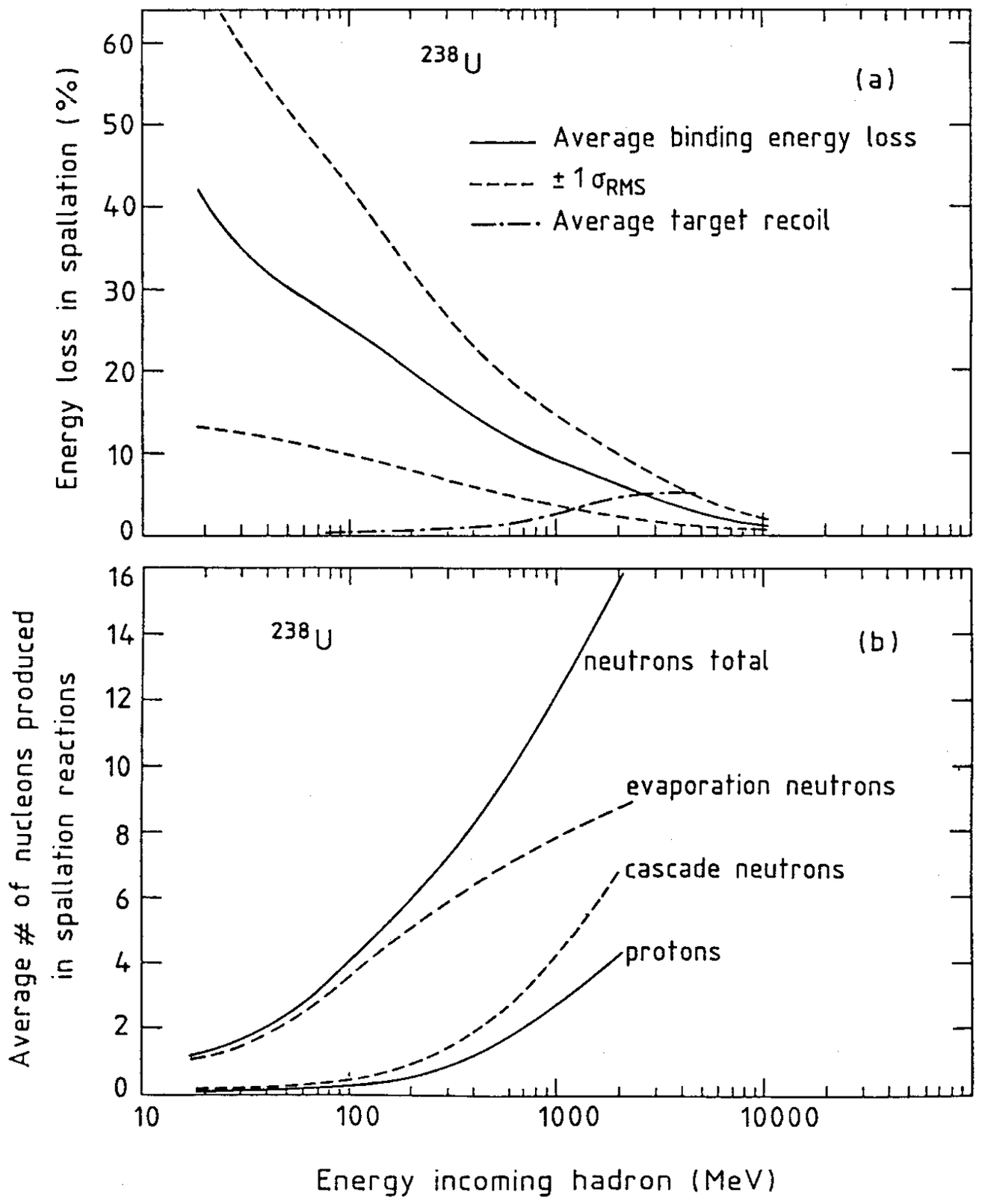
238U
(a)
Average binding energy loss
± 1 σRMS
Average target recoil
Energy loss in spallation (%)
60
50
40
30
20
10
0
238U
(b)
neutrons total
evaporation neutrons
cascade neutrons
protons
Average # of nucleons produced in spallation reactions
16
14
12
10
8
6
4
2
0
10
100
1000
10000
Energy incoming hadron (MeV)

FIGURE 11

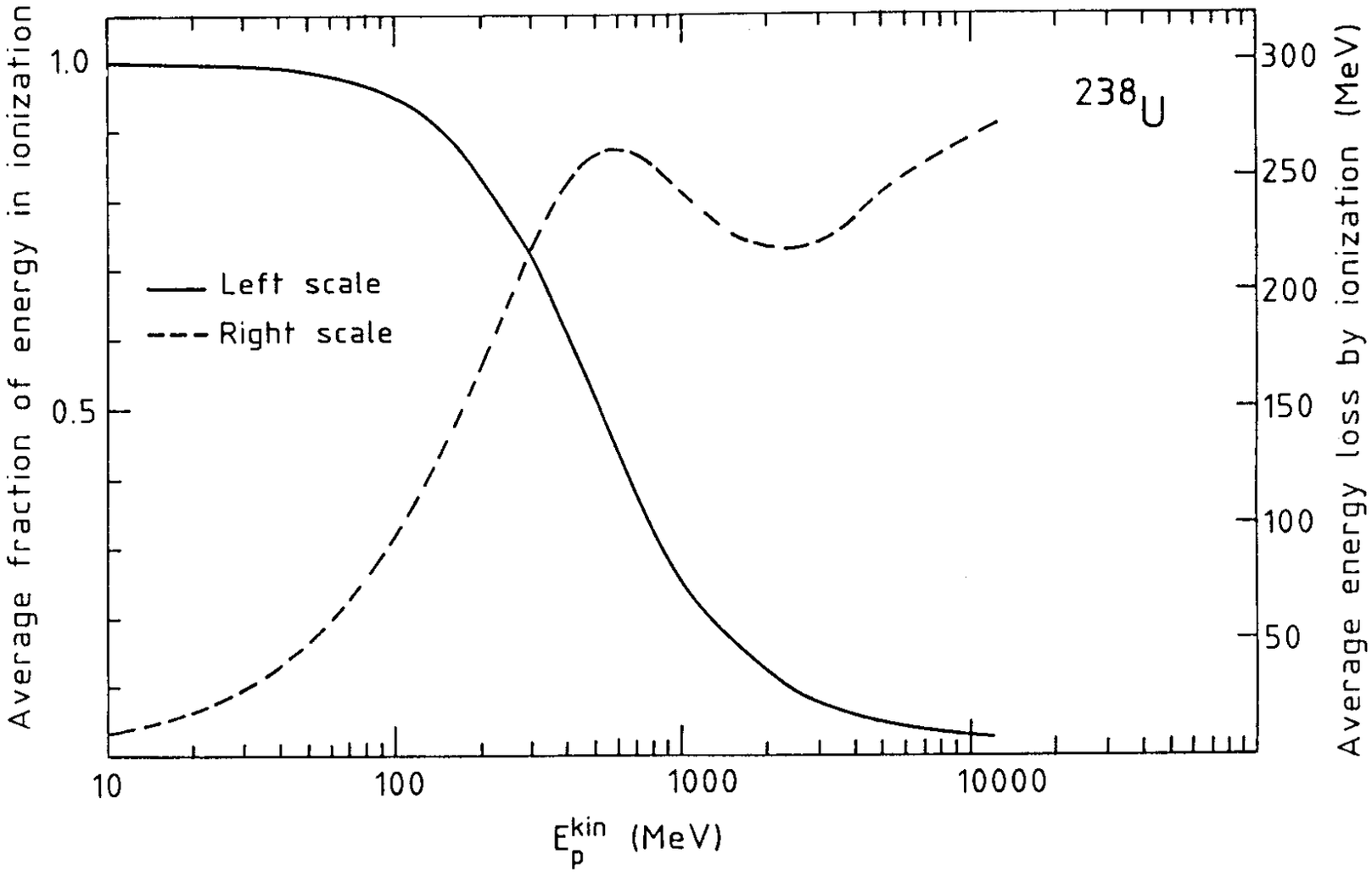
Average fraction of energy in ionization
1.0
0.5
Left scale
Right scale
^{238}U
300
250
200
150
100
50
Average energy loss by ionization (MeV)
10
100
1000
10000
E_p^{kin} (MeV)

FIGURE 12

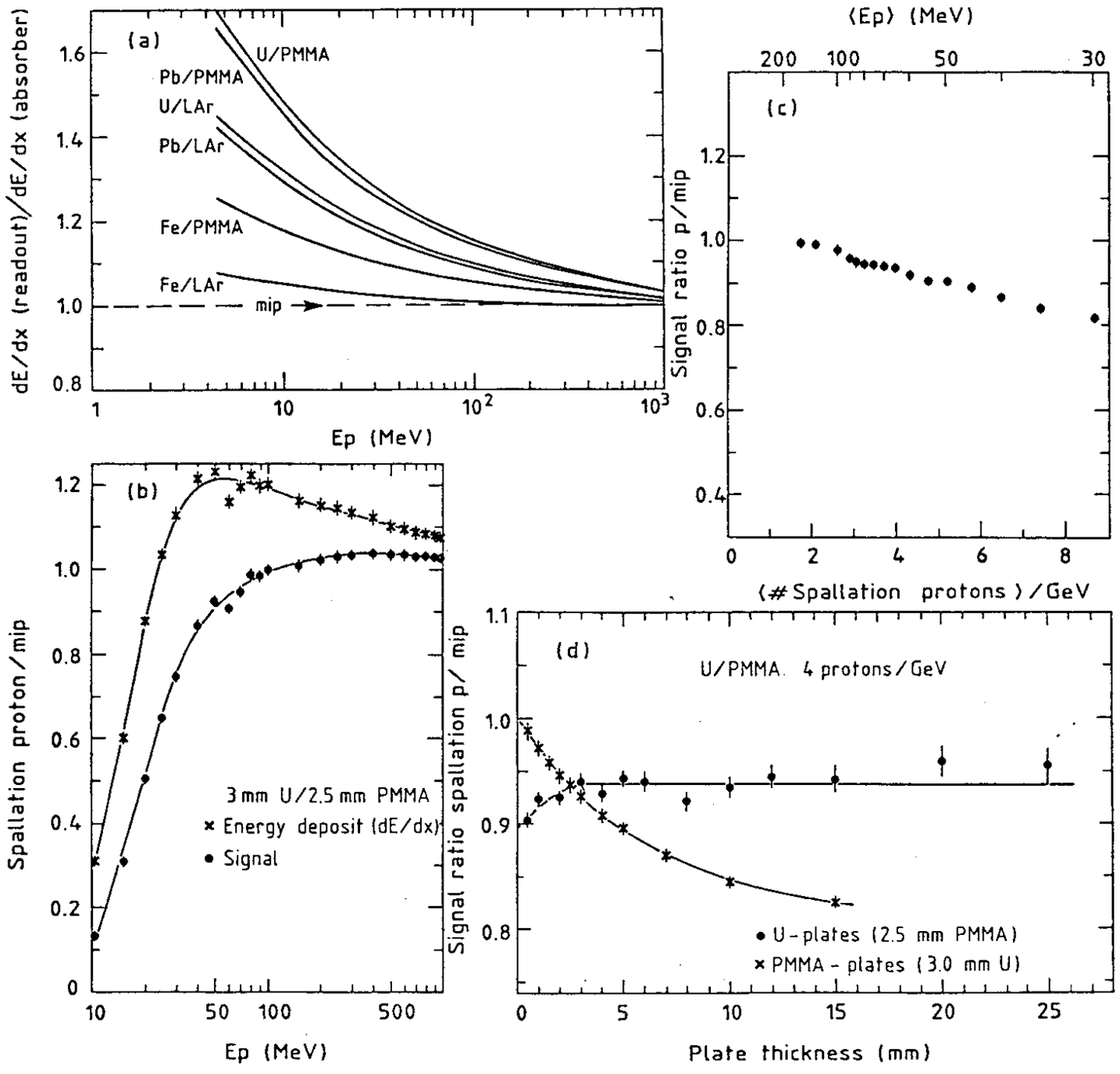
(a)
U/PMMA
Pb/PMMA
U/LAr
Pb/LAr
Fe/PMMA
Fe/LAr
mip
dE/dx (readout)/dE/dx (absorber)
Ep (MeV)
(b)
3 mm U/2.5 mm PMMA
× Energy deposit (dE/dx)
• Signal
Spallation proton/mip
Ep (MeV)
(c)
⟨Ep⟩ (MeV)
Signal ratio p/mip
(# Spallation protons)/GeV
(d)
U/PMMA. 4 protons/GeV
• U-plates (2.5 mm PMMA)
× PMMA-plates (3.0 mm U)
Signal ratio spallation p/mip
Plate thickness (mm)

FIGURE 13

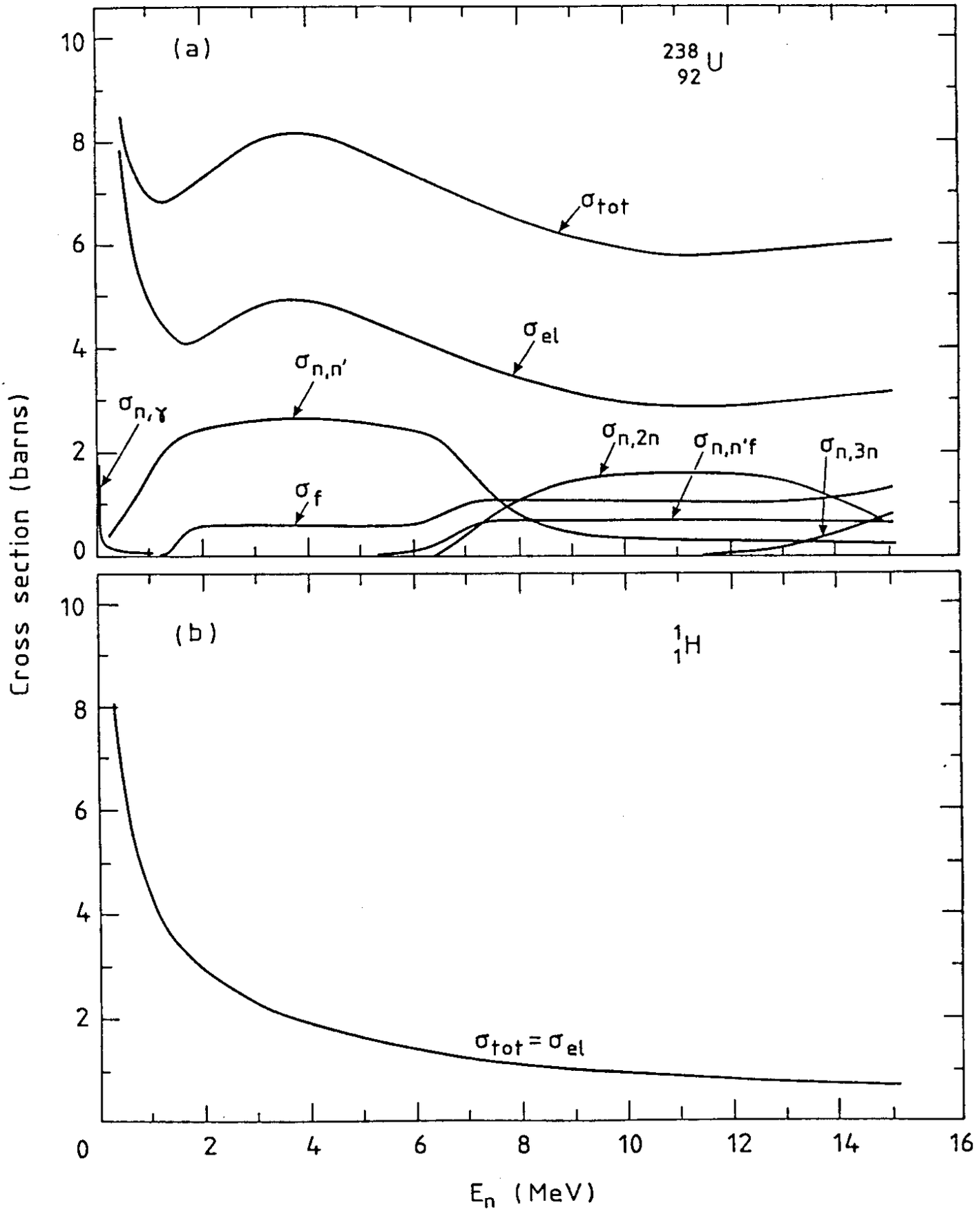
(a)
$^{238}_{92}U$
σ_{tot}
σ_{el}
$\sigma_{n,n'}$
$\sigma_{n,\gamma}$
$\sigma_{n,2n}$
$\sigma_{n,n'f}$
$\sigma_{n,3n}$
σ_f
(b)
$^{1}_{1}H$
$\sigma_{tot} = \sigma_{el}$
Cross section (barns)
E_n (MeV)
0
2
4
6
8
10
12
14
16

FIGURE 14

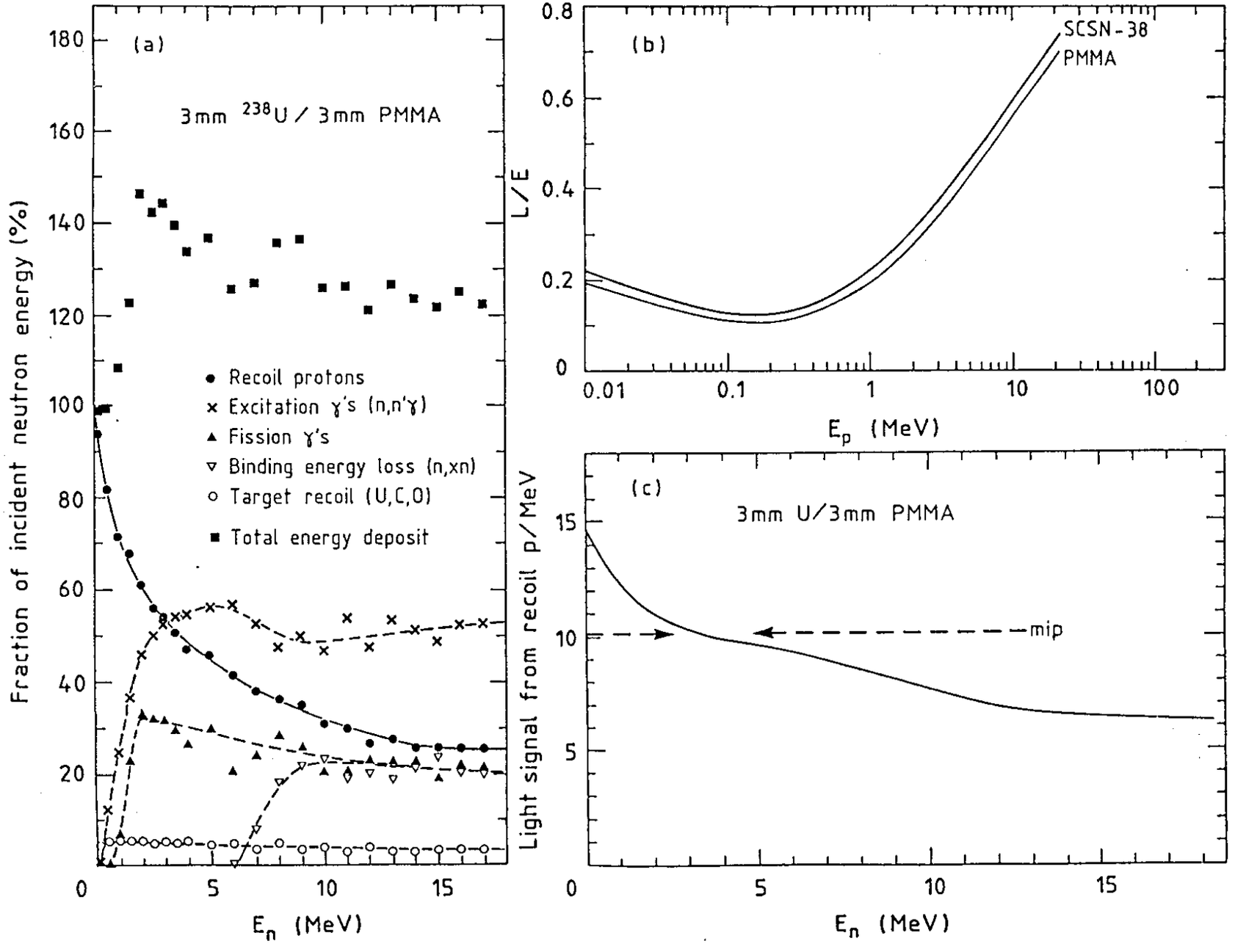
(a)
3mm ^{238}U / 3mm PMMA
Recoil protons
Excitation γ's (n,n'γ)
Fission γ's
Binding energy loss (n,xn)
Target recoil (U,C,O)
Total energy deposit
Fraction of incident neutron energy (%)
E_n (MeV)
(b)
SCSN-38
PMMA
L/E
E_p (MeV)
(c)
3mm U/3mm PMMA
mip
Light signal from recoil p/MeV
E_n (MeV)

FIGURE 15

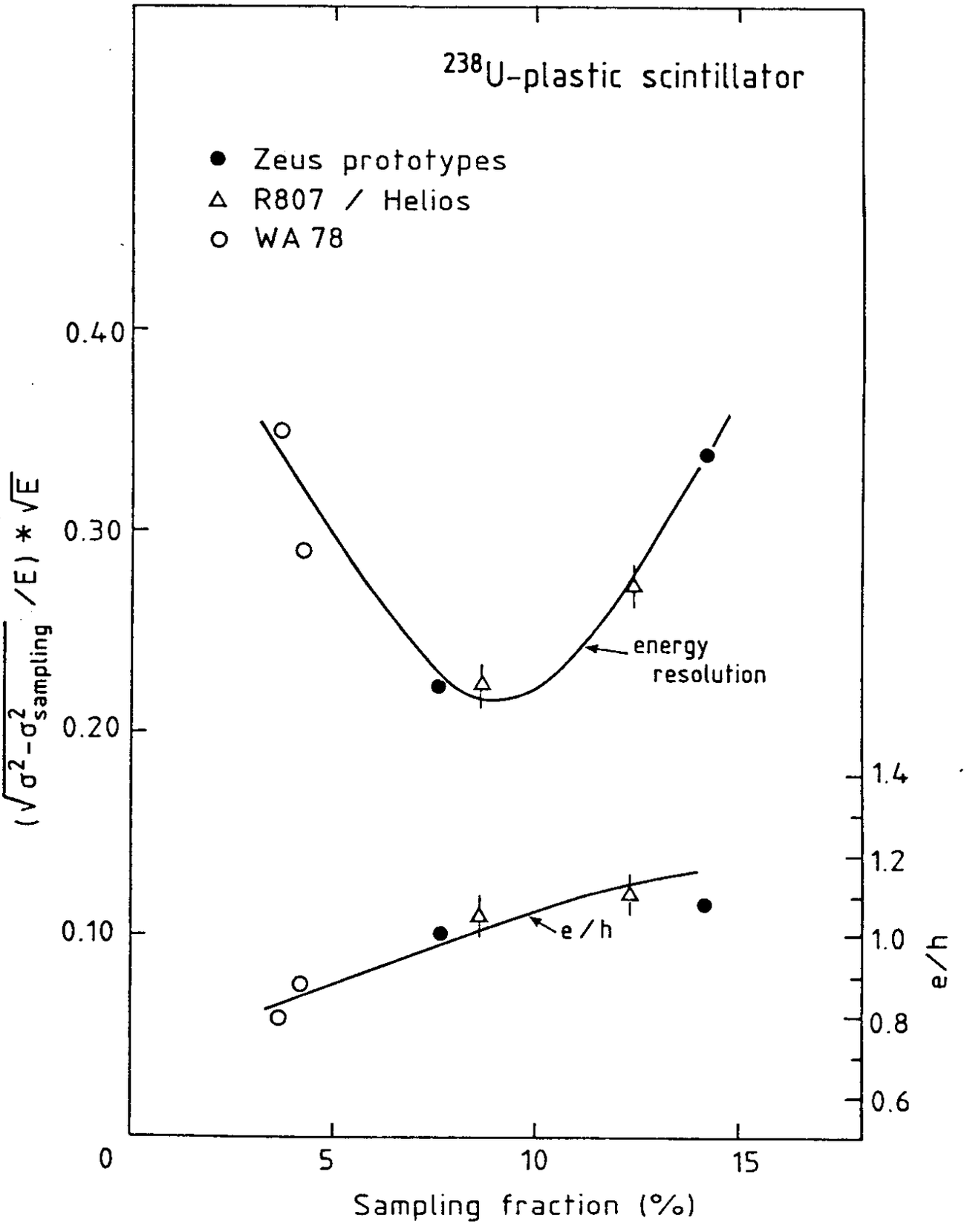
^{238}U-plastic scintillator
Zeus prototypes
R807 / Helios
WA 78
energy resolution
e/h
$(\sqrt{\sigma^2-\sigma^2_{sampling}}/E) * \sqrt{E}$
Sampling fraction (%)
0.40
0.30
0.20
0.10
0
5
10
15
1.4
1.2
1.0
0.8
0.6
e/h

FIGURE 16

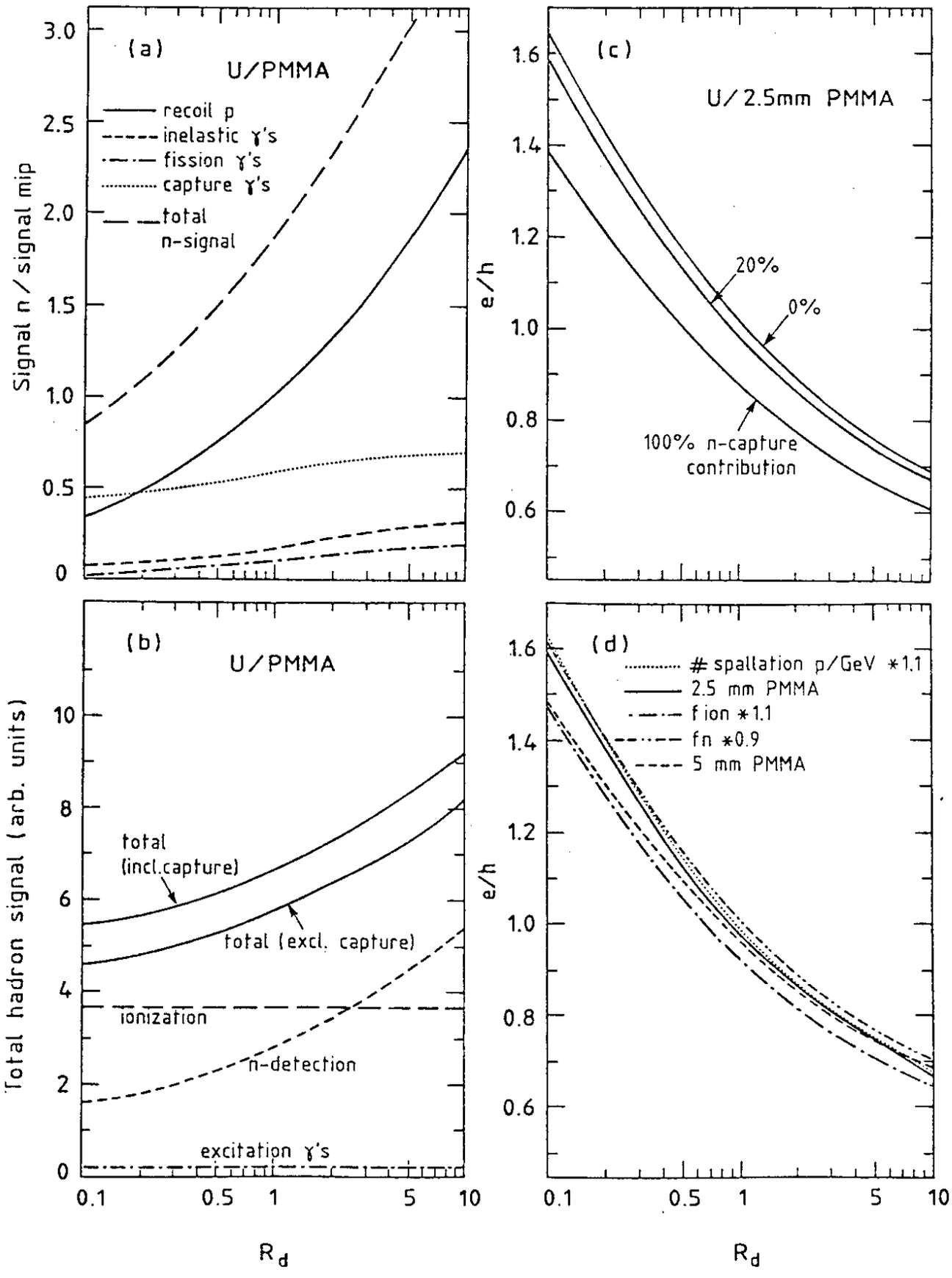
(a)
U/PMMA
recoil p
inelastic γ's
fission γ's
capture γ's
total n-signal
Signal n / signal mip
(b)
U/PMMA
total (incl.capture)
total (excl. capture)
ionization
n-detection
excitation γ's
Total hadron signal (arb. units)
R_d
(c)
U/2.5mm PMMA
20%
0%
100% n-capture contribution
e/h
(d)
spallation p/GeV *1.1
2.5 mm PMMA
f ion *1.1
fn *0.9
5 mm PMMA
e/h
R_d

FIGURE 17

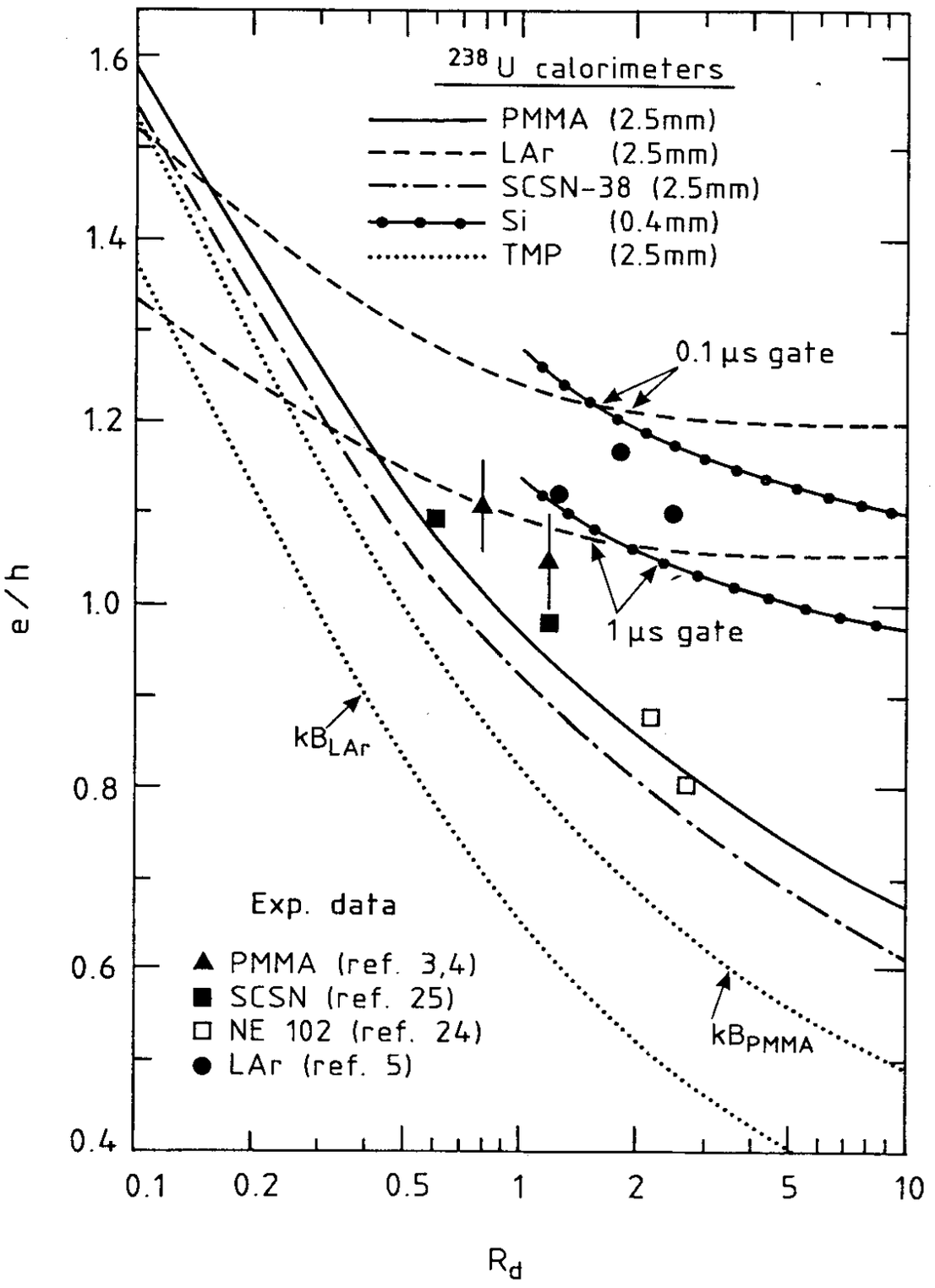
^{238}U calorimeters
PMMA (2.5mm)
LAr (2.5mm)
SCSN-38 (2.5mm)
Si (0.4mm)
TMP (2.5mm)
0.1 µs gate
1 µs gate
kB$_{LAr}$
kB$_{PMMA}$
Exp. data
PMMA (ref. 3,4)
SCSN (ref. 25)
NE 102 (ref. 24)
LAr (ref. 5)
e / h
R$_d$
1.6
1.4
1.2
1.0
0.8
0.6
0.4
0.1
0.2
0.5
1
2
5
10

FIGURE 18

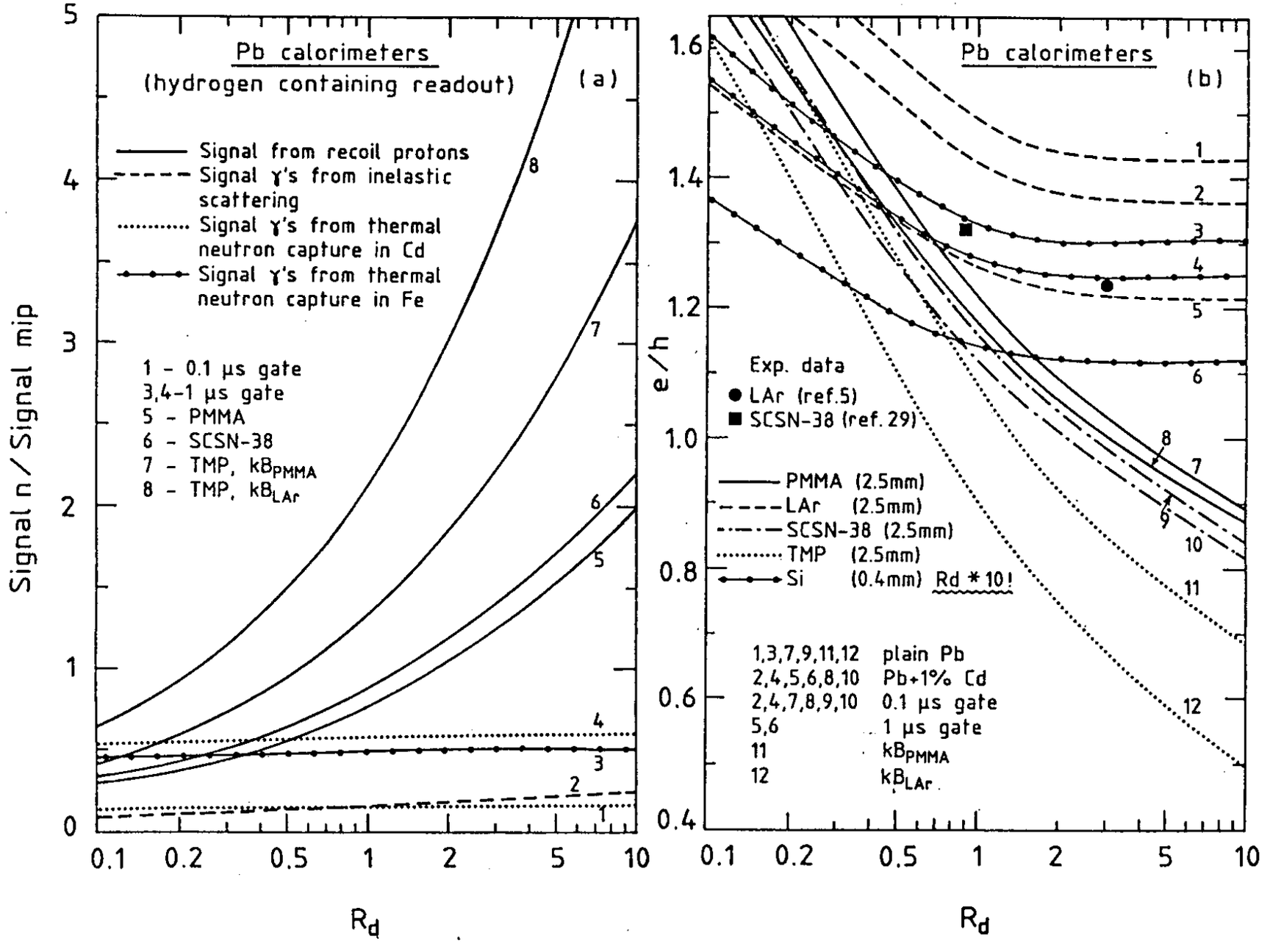
Pb calorimeters
(hydrogen containing readout)
(a)
Signal from recoil protons
Signal γ's from inelastic scattering
Signal γ's from thermal neutron capture in Cd
Signal γ's from thermal neutron capture in Fe
1 - 0.1 μs gate
3,4-1 μs gate
5 - PMMA
6 - SCSN-38
7 - TMP, kB_PMMA
8 - TMP, kB_LAr
Signal n / Signal mip
R_d
Pb calorimeters
(b)
Exp. data
LAr (ref.5)
SCSN-38 (ref.29)
PMMA (2.5mm)
LAr (2.5mm)
SCSN-38 (2.5mm)
TMP (2.5mm)
Si (0.4mm) Rd * 10!
1,3,7,9,11,12 plain Pb
2,4,5,6,8,10 Pb+1% Cd
2,4,7,8,9,10 0.1 μs gate
5,6 1 μs gate
11 kB_PMMA
12 kB_LAr
e / h
R_d

FIGURE 19

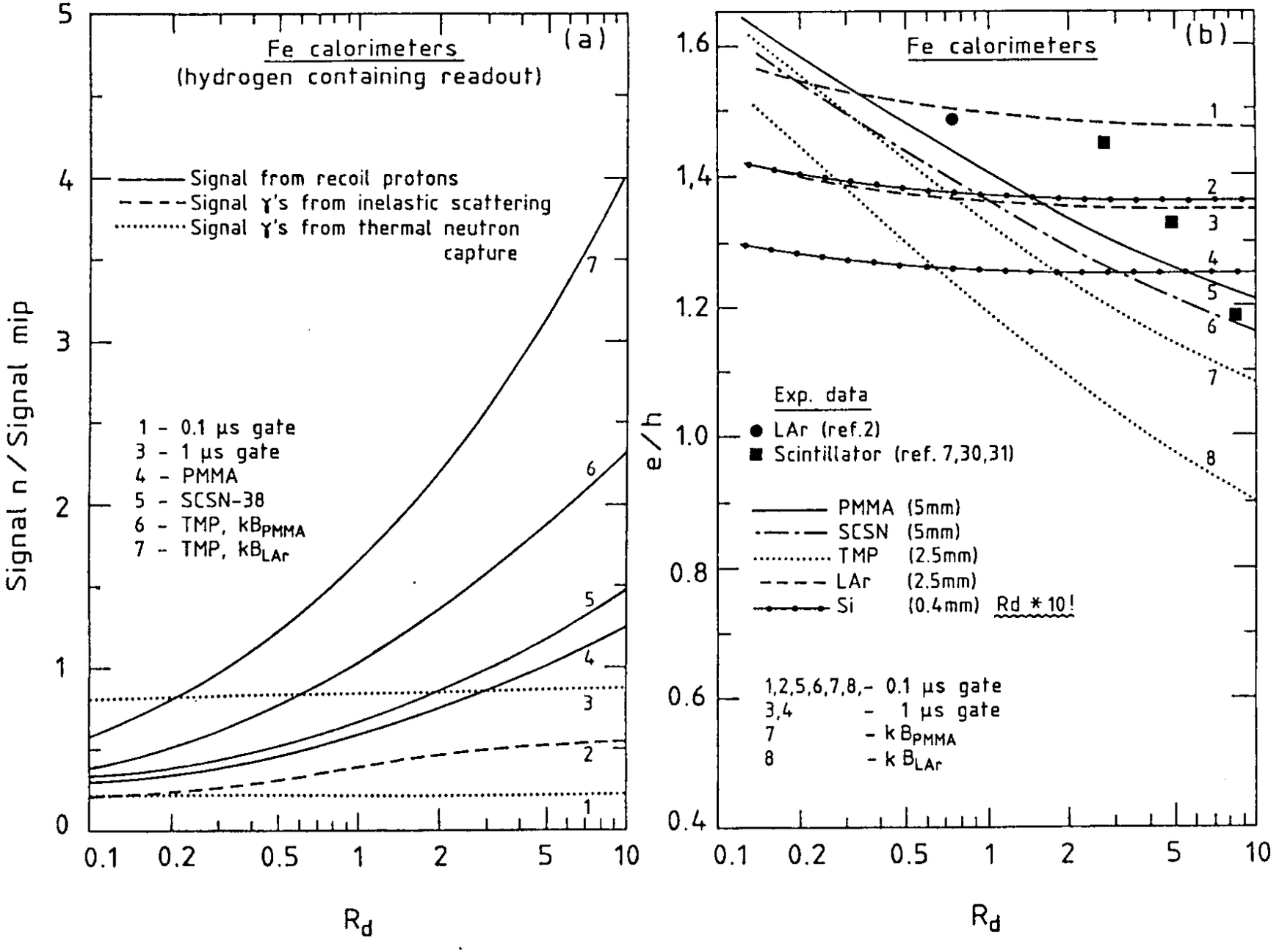
Fe calorimeters
(hydrogen containing readout)
(a)
Signal from recoil protons
Signal γ's from inelastic scattering
Signal γ's from thermal neutron capture
1 - 0.1 μs gate
3 - 1 μs gate
4 - PMMA
5 - SCSN-38
6 - TMP, kB_PMMA
7 - TMP, kB_LAr
Signal n / Signal mip
R_d
Fe calorimeters
(b)
Exp. data
LAr (ref.2)
Scintillator (ref. 7,30,31)
PMMA (5mm)
SCSN (5mm)
TMP (2.5mm)
LAr (2.5mm)
Si (0.4mm) Rd * 10!
1,2,5,6,7,8,- 0.1 μs gate
3,4 - 1 μs gate
7 - k B_PMMA
8 - k B_LAr
e / h
R_d

FIGURE 20

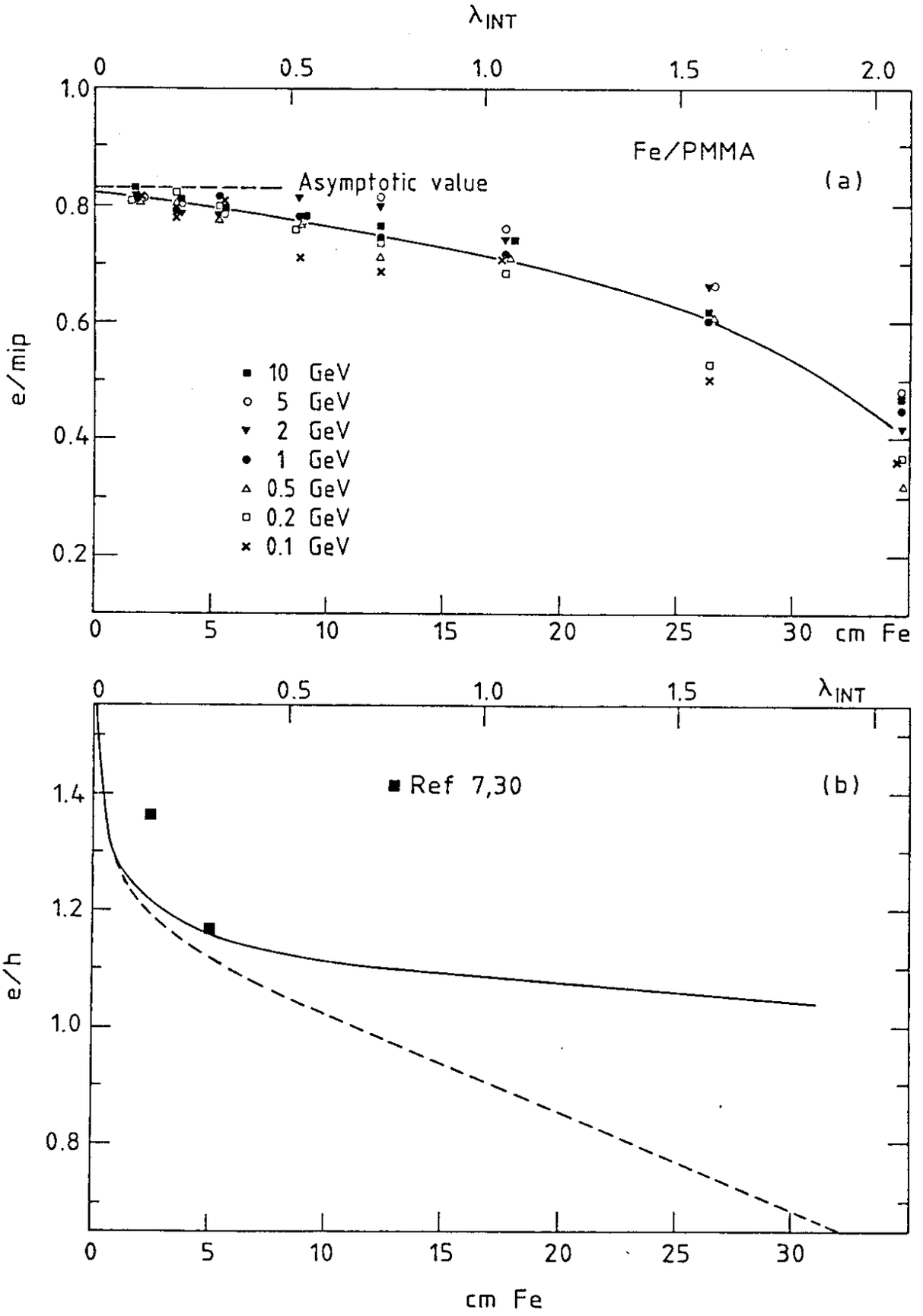
λINT
0
0.5
1.0
1.5
2.0
Fe/PMMA
(a)
Asymptotic value
e/mip
1.0
0.8
0.6
0.4
0.2
10 GeV
5 GeV
2 GeV
1 GeV
0.5 GeV
0.2 GeV
0.1 GeV
0
5
10
15
20
25
30
cm Fe
λINT
Ref 7,30
(b)
e/h
1.4
1.2
1.0
0.8
cm Fe

FIGURE 21

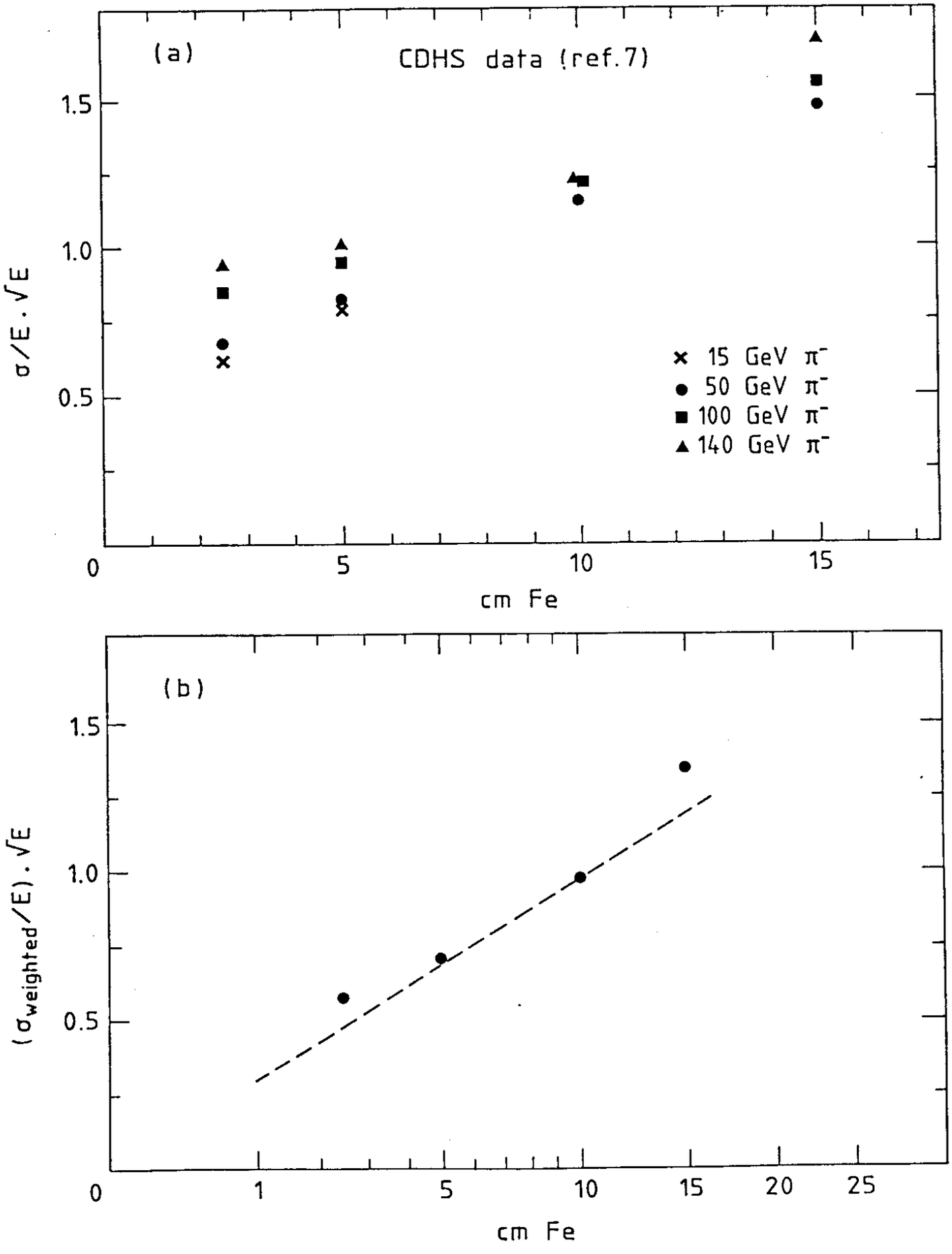
(a)
CDHS data (ref.7)
σ/E . √E
1.5
1.0
0.5
0
5
10
15
cm Fe
× 15 GeV π⁻
● 50 GeV π⁻
■ 100 GeV π⁻
▲ 140 GeV π⁻
(b)
(σweighted/E) . √E
1.5
1.0
0.5
0
1
5
10
15
20
25
cm Fe

FIGURE 22

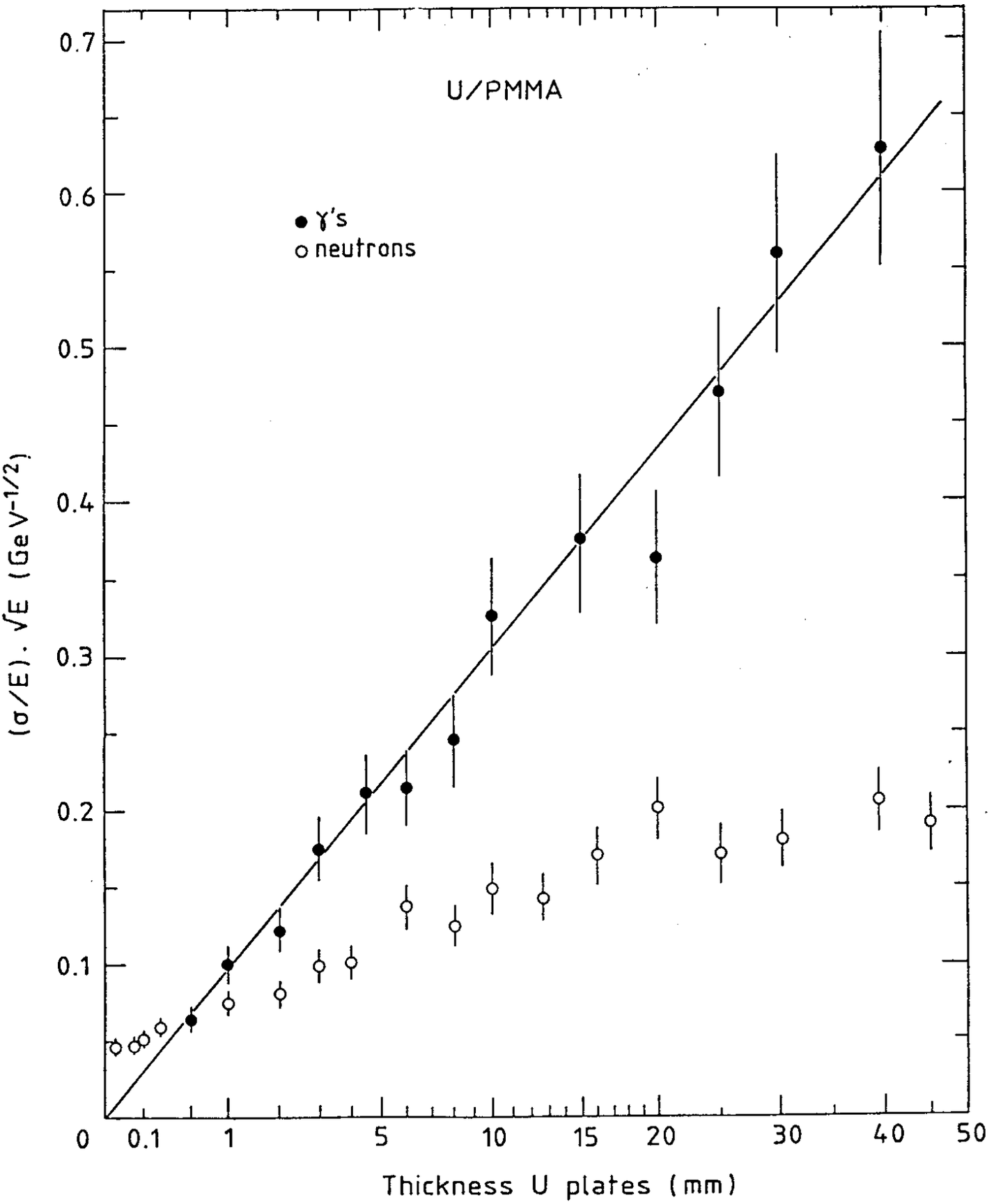
U/PMMA
● γ's
○ neutrons
(σ/E). √E (GeV^-1/2)
0.7
0.6
0.5
0.4
0.3
0.2
0.1
0
0.1
1
5
10
15
20
30
40
50
Thickness U plates (mm)

FIGURE 23

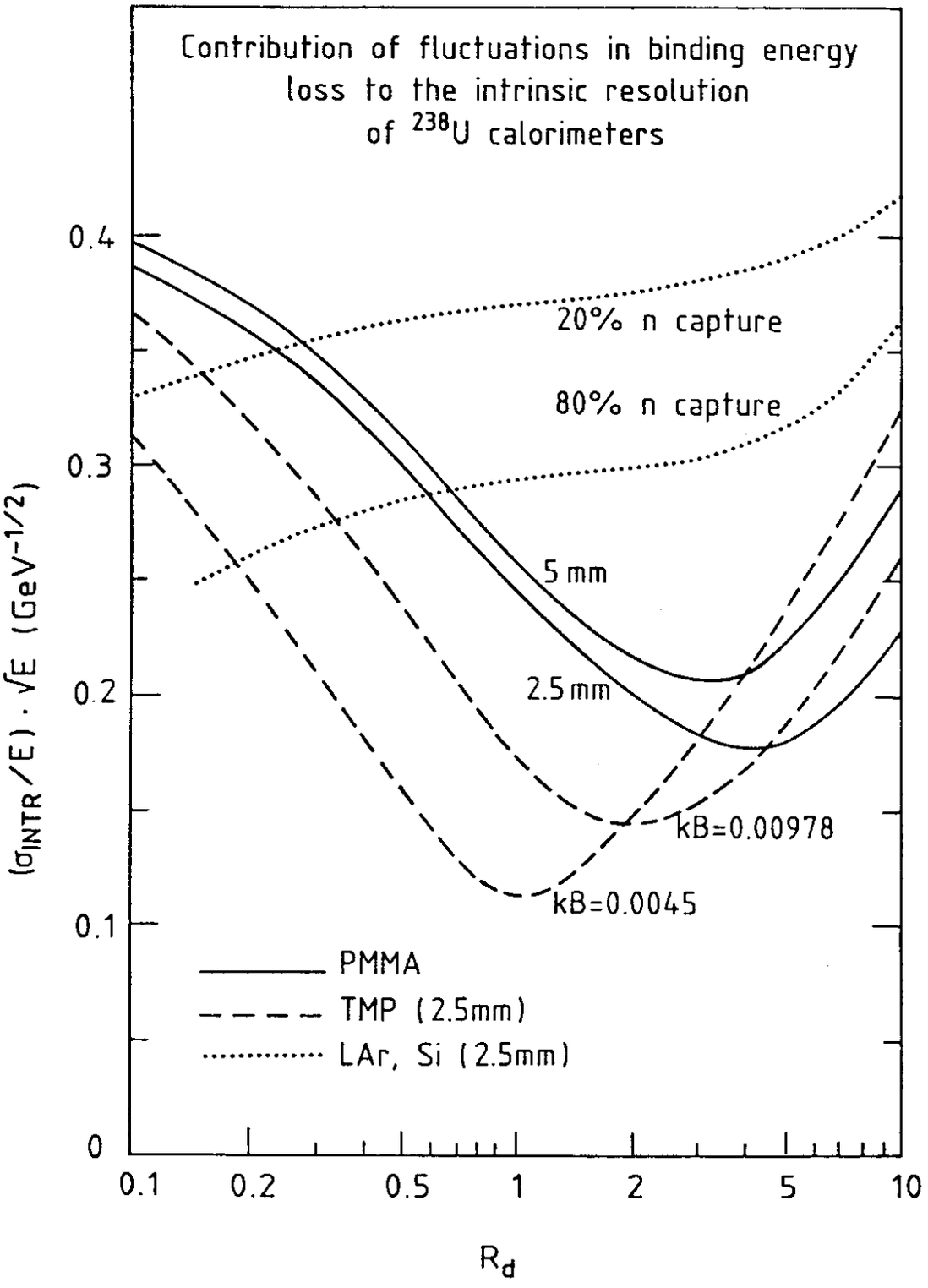
Contribution of fluctuations in binding energy loss to the intrinsic resolution of ^{238}U calorimeters
$(\sigma_{INTR}/E)\cdot\sqrt{E}$ (GeV$^{-1/2}$)
0.4
0.3
0.2
0.1
0
20% n capture
80% n capture
5 mm
2.5 mm
kB=0.00978
kB=0.0045
PMMA
TMP (2.5mm)
LAr, Si (2.5mm)
0.1
0.2
0.5
1
2
5
10
R_d

FIGURE 24

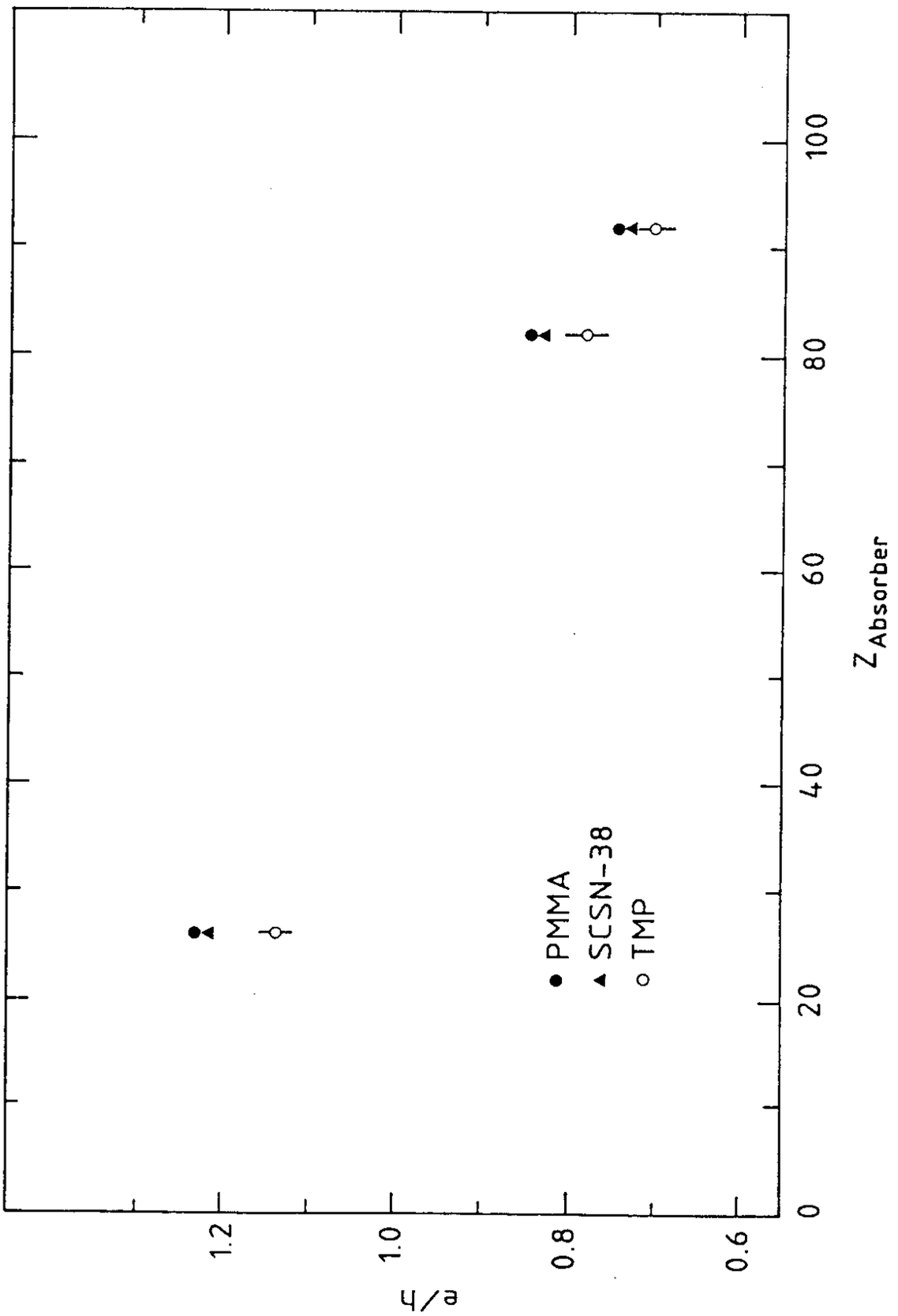

FIGURE 25

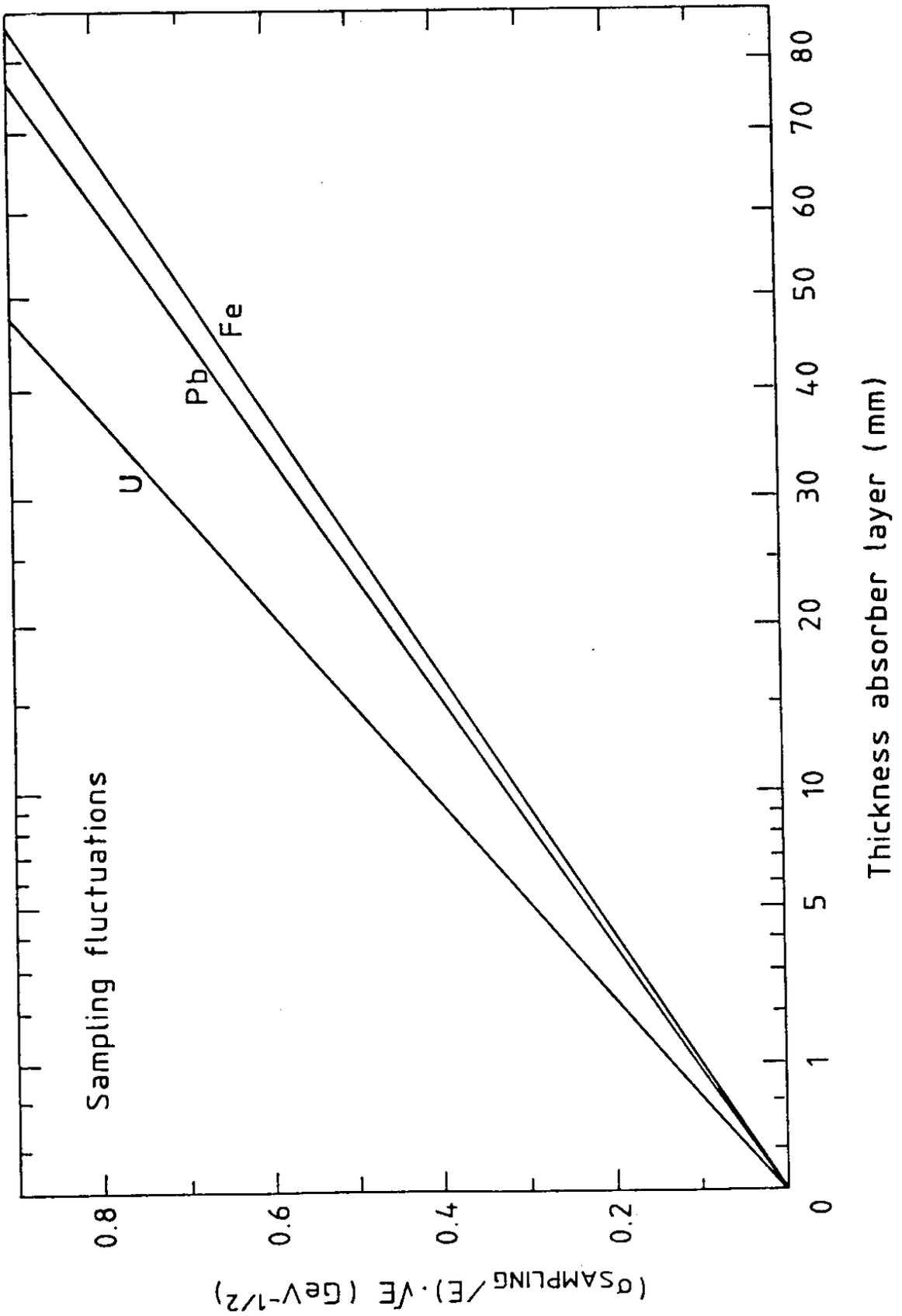
Sampling fluctuations
U
Pb
Fe
0.8
0.6
0.4
0.2
0
1
5
10
20
30
40
50
60
70
80
Thickness absorber layer (mm)
(σSAMPLING/E)·√E (GeV-1/2)

FIGURE 26

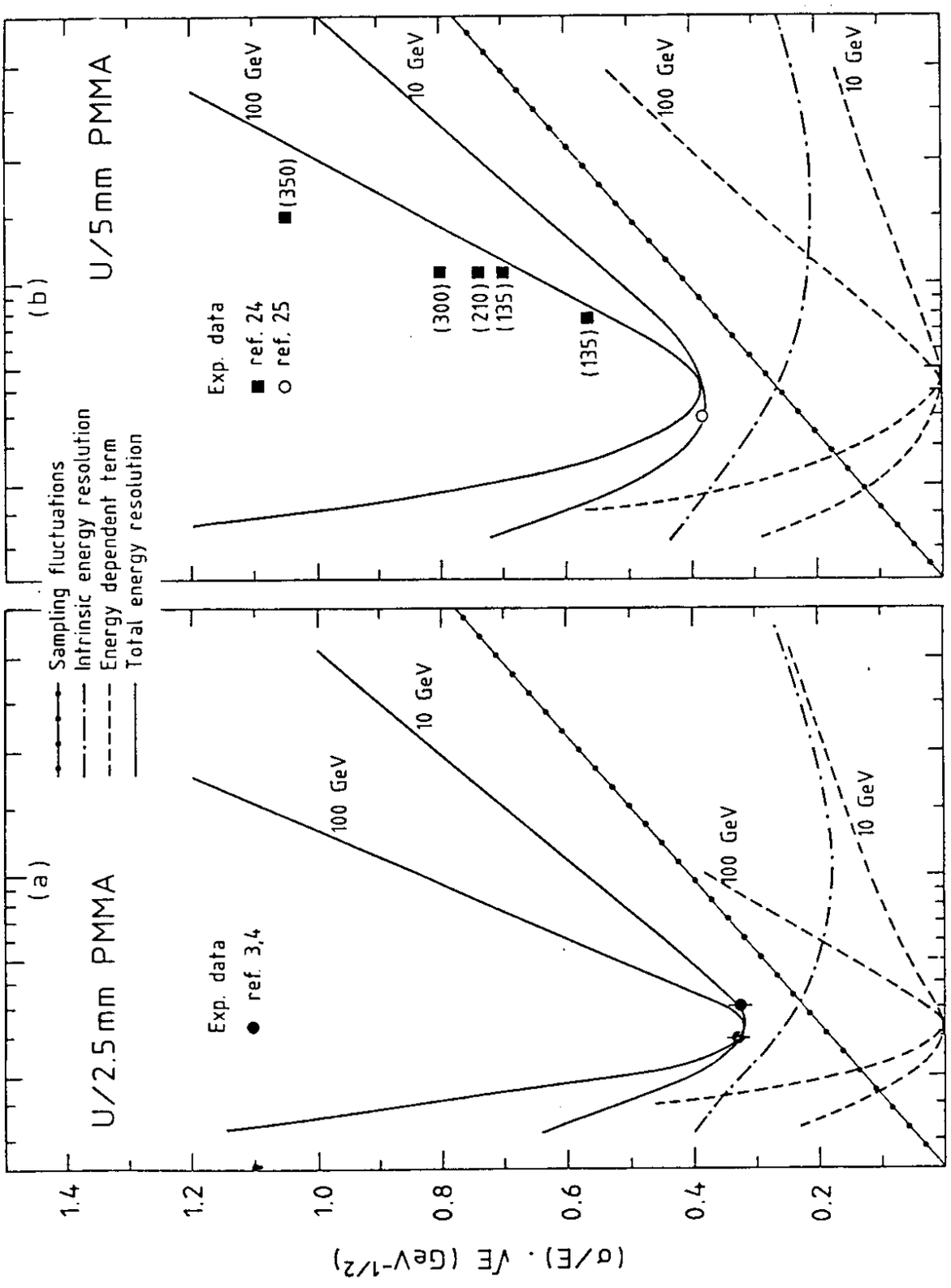
(a)
U/2.5 mm PMMA
(b)
U/5 mm PMMA
Sampling fluctuations
Intrinsic energy resolution
Energy dependent term
Total energy resolution
Exp. data
ref. 3,4
ref. 24
ref. 25
100 GeV
10 GeV
(350)
(300)
(210)
(135)
(σ/E) · √E (GeV-1/2)
mm U

FIGURE 27

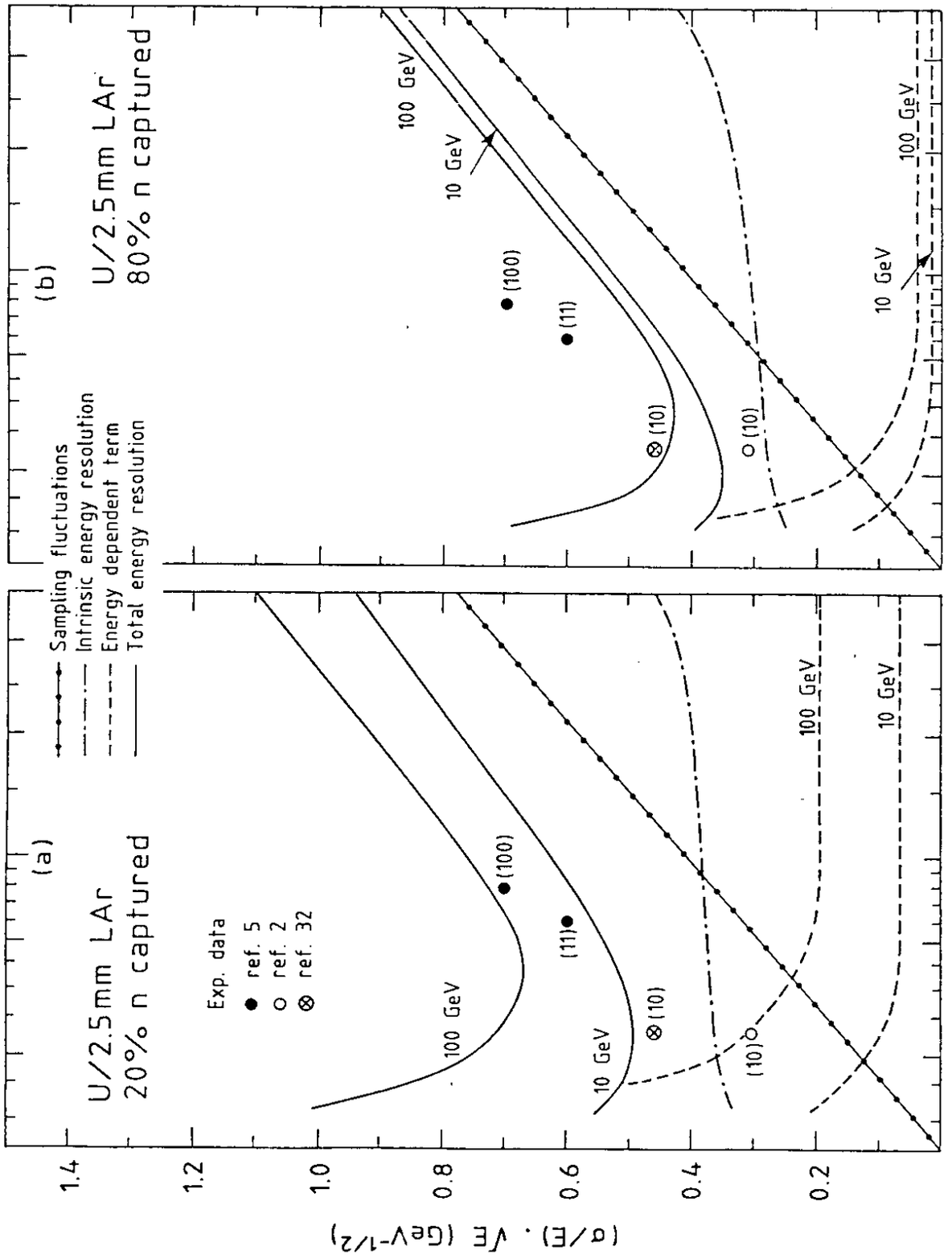
(a)
U/2.5mm LAr
20% n captured
(b)
U/2.5mm LAr
80% n captured
Sampling fluctuations
Intrinsic energy resolution
Energy dependent term
Total energy resolution
Exp. data
ref. 5
ref. 2
ref. 32
100 GeV
10 GeV
(100)
(11)
(10)
(σ/E) · √E (GeV-1/2)
mm U

FIGURE 28

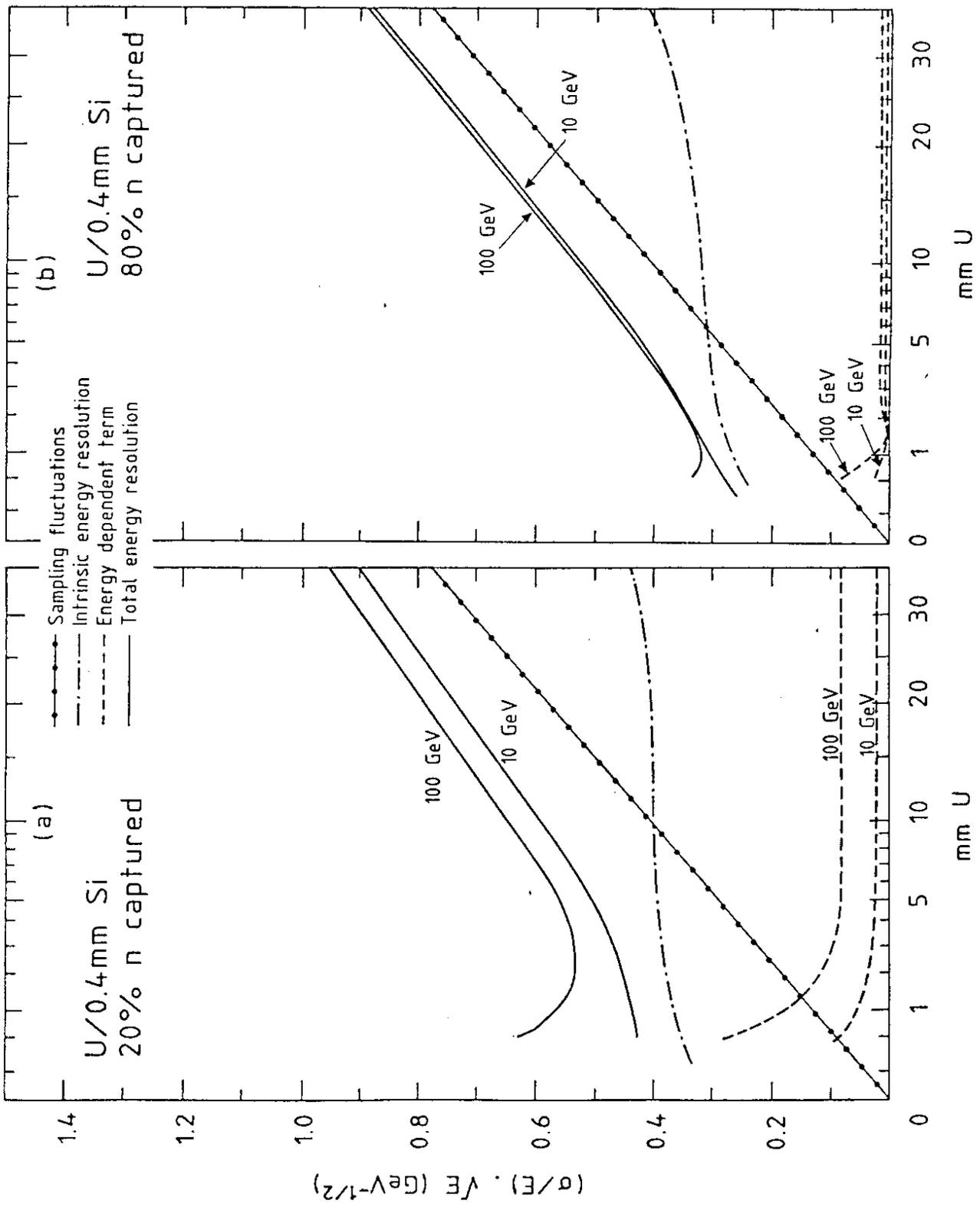
(a)
U/0.4mm Si
20% n captured
(b)
U/0.4mm Si
80% n captured
Sampling fluctuations
Intrinsic energy resolution
Energy dependent term
Total energy resolution
100 GeV
10 GeV
mm U
(σ/E) . √E (GeV-1/2)

FIGURE 29

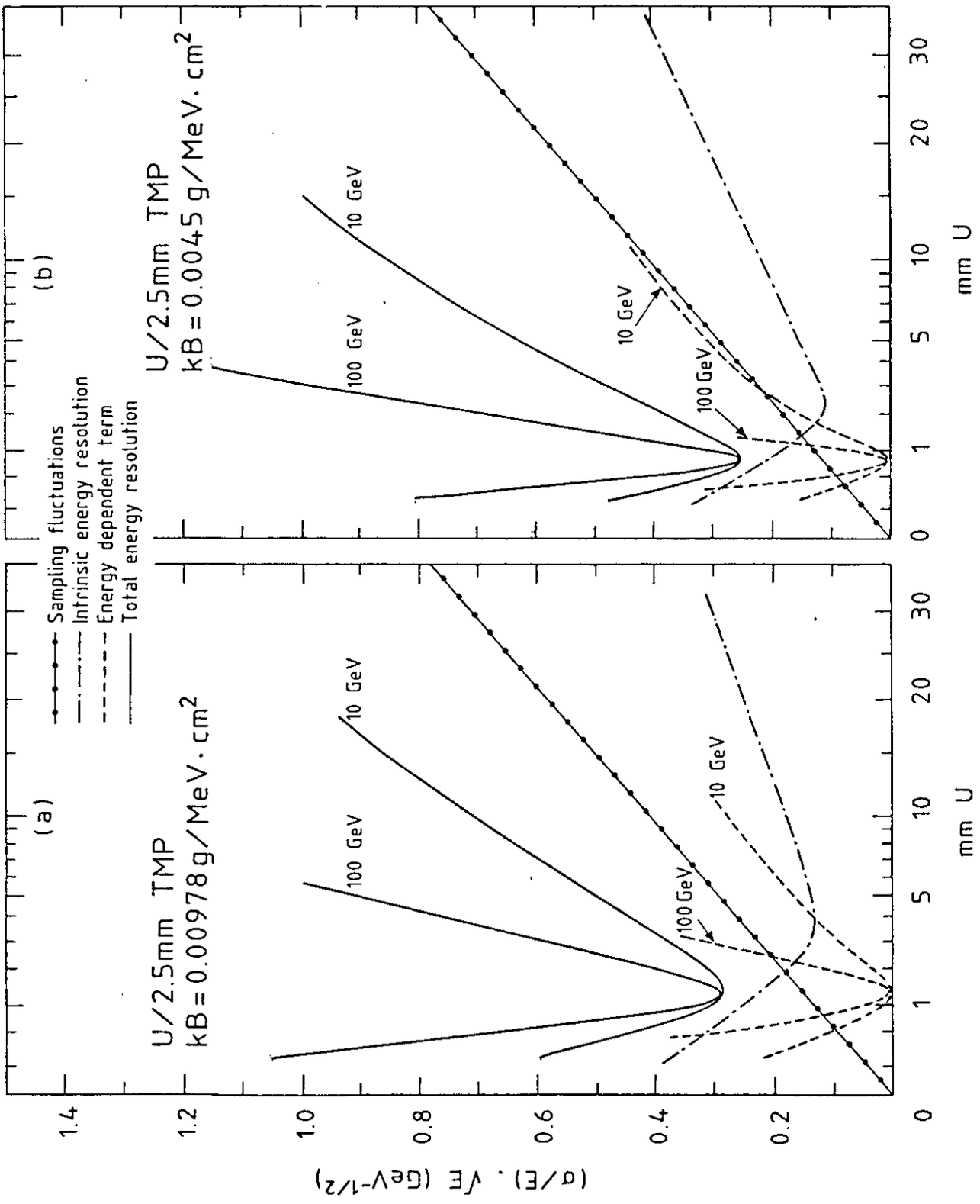
(a)
(b)
U/2.5mm TMP
kB = 0.00978 g/MeV · cm²
U/2.5mm TMP
kB = 0.0045 g/MeV · cm²
Sampling fluctuations
Intrinsic energy resolution
Energy dependent term
Total energy resolution
10 GeV
100 GeV
(σ/E) · √E (GeV-1/2)
mm U

FIGURE 30

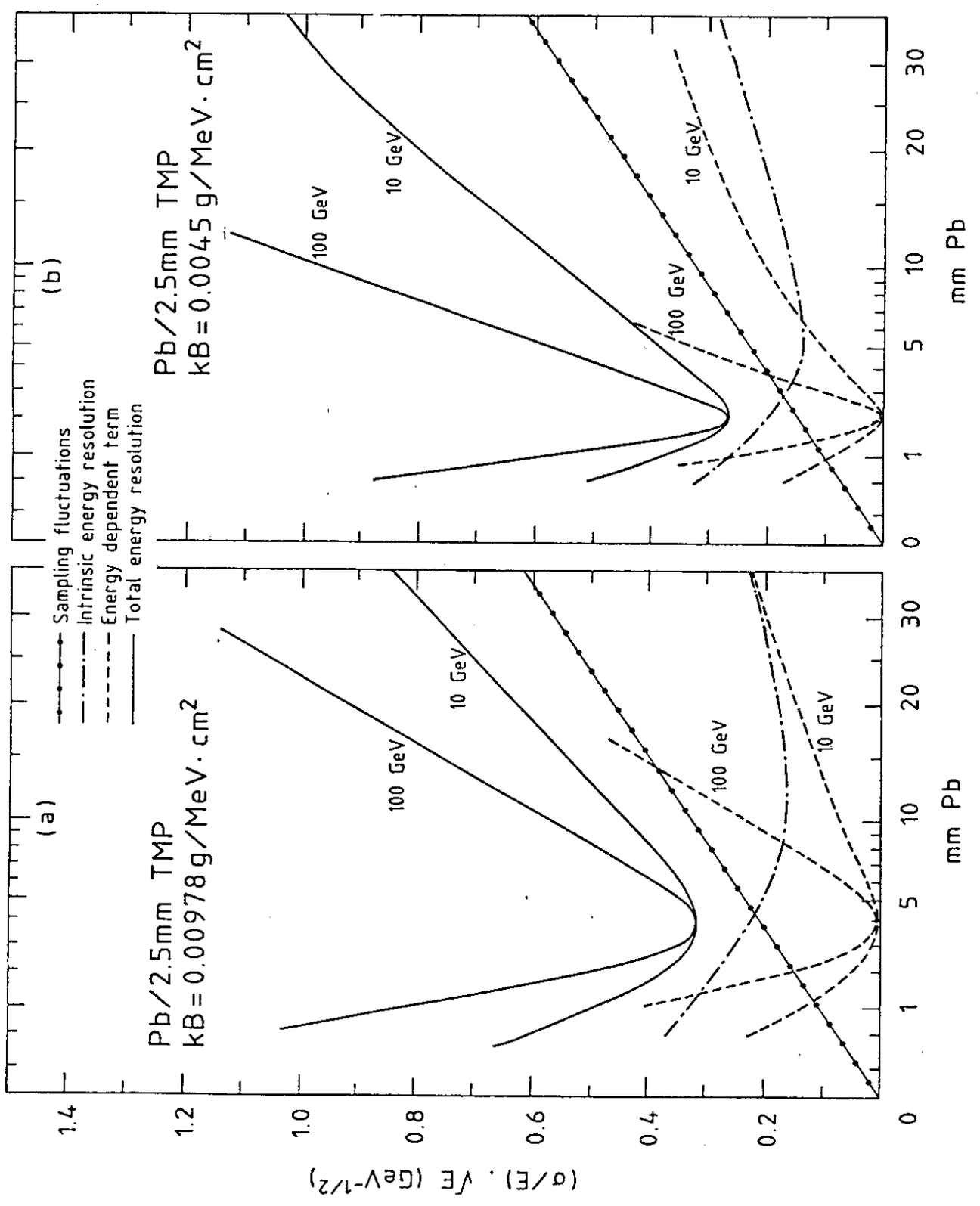
(a)
(b)
Pb/2.5mm TMP
kB=0.00978 g/MeV·cm²
Pb/2.5mm TMP
kB=0.0045 g/MeV·cm²
Sampling fluctuations
Intrinsic energy resolution
Energy dependent term
Total energy resolution
100 GeV
10 GeV
(σ/E) · √E (GeV-1/2)
mm Pb

FIGURE 31

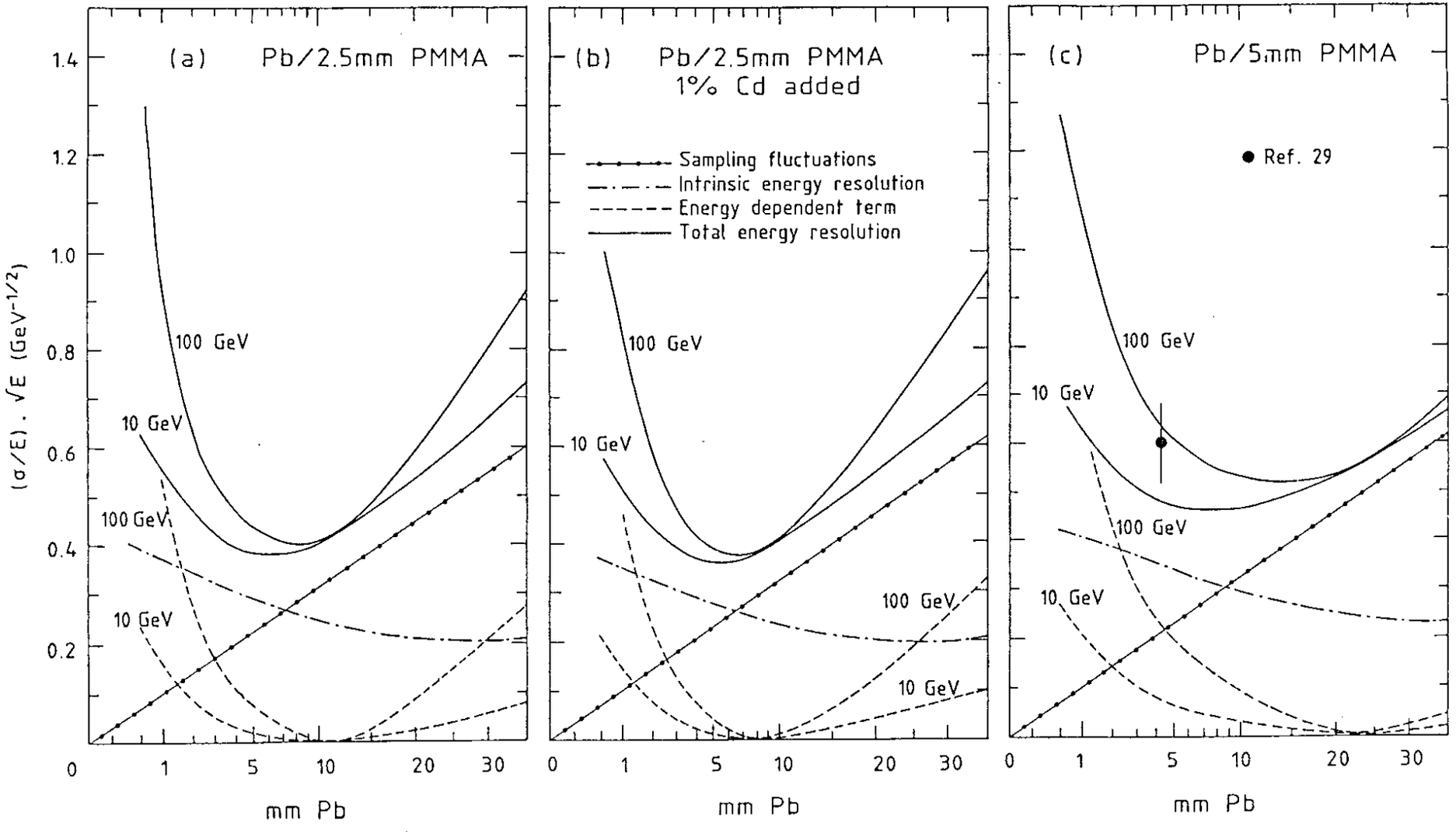
(a) Pb/2.5mm PMMA
(b) Pb/2.5mm PMMA
1% Cd added
(c) Pb/5mm PMMA
Sampling fluctuations
Intrinsic energy resolution
Energy dependent term
Total energy resolution
Ref. 29
100 GeV
10 GeV
(σ/E) . √E (GeV^-1/2)
mm Pb
0
1
5
10
20
30
0.2
0.4
0.6
0.8
1.0
1.2
1.4

FIGURE 32

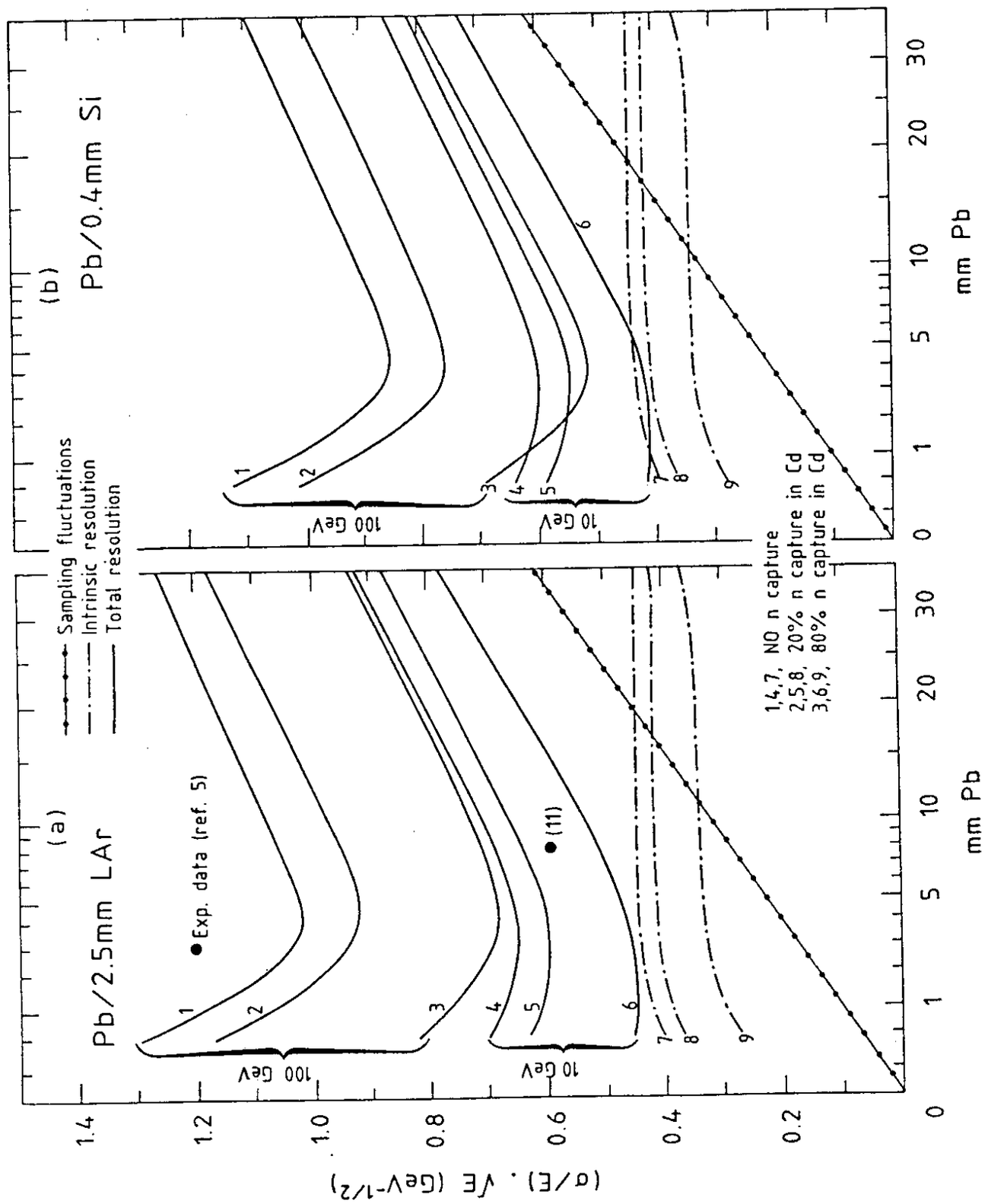
(a)
Pb/2.5mm LAr
(b)
Pb/0.4mm Si
Sampling fluctuations
Intrinsic resolution
Total resolution
Exp. data (ref. 5)
(11)
100 GeV
10 GeV
1,4,7, NO n capture
2,5,8, 20% n capture in Cd
3,6,9, 80% n capture in Cd
(σ/E) . √E (GeV-1/2)
mm Pb

FIGURE 33

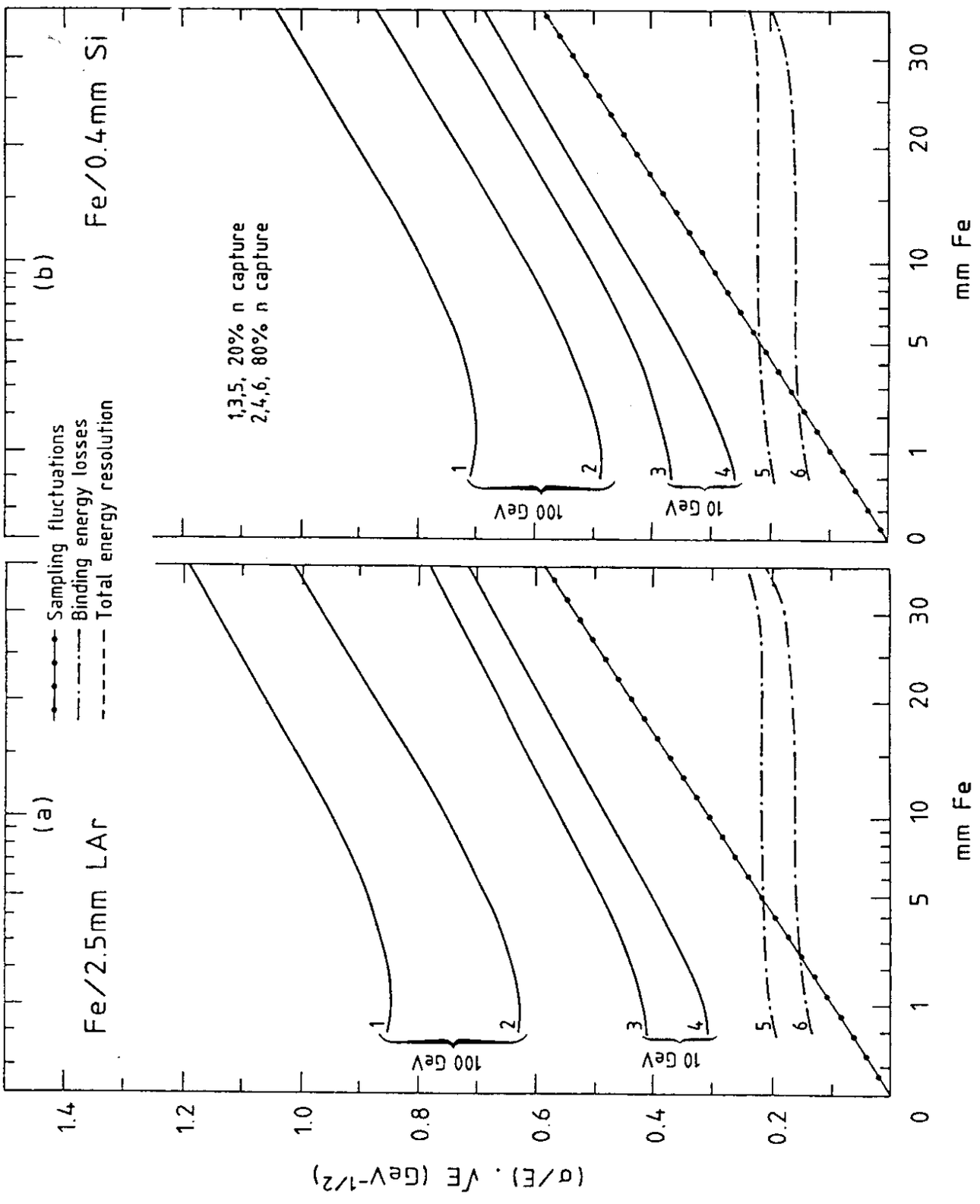
(a)
Fe/2.5mm LAr
(b)
Fe/0.4mm Si
Sampling fluctuations
Binding energy losses
Total energy resolution
1,3,5, 20% n capture
2,4,6, 80% n capture
100 GeV
10 GeV
1
2
3
4
5
6
(σ/E) . √E (GeV-1/2)
mm Fe
mm Fe

FIGURE 34

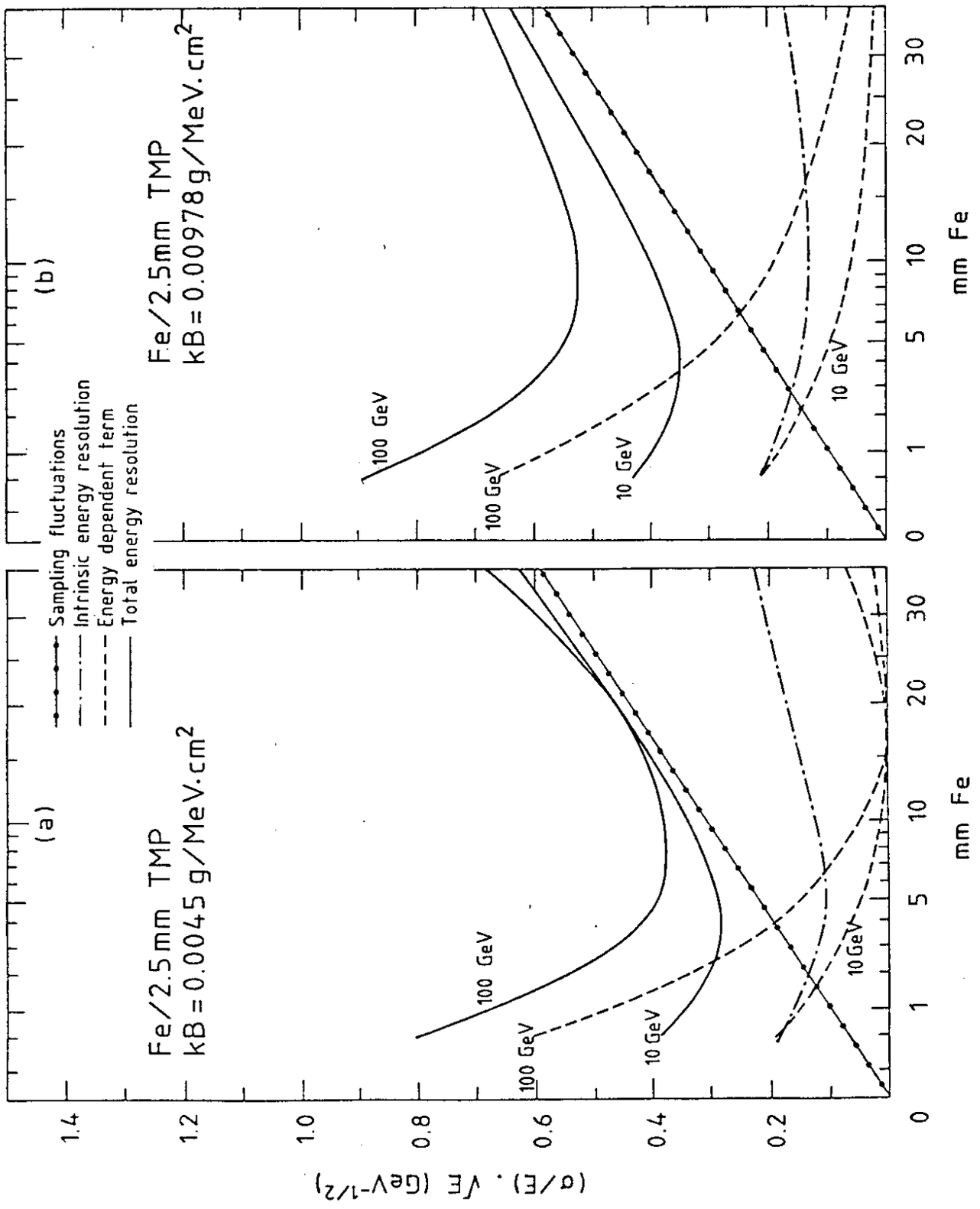
(a)
(b)
Fe/2.5mm TMP
kB = 0.0045 g/MeV·cm²
Fe/2.5mm TMP
kB = 0.00978 g/MeV·cm²
Sampling fluctuations
Intrinsic energy resolution
Energy dependent term
Total energy resolution
100 GeV
10 GeV
(σ/E) · √E (GeV-1/2)
mm Fe

FIGURE 35

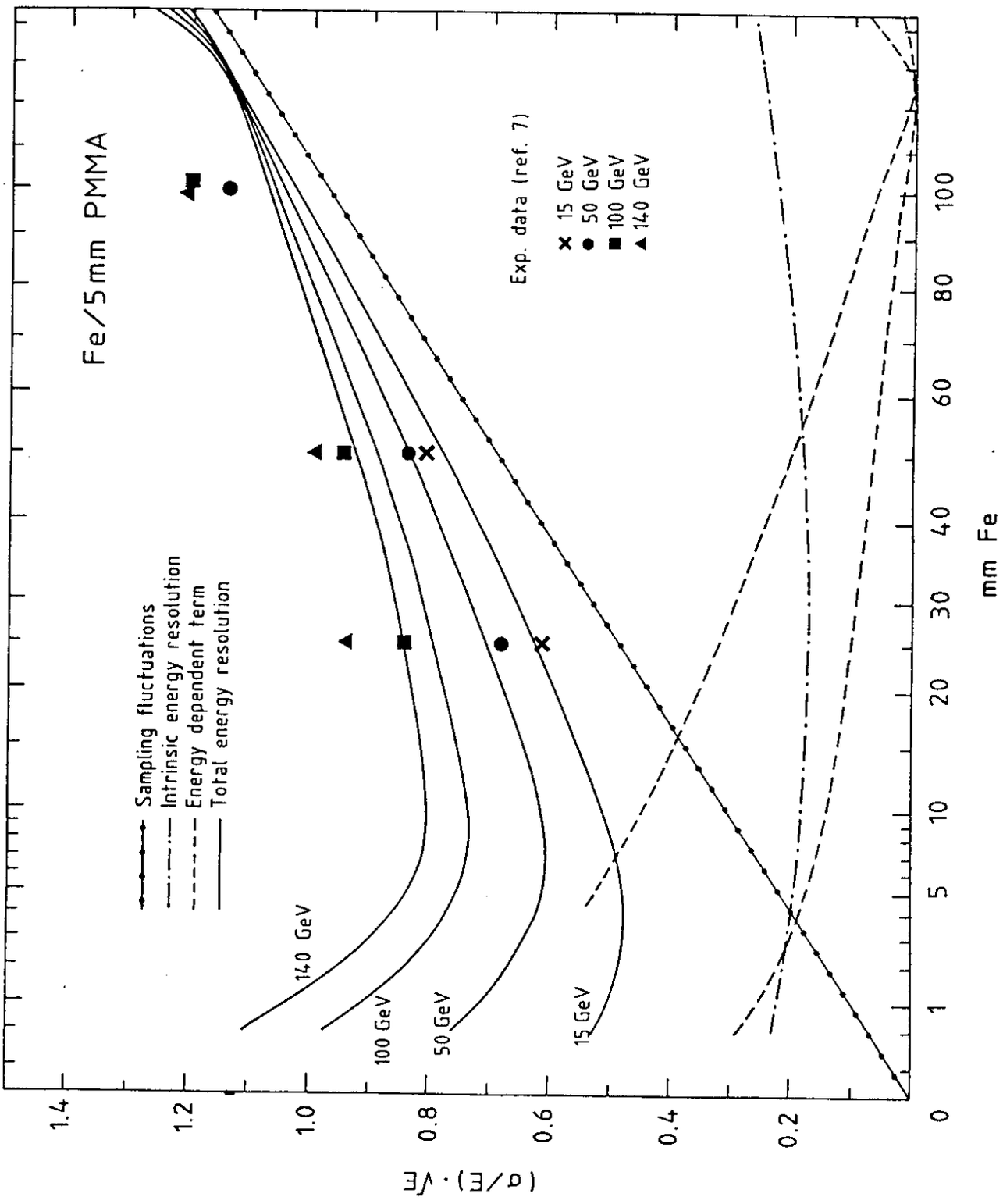
Fe/5mm PMMA
Sampling fluctuations
Intrinsic energy resolution
Energy dependent term
Total energy resolution
Exp. data (ref. 7)
15 GeV
50 GeV
100 GeV
140 GeV
140 GeV
100 GeV
50 GeV
15 GeV
(σ/E)·√E
mm Fe
0
1
5
10
20
30
40
60
80
100
0.2
0.4
0.6
0.8
1.0
1.2
1.4

FIGURE 36